



UNIVERSITAT
POLITÈCNICA
DE VALÈNCIA

Developing preclinical devices for neuroscience research in the fields of animal tracking, fMRI acquisition, and 3D histology cutting

Dissertation submitted in partial fulfillment of the requirements
for the degree of
Doctor of Philosophy

January 29, 2019

Author: **Darío Rubén Quiñones Colomer**

Director: **Prof. Dr. David Moratal Pérez**

Center for Biomaterials and Tissue Engineering
Universitat Politècnica de València
Valencia, Spain

Dr. Santiago Canals Gamoneda

Instituto de Neurociencias
Consejo Superior de Investigaciones Científicas
Universidad Miguel Hernández
San Juan de Alicante, Spain

Supervisor **Prof. Dr. David Moratal Pérez**
Universitat Politècnica de València

Co-Supervisor **Dr. Santiago Canals Gamoneda**
Instituto de Neurociencias de Sant Joan -
CSIC, Universidad Miguel Hernández

Members of the Jury Miguel Maravall Rodríguez
University of Sussex

Enrique Domingo Guijarro Estelles
Universitat Politècnica de València

Vicent Manuel Teruel Martí
Universitat de València

Members of the reviewers committee Javier Calpe Maravilla
Universitat de València

Miguel Maravall Rodríguez,
University of Sussex

André Marques-Smith
University College London

The research described in this thesis was carried out at the Polytechnic University of Valencia (Universitat Politècnica de València), Valencia, Spain in an extremely close collaboration with the Neuroscience Institute - Spanish National Research Council - Miguel Hernández University (Instituto de Neurociencias - Consejo Superior de Investigaciones Científicas - Universidad Miguel Hernández), San Juan de Alicante, Spain. This work was supported in part by the Spanish Ministerio de Economía y Competitividad (MINECO) and FEDER funds under grants BFU2015-64380-C2-2-R (D.M.) and BFU2015-64380-C2-1-R, by EU Horizon 2020 Program 668863-SyBil-AA grant (S.C.). S.C. acknowledges financial support from the Spanish State Research Agency, through the “Severo Ochoa” Programme for Centres of Excellence in R&D (ref. SEV-2013-0317) and by a grant “Ayudas para la formación de personal investigador (FPI)” from the Vicerrectorado de Investigación, Innovación y Transferencia of the Universitat Politècnica de València.

Acknowledgments

A David Moratal, per confiar en mi des del primer moment. Gràcies a tu he pogut millorar molt tant en la meua carrera professional com en la meua vida personal. Moltes gràcies David per aquests anys.

A Santiago Canals, por su colaboración, gracias a la cual he podido aportar mis ideas al campo de la neurociencia.

A todos los “*Moratalistas*”, por estos cuatro años juntos. Estoy muy agradecido por todo su apoyo e innumerables momentos divertidos, ya que sin ellos no hubiera podido llegar al final de esta etapa. Especialmente a Aarón Cuevas por su infinita paciencia y por intentar enseñarme todo lo que necesitaba para avanzar en el proyecto.

I would like to sincerely express my gratitude to Adam Kampff and his team for including me as one of their team/family. I have enjoyed a lot during my stay in your lab and I have learnt so many things. Thank you! I am also very grateful to Gonçalo Lopes, Danbee Kim, Cedric Honnet for being part of the Hive Tracker team and giving me the opportunity to learn from them in a lot of aspects.

A Ricardo Pérez y Juan Antonio García Manrique, por su incansable colaboración durante todos estos años. Sin vosotros no hubiera sido posible conseguir muchas de las cosas que he conseguido. ¡Gracias Peregrinos!

A mi familia, porque no hay palabras que puedan expresar mi gratitud hacia ellos. Porque siempre están ahí, aguantando mis tropiezos y mis desdichas sin

esperar nada a cambio. Nada de lo que he logrado hasta ahora hubiera sido posible sin su apoyo.

A Julia Gómez, por apoyarme, soportarme y estar siempre a mi lado tanto en los tiempos malos y en los buenos de esta tesis. ¡Gracias Pollito!

A Víctor González por abrirme las puertas del IVO y estar siempre dispuesto a ayudar en los proyectos que hemos llevado a cabo juntos.

A David Ibáñez por enseñarme a ser constante, además de darme todo su apoyo y energía cada día que he ido a verle. ¡Gracias!

Abstract

Neuroscience is a field that covers many specialties. The objective of this thesis is to correct some technological deficiencies that exist in current methods of animal experimentation in neuroscience. In this thesis, six projects are presented, which will aim to improve the “*Principle of the three Rs*” in animal experimentation enunciated by the English biologists W. M. S. Russell and R. L. Burch.

In the present era of impressive progress in neuroscience, it is still not arguable that a complete understanding of the brain cannot be possible without a comparable understanding of animal behavior. In order to study the behavior of laboratory animals, various tools are needed, being a reliable tracking system one of the most important to follow large populations of individual subjects that interact in complex manners. Several visual tracking tools are currently available. However, they all have some drawbacks. For example, in a situation where an animal is inside a cave, or is in close proximity to other animals, tracking cameras cannot always detect the precise location or movement of the animal. For this reason, environments that have been enriched in order to attempt to re-create the natural habitat of the animals under experiment, cannot be used, as the data gathered is insufficient/inaccurate.

In order to improve the current tracking systems, the RFID Assisted Tracking Tile (RATT) is presented. RATT is a tracking system based on passive Radio Frequency IDentification (RFID) technology and it is composed of electronic tiles. Using several tiles, a large surface area, on which the animals can move freely, can be built. This enables the more accurate identification of the animals, as well as the tracking of their movements. This system, which can also be combined

with a visual tracking system, paves the way for complete behavioral studies in enriched environments.

With the premise that positional tracking systems could be of great benefit in a number of other fields, including performance art, athletics, neuroscience and medicine, a new follow-up project was launched.

Commercially-available tracking solutions can track the movements of a human being inside a room with millimetric precision. However, these systems can track only a very small number of subjects at a time; are too expensive to be widely accessible; and their tracking devices are too large and too inaccurate for research or clinical use. Here, a small and lightweight wireless device, which piggybacks on current commercial solutions in order to provide scalable, affordable, and highly accurate positional tracking, is presented. This device can be used to track the movements of humans and other freely moving subjects for research purposes.

Given the ability to track animals and thus conduct thorough behavioral experiments, it is possible to observe how the subjects behave from an external viewpoint. However, if we want to understand what is going on in the brains of these subjects, it is necessary to apply other analysis techniques, for example the study of Blood Oxygen Level Dependent (BOLD) signals. BOLD signals are based on vascular responses to neuronal activation and are used extensively in clinical and preclinical research studies. In preclinical settings, animals are usually anesthetized. However, anesthetics cause changes in the physiology of the animals, e.g. hypothermia, and this has the potential to disrupt functional MRI (fMRI) signals. In order to avoid hypothermia in anesthetized rodents, TherMouseDuino is presented. This is an Open-Source automatic temperature control system, which reduces temperature fluctuations, thus providing robust conditions in which to perform fMRI experiments.

In biology and neuroscience courses, brain anatomy is generally taught using Magnetic Resonance Imaging (MRI) or histological sections of different planes. These show the most important macroscopic areas in an animals' brain. However, this method is neither dynamic nor intuitive. An anatomical Three-Dimensional (3D) printed rat brain with educative purposes is presented in this thesis. Hand manipulation of the structure, facilitated by the scaling up of its dimensions, together with the ability to dismantle the "*brain*" into some of main its constituent parts, facilitates the understanding of the 3D organization of the nervous system. This is an alternative and improved method for teaching students in general and biologists, in particular, the rat brain anatomy.

Once tools for behavioral experiments, signals from the brain, and 3D-printed models of the brain are obtained, we can go further and make histological cuts in the actual brains of rats/mice. But this is not something new. The study of tissue has always been an important part of the subject of biology. Hence, obtaining samples of tissue has been vital to morphological and functional research. The tools mainly used to obtain slices of tissue are microtomes and vibratomes. However, it is impossible to obtain a full 3D structure (e.g. long-haul tract) of a tissue sample with these devices. In this thesis, an automatic positioning device for the 3D cutting of living or fixed tissue samples is presented. This device paves the way for researchers to make cuts in sample tissue along different planes and in different directions, by maximizing the tract that appears in a slice.

The final project presented is not related to neuroscience, but it uses all of the knowledge of this thesis to develop devices for clinical research. Worldwide, cancer is one of the main causes of death, lung cancer being one of the most aggressive. There are several techniques for the treatment of lung cancer, among which radiotherapy is one of the most effective and least invasive for the patient. However, it has associated difficulties due to the moving target tumor. It is possible to reduce the side effects of radiotherapy by effectively tracking a tumor and reducing target irradiation margins. This thesis presents a custom electromechanical system that follows the movement of a lung tumor. The developed device helps the verification of individualized radiation treatment plans and permits the improvement of radiotherapy quality assurance procedures.

All the projects mentioned above are intended to help improve clinical and preclinical research, especially in the field of neuroscience. In addition, they intend to improve the application of the principle of the three Rs (Replacement, Reduction, Refinement) in the animal experimentation.

Resumen

La neurociencia es un campo que abarca muchas especialidades. El objetivo de esta tesis es subsanar algunas carencias tecnológicas que existen en los métodos actuales de experimentación animal en neurociencia. En esta tesis, se presentan seis proyectos, que tendrán como objetivo mejorar el “*Principio de las tres R*”, el cual fue enunciado por los biólogos ingleses W. M. S. Russell y R. L. Burch, durante la experimentación animal.

El comportamiento es uno de los aspectos más importantes de la vida animal. Depende de los vínculos entre los animales, sus sistemas nerviosos y sus entornos. Para estudiar el comportamiento de los animales de laboratorio, se necesitan varias herramientas, pero una herramienta de seguimiento es esencial para llevar a cabo un estudio de comportamiento exhaustivo. Varias herramientas de seguimiento visual están actualmente disponibles. Sin embargo, todas tienen algunos inconvenientes. Por ejemplo, en una situación en la que un animal está dentro de una madriguera o cerca de otros animales, las cámaras de rastreo (*tracking*) no siempre pueden detectar la ubicación precisa o el movimiento del animal. Por esta razón, los entornos enriquecidos para intentar recrear el hábitat natural de los animales en experimentación no pueden utilizarse, ya que los datos recopilados son insuficientes/inexactos.

Con la finalidad de mejorar los experimentos de tracking *RFID Assisted Tracking Tile (RATT)* es presentado en esta tesis. RATT es un sistema de seguimiento basado en tecnología de identificación pasiva de radiofrecuencia (RFID) y está compuesto por baldosas electrónicas con las que se puede construir una gran superficie, sobre la cual los animales pueden moverse libremente. Esto

permite la identificación más precisa de los animales, así como el seguimiento de sus movimientos. Este sistema, que también se puede combinar con un sistema de seguimiento con cámaras, allana el camino para estudios completos de comportamiento en entornos enriquecidos.

Con la premisa de que los sistemas de seguimiento posicional podrían ser de gran beneficio en otros campos, como atletismo, neurociencia y medicina, se lanzó un nuevo proyecto de seguimiento.

Las soluciones de rastreo disponibles comercialmente pueden rastrear los movimientos de un ser humano dentro de una habitación con una precisión milimétrica. Sin embargo, estos sistemas pueden rastrear solo una cantidad muy pequeña de sujetos a la vez; son demasiado caros para ser ampliamente accesibles; y sus dispositivos de rastreo son demasiado grandes e inexactos para la investigación o el uso clínico. Aquí, se presenta un dispositivo inalámbrico pequeño y liviano, que se complementa con las soluciones comerciales actuales para proporcionar un seguimiento posicional escalable, asequible y altamente preciso. Este dispositivo se puede utilizar para rastrear los movimientos de humanos y otros sujetos que se mueven libremente con fines de investigación.

Dada la capacidad de rastrear animales y, por lo tanto, realizar experimentos de comportamiento exhaustivos, es posible observar cómo se comportan los sujetos desde un punto de vista externo. Sin embargo, si queremos comprender lo que sucede en el cerebro de estos sujetos, es necesario aplicar otras técnicas de análisis, por ejemplo, el estudio de señales dependientes del nivel de oxígeno en la sangre (BOLD, por sus siglas en inglés).

Las señales BOLD se basan en las respuestas vasculares a la activación neuronal y se utilizan ampliamente en estudios de investigación clínicos y preclínicos. En entornos preclínicos, los animales suelen ser anestesiados. Sin embargo, los anestésicos causan cambios en la fisiología de los animales, p. Ej. hipotermia, y esto tiene el potencial de alterar las señales funcionales de MRI (fMRI). Para evitar la hipotermia en roedores anestesiados, se presenta *TherMouseDuino*. Este es un sistema de control automático de temperatura de código abierto, que reduce las fluctuaciones de la temperatura, lo que proporciona condiciones sólidas para realizar experimentos de resonancia magnética funcional.

En los cursos de biología y neurociencia, la anatomía del cerebro se enseña generalmente utilizando imágenes de resonancia magnética (IRM) o secciones histológicas de diferentes planos. Estos muestran las áreas macroscópicas más importantes en el cerebro de un animal. Sin embargo, este método no es dinámico ni intuitivo. En esta tesis se presenta un cerebro de rata impreso en 3D con fines

educativos. La manipulación manual de la estructura, facilitada por la ampliación de sus dimensiones, junto con la capacidad de desmontar el “*cerebro*” en algunas de sus partes principales, facilita la comprensión de la organización 3D del sistema nervioso. Este es un método alternativo y mejorado para enseñar a los estudiantes en general y a los biólogos, en particular, la anatomía del cerebro de rata.

Una vez que se han obtenido las herramientas para los experimentos de comportamiento, las señales del cerebro y los modelos impresos en 3D del cerebro, podemos ir más lejos y hacer cortes histológicos en los cerebros reales de las ratas/ratones. Pero esto no es algo nuevo. El estudio del tejido siempre ha sido una parte importante de la biología. Por lo tanto, la obtención de muestras de tejido ha sido vital para la investigación morfológica y funcional. Las herramientas utilizadas principalmente para obtener cortes de tejido son micrótomos y vibrátomos. Sin embargo, no es imposible obtener una estructura 3D completa (Por ejemplo, un tracto completo) de una muestra de tejido con estos dispositivos. En esta tesis, se presenta un dispositivo de posicionamiento automático para el corte 3D de muestras de tejido vivo o fijado. Este dispositivo abre nuevas posibilidades para que los investigadores realicen cortes en el tejido de la muestra a lo largo de diferentes planos y en diferentes direcciones, maximizando el tracto que aparece en una rebanada.

El proyecto final presentado no está relacionado con la neurociencia, pero utiliza todo el conocimiento de esta tesis para desarrollar dispositivos para la investigación clínica. En todo el mundo, el cáncer es una de las principales causas de muerte, y el cáncer de pulmón es uno de las más agresivos. Existen varias técnicas para el tratamiento del cáncer de pulmón, entre las cuales la radioterapia es una de las más efectivas y menos invasivas para el paciente. Sin embargo, tiene dificultades asociadas debido a que el tumor es una diana móvil. Es posible reducir los efectos secundarios de la radioterapia mediante el seguimiento efectivo de un tumor y la reducción de los márgenes de irradiación objetivos. Esta tesis presenta un sistema electromecánico personalizado que sigue el movimiento de un tumor de pulmón. El dispositivo desarrollado ayuda a verificar los planes de tratamiento de radioterapia individualizados y permite mejorar los procedimientos de la calidad de la radioterapia.

Todos los proyectos mencionados anteriormente pretenden ayudar a la mejora de la investigación clínica y preclínica, especialmente en el campo de la neurociencia. Además pretenden mejorar la aplicación del principio de las tres R (Reemplazo, Reducción, Refinamiento) en la experimentación con animales.

Resum

La neurociència és un camp que abasta moltes especialitats. L'objectiu d'aquesta tesi és esmenar algunes manques tecnològiques que existeixen en els mètodes actuals d'experimentació animal en neurociència. En aquesta tesi, es presenten sis projectes, que tindran com a objectiu millorar el “*Principi de les tres R*”, el qual va ser enunciat pels biòlegs anglesos W. M. S. Russell i R. L. Burch, durant l'experimentació animal.

El comportament és un dels aspectes més importants de la vida animal. Depèn dels vincles entre els animals, els seus sistemes nerviosos i els seus entorns. Per estudiar el comportament dels animals de laboratori, es necessiten diverses eines, però una eina de seguiment és essencial per a dur a terme un estudi de comportament exhaustiu. Diverses eines de seguiment visual estan actualment disponibles. No obstant això, totes tenen alguns inconvenients. Per exemple, en una situació en la qual un animal està dins d'un cau o prop d'altres animals, les cambres de rastreig (tracking) no sempre poden detectar la ubicació precisa o el moviment de l'animal. Per aquesta raó, els entorns enriquits per a intentar recrear l'hàbitat natural dels animals en experimentació no poden utilitzar-se, ja que les dades recopilades són insuficients/inexactes.

Amb la finalitat de millorar els experiments de tracking/seguiment *RFID Assisted Tracking Tile (RATT)* és presentat en aquesta tesi. RATT es un sistema de seguiment basat en tecnologia d'identificació passiva de radiofreqüència (RFID) i està compost per rajoles electròniques amb les quals es pot construir una gran superfície, sobre la qual els animals poden moures lliurement. Això permet la identificació més precisa dels animals, així com el seguiment dels seus moviments.

Aquest sistema, que també es pot combinar amb un sistema de seguiment amb cambres, aplanar el camí per a estudis complets de comportament en entorns enriquits.

Amb la premissa que els sistemes de seguiment posicional podrien ser de gran benefici en un altres camps, com a atletisme, neurociència i medicina, es va llançar un nou projecte de seguiment.

Les solucions de rastreig disponibles comercialment poden rastrejar els moviments d'un ésser humà dins d'una habitació amb una precisió mil·limètrica. No obstant això, aquests sistemes poden rastrejar només una quantitat molt xicoteta de subjectes alhora; són massa cars per a ser àmpliament accessibles; i els seus dispositius de rastreig són massa grans i inexactes per a la investigació o l'ús clínic. Ací, es presenta un dispositiu sense fil xicotet i lleuger, que es complementa amb les solucions comercials actuals per a proporcionar un seguiment posicional, assequible i altament precís. Aquest dispositiu es pot utilitzar per a rastrejar els moviments d'humans i altres subjectes que es mouen lliurement amb finalitats d'investigació.

Donada la capacitat de rastrejar animals i, per tant, realitzar experiments de comportament exhaustius, és possible observar com es comporten els subjectes des d'un punt de vista extern. No obstant això, si volem comprendre el que succeeix en el cervell d'aquests subjectes, és necessari aplicar altres tècniques d'anàlisi, per exemple, l'estudi de senyals dependents del nivell d'oxigen en la sang (BOLD, per les seues sigles en anglès).

Els senyals BOLD es basen en les respostes vasculars a l'activació neuronal i s'utilitzen àmpliament en estudis d'investigació clínics i preclínics. En entorns preclínics, els animals solen ser anestesiats. No obstant això, els anestèsics causen canvis en la fisiologia de els animals, per exemple hipotèrmia, i això té el potencial d'alterar els senyals funcionals de MRI (fMRI). Per a evitar la hipotèrmia en rosegadors anestesiats, es presenta TherMouseDuino. Aquest és un sistema de control automàtic de temperatura de codi obert, que redueix les fluctuacions de la temperatura, la qual cosa proporciona condicions sòlides per a realitzar experiments de ressonància magnètica funcional. En els cursos de biologia i neurociència, l'anatomia del cervell s'ensenya generalment utilitzant imatges de ressonància magnètica (IRM) o seccions histològiques de diferents plans. Aquests mostren les àrees macroscòpiques més importants en el cervell de un animal. No obstant això, aquest mètode no és dinàmic ni intuïtiu. En aquesta tesi es presenta un cervell de rata imprès en 3D amb finalitats educatius. La manipulació manual de l'estructura, facilitada per l'ampliació de les seues dimensions, juntament amb la capacitat de desmuntar el "cervell" en algunes de les seues parts principals,

facilita la comprensió de l'organització 3D del sistema nerviós. Aquest és un mètode alternatiu i millorat per a ensenyar a els estudiants en general i als biòlegs, en particular, l'anatomia del cervell de rata.

Una vegada que s'han obtingut les eines per als experiments de comportament, els senyals del cervell i els models impresos en 3D del cervell, podem anar més lluny i fer talls histològics en els cervells reals de les rates/ratolins. Però això no és alguna cosa nova. L'estudi del teixit sempre ha sigut una part important de la biologia. Per tant, l'obtenció de mostres de teixit ha sigut vital per la investigació morfològica i funcional. Les eines utilitzades principalment per a obtindre talls de teixit són micròtoms i vibràtoms. No obstant això, no és impossible obtindre una estructura 3D completa (Per exemple, un tracte complet) d'una mostra de teixit amb aquests dispositius. En aquesta tesi, es presenta un dispositiu de posicionament automàtic per al tall 3D de mostres de teixit viu o fixat. Aquest dispositiu obri noves possibilitats perquè els investigadors realitzen corts en el teixit de la mostra al llarg de diferents plans i en diferents direccions, maximitzant el tracte que apareix en una llesca.

El projecte final presentat no està relacionat amb la neurociència, però utilitza tot el coneixement d'aquesta tesi per a desenvolupar dispositius per a la investigació clínica. A tot el món, el càncer és una de les principals causes de mort, i el càncer de pulmó és un de les més agressius. Existeixen diverses tècniques per al tractament del càncer de pulmó, entre les quals la radioteràpia és una de les més efectives i menys invasives per al pacient. No obstant això, té dificultats associades pel fet que el tumor és una diana mòbil. És possible reduir els efectes secundaris de la radioteràpia mitjançant el seguiment efectiu d'un tumor i la reducció de els marges d'irradiació objectius. Aquesta tesi presenta un sistema electromecànic personalitzat que segueix el moviment de un tumor de pulmó. El dispositiu desenvolupat ajuda a verificar els plans de tractament de radioteràpia individualitzats i permet millorar els procediments de la qualitat de la radioteràpia.

Tots els projectes esmentats anteriorment pretenen ajudar a la millora de la recerca clínica i preclínica, especialment en el camp de la neurociència. A més pretenen millorar l'aplicació del principi de les tres R (Reemplaçament, Reducció, Refinament) en l'experimentació amb animal.

Contents

Colophon	4
Acknowledgements	iii
Abstract	v
Resumen	ix
Resum	xiii
Contents	xvii
1 Introduction	1
1.1 Cognitive and Behavioral Neuroscience	2
1.2 Animal Experimentation	4
1.3 Motivation	7
1.4 Objectives.....	9
1.5 Thesis Structure	9

- 2 RATT: RFID Assisted Tracking Tile. 13**
- 2.1 Introduction 14**
 - 2.1.1 Behavior Experiments 15
 - 2.1.2 Computer Vision Tracking Systems 16
 - 2.1.3 Radio Frequency Tracking Systems 19
 - 2.1.4 Mixed Tracking Systems 19
 - 2.1.5 Radio Frequency Identification (RFID) 20
 - 2.1.5.1 Inductive Coupling 20
 - 2.1.5.2 Differentiation Features of RFID Systems 22
 - 2.1.5.3 Tag Construction Formats 23
 - 2.1.6 RATT Features 24
- 2.2 Materials and Methods 26**
 - 2.2.1 RATT System Concept 26
 - 2.2.2 Software 27
 - 2.2.3 System Core: LPC4088-ARM cortex 28
 - 2.2.4 RFID Tags 30
 - 2.2.5 ISO/IEC 15693 30
 - 2.2.6 Smith Chart 30
 - 2.2.7 Connectors 31
 - 2.2.8 The TRF7960A 31
 - 2.2.9 UDP Communication 32
- 2.3 Results 33**
 - 2.3.1 RATT Tile Virtual Concept 33
 - 2.3.2 Control Board 34
 - 2.3.3 RF Board 36
 - 2.3.4 RFID Antenna Design 36
 - 2.3.5 RFID Antenna Simulation 40
 - 2.3.6 Structure 41
 - 2.3.7 Triangulation Algorithm 44
 - 2.3.8 Artificial Vision 45
 - 2.3.9 Data Acquisition 47
 - 2.3.10 Overall 48
 - 2.3.11 MultiRATT Tile 51

2.4	Conclusions	52
3	HIVE Tracker	55
3.1	Introduction.....	56
3.1.1	Applications in Performing Arts and Athletics	56
3.1.2	Applications in Neuroscience and Medicine	57
3.1.3	Current State-of-the-art in Positional Tracking	57
3.1.4	Affordable, Smaller, and more Scalable	58
3.2	Materials and Methods	58
3.2.1	Valve Tracking System	59
3.2.2	Signal Processing	61
3.2.2.1	Photodiode circuit	61
3.2.2.2	Acquisition Hardware: Teensy	61
3.2.2.3	Acquisition Software: BONSAI	62
3.2.2.4	Triangulation Algorithm	63
3.3	Results and Discussion.....	63
3.3.1	Tracking: inside an ideal room	63
3.3.2	Tracking: in a non ideal room	64
3.3.3	Light Reflections	65
3.3.4	Tracking Refresh Rate	66
3.4	PCB Prototype	67
3.4.1	Hardware	67
3.4.2	Firmware	68
3.4.3	Size/Accuracy Trade-off	70
3.4.4	Cost	71
3.4.5	Autonomy	72
3.5	Conclusion	72
4	TherMouseDuino	73
4.1	Introduction.....	74
4.2	Materials and Methods	76
4.2.1	Overview	76
4.2.2	Heating System	77

4.2.3 Acquisition Device	78
4.2.4 Microcontroller	79
4.2.5 USB Host Module	80
4.2.6 RS-232 Communication Module	80
4.2.7 LCD User Interface	81
4.2.8 Model Identification	81
4.2.9 PID Control	82
4.2.10 Animals and MRI Acquisition Protocol	83
4.2.11 Surgery for fMRI experiments	83
4.2.12 fMRI data extraction	84
4.3 Results and Discussion	85
4.3.1 Experimental Identification Results	85
4.3.2 Control System Design Results	87
4.4 Conclusion	90
5 A Tangible Educative 3D Printed Atlas of the Rat Brain	93
5.1 Introduction	94
5.2 Materials and Methods	95
5.2.1 Data Selection: The 8 Most Relevant Macroscopic Areas in the Rat Brain	97
5.2.2 Three-Dimensional Reconstruction of the Desired Areas	99
5.2.3 Transforming the Facet Body into an Editable Solid Body	100
5.2.4 Rapid Prototyping	101
5.3 Results	103
5.4 Discussion	105
5.5 Conclusions	106
6 Automatic Device for Cutting 3D Tissue	107
6.1 Introduction	108
6.1.1 Histology	108
6.1.2 Microtome and Vibratome	108
6.2 Materials and Methods	110
6.2.1 System Concept	110

6.2.2 System Parts	112
6.2.3 Manufacturing materials	113
6.2.4 Acquisition System	114
6.3 Results and Discussion	114
6.3.1 Systems Specifications	114
6.3.2 Slicing test	116
6.3.3 Graphical User Interface	117
6.4 Conclusions	118
7 Lung Tumor Movement Simulator	119
7.1 Preface	120
7.2 Introduction	120
7.3 Materials and Methods	123
7.3.1 Linear Accelerator	123
7.3.2 Electromechanical Components	124
7.3.3 Microcontroller	124
7.3.4 Manufacture and Material	125
7.4 Results	125
7.4.1 Prototype Design	125
7.4.2 Movement and Path Simulation	127
7.4.3 Synchronizing the Movements	128
7.4.4 Path Verification	129
7.5 Discussion	131
7.6 Conclusions	133
8 Conclusions and Outlook	135
8.1 On the tracking devices	135
8.2 On the control temperature devices	136
8.3 On the 3D printed brain	137
8.4 On the histological cuts	137
8.5 On the tumor movement simulator	138
8.6 On the future work	138

9 Contributions	139
9.1 Research Internship	139
9.2 Publications in Journals	139
9.2.1 International Journals.....	139
9.2.2 National Journals	140
9.3 Patents	140
9.4 Publications in International Conference Proceedings	141
9.5 Awards and Honours	141
9.6 Others	142
9.7 Final Master Project Supervision	142
9.8 Final Degree Project Supervision	143
List of Figures	145
List of Tables	149
Abbreviations and Acronyms	151
Bibliography	155

Chapter 1

Introduction

“New technologies to probe the nervous system are propelling innovation and discovery at blinding speed, but are our trainees prepared to maximize this power? The growing role of engineering in research, such as materials, computing, electronics, and devices, compels us to rethink neuroscience education. Core technology requirements, cross-disciplinary education, open-source resources, and experiential learning are new ways we can efficiently equip future leaders to make the next disruptive discoveries.”– Brian Litt, 2015

Scientists have been interested in the brain from the beginning of scientific research, its diseases and why human beings behave as they do. The earliest study of the nervous system dates back to the Ancient Egyptians. The surgical practice of drilling or scraping a hole into the skull, known as Trepanation, was first recorded during the Neolithic period (10,000 BC to 2,000 BC approx.); the aim of this was to cure headaches or mental disorders by relieving cranial pressure [1].

From the nineteenth century, there have been significant advances in neuroscientific knowledge, thanks to well-known researchers such as Golgi, Santiago Ramón y Cajal, Flourens, and Broca among others. The Golgi stain first enabled the visualization of individual neurons (see Figure 1.1). Santiago Ramón y Cajal who created the neuron doctrine, which is the concept that the nervous system is made up of discrete individual cells. Jean Pierre Flourens pioneered the experimental method of creating localized lesions in the brains of rabbits and pigeons and carefully observing their effects on motor skills, sensibility and behavior. Paul Broca suggested that certain cortical regions of the brain were responsible for specific functions.

The Brodmann cerebral cytoarchitectonic, which dates from this era, today through current neuroimaging techniques, continues to show that distinct areas of the cortex are activated in the execution of specific tasks [2]. Thanks to technological advances in the twentieth century, understanding of neurons and the nervous system as a whole became increasingly precise and molecular. For example, in 1952, Alan Lloyd Hodgkin and Andrew Huxley presented the first “*Action potential*” mathematical model for the transmission of electrical signals in the neurons of the giant axon of a squid, and how these neurons are initiated and propagated. It is known as the *Hodgkin-Huxley model* [4].

1.1 Cognitive and Behavioral Neuroscience

Cognitive neuroscience addresses the question of how psychological functions are produced by neural circuits [5]. The emergence of new measurement techniques, such as neuroimaging, electrophysiology and human genetic analysis, combined with sophisticated experimental techniques of cognitive psychology allow neuroscientists and psychologists to address abstract concepts, such as

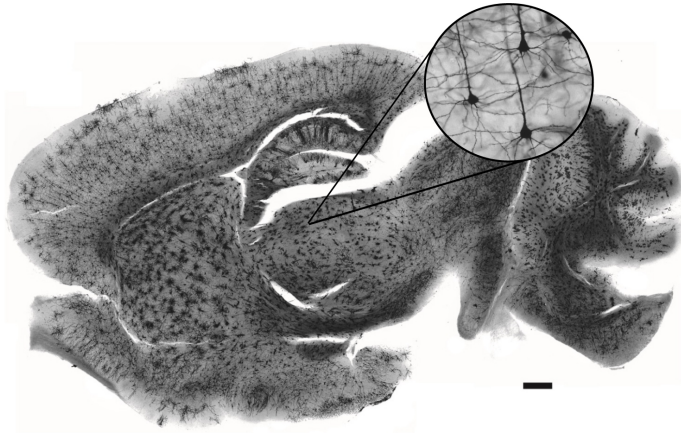


Figure 1.1. Neurons in all brain regions are evenly and reliably stained with the Golgi-Cox protocol. Modified figure from Zaqout et Al.[3].

cognition and human emotion, and how these are mapped to specific neuronal substrates.

Although many studies still maintain a reductionist stance in the search for a neurobiological basis of cognitive phenomena, recent research shows that there is an interaction between neuroscientific findings and conceptual research, which integrates both perspectives. For example, neuroscientific research on empathy called for an interdisciplinary debate involving philosophy, psychology and psychopathology [6]. In addition, the neuroscientific identification of multiple memory systems, related to different areas of the brain has challenged the idea of memory as a literal reproduction of the past, and supports a vision of memory as a generative, constructive and dynamic process [7].

Neuroscience is also applied to with social and behavioral sciences [8], as well as with new interdisciplinary fields such as neuroeconomics [9], decision theory [10], social neuroscience [11] and neuromarketing [12] in order to address complex questions about the brain's interaction with the environment. For example, behavioural neuroscientists are generating a comprehensive set of assays for social interaction, communication and repetitive behaviours based on rodent experiments to test hypotheses about the causes of autism [8]. Another example is a study on consumer responses narrative videos in energy efficiency social

marketing, for example, uses EEG to investigate the neural correlations associated [13].

Ultimately, neuroscientists hope to understand all aspects of the nervous system, including how it works, how it develops, and how it can be altered or repaired. The specific topics that form the main focus of research change over time, driven both by a knowledge base in constant expansion and the availability of increasingly sophisticated technical methods. In the long term, improvements in technology have been the main drivers of progress. Advances in electron microscopy, computers, electronics, functional brain imaging and, more recently, genetics and genomics, have all been important drivers of progress.

1.2 Animal Experimentation

The use of animals for scientific purposes presents a great moral dilemma for society today. Although social progress has led to greater empathy towards animals, it is true that animal experimentation has led to a large number of scientific advances over the years, especially in the field of biomedicine. This type of experimentation has greatly assisted the study of diseases and their causes, a situation which would not have been possible otherwise. However, it is mandatory to follow a series of rules and guidelines when working with animals for experimentation.

The purpose of these guidelines is to prevent unnecessary or excessive suffering when the animals are used. Law 32/2007 of November 7, 2007, and its subsequent amendment by law 6/2013 of June 11 establish the Spanish regulatory framework regarding the care of animals, in their exploitation, their transportation, experimentation and sacrifice. This legislation is under Directive 2010/63/EU of the European Parliament and of the Council, of September 22, 2010, on the protection of animals used for scientific purposes.

Both the regulations and the derived guides are based on the “Principle of the three Rs” enunciated by the English biologists W. M. S. Russell and R. L. Burch at the beginning of the decade of the 60s [14]. This principle aims to ensure a real need for the use of animals during research, but using alternative methods when it is possible. The techniques that this principle suggests are [15]:

- **Reduction:** The purpose is to keep to a minimum the number of animals used for experimental purposes. Some examples of this are the use of animals that are as homogeneous as possible, obtaining the maximum information from each animal and increasing the precision of the experiments.
- **Refinement:** This means reducing stress and pain as much as possible in order to ensure the welfare of the animals. Some examples here are the use of non-invasive methods, reduction in the duration of the experiments and improvement in the conditioning of the animal. This point is of particular interest as it tends to the results obtained in the experiments. Being in pain produces physiological changes in animals that can alter results.
- **Replacement:** This consists of the replacement of live animals with other methods that use previous studies, computer models, physicochemical systems, cell cultures, tissues and organs, human volunteers, etc.

The animals most commonly used in research are the Norwegian rat (*Rattus norvegicus*) and the laboratory mouse (*Mus musculus laboratorius*), especially in biomedical research. One of the reasons for their use is the detailed knowledge of the sequences of both genomes [16]. This knowledge makes it possible to compare these genomes with the genomes of other mammals, such as man. However, historically, several discoveries were made in other animal models (see Figure 1.2) and these had a considerable impact on neuroscience knowledge.

Squids were used to study the mechanisms underlying action potential generation because of their giant axons, which allow the insertion of voltage-clamp electrodes[17].

Frogs were used to study the mechanisms of synaptic transmission because of the simple behavior and large size of the synapses involved [18].

Horseshoe crabs were used to study mechanisms of retinal physiology, including lateral inhibition, because of the accessibility of individual nerve cells and the convenient structure of the compound eye [19].

Aplysia was used to study the neurobiology of learning and memory because of its capacity for simple forms of learning and the easily identifiable and accessible neurons that mediate these behaviors [20].

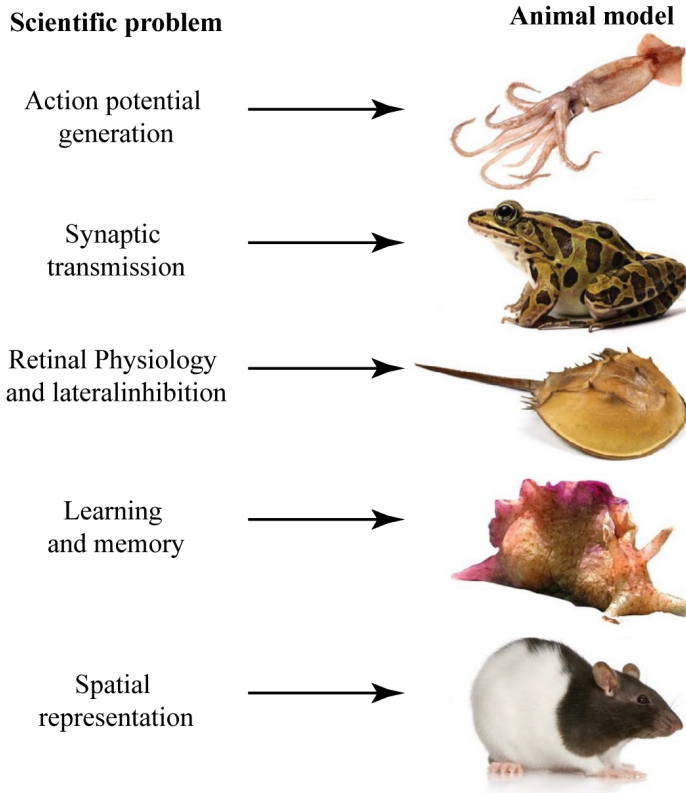


Figure 1.2. The most famous animal models for experimentation

Fruit flies (*Drosophila*) has enabled milestone discoveries in nervous system development and function [21].

Rats are used to study the neural components of spatial representation [22], [23] because of their exploratory behavior and size, which enables neural recordings during free behavior. The neuroethological approach taken in these studies is described by O’Keefe and Nadel [section 4.7. LOF [22]].

The laboratory mouse has a significant advantage in terms of genetic modification methods. However, the laboratory rat is larger in size, which means greater ease for repeated sampling and surgical modifications. Over the years, the number of pure strains for both species has been increasing. In addition,

there has been the use of many species with genetic mutations that can simulate different research models [14].

The laboratory mouse is recognized as the main model for modern genetic research. It is also used in a variety of types of research such as oncology, immunology, toxicology, cardiology, etc. They are prized for qualities such as their small size, short gestation time and ease of breeding in the laboratory [24].

1.3 Motivation

As stated in the introduction, Neuroscientific knowledge is continuously advancing in all aspects of the field. However, despite this it is still necessary to use animals for experimentation.

Based on one of the three Rs, the “R” of *Refinement*, this thesis aims to use technology to provide novel devices for reducing stress and pain in these animals as much as possible in order to ensure their welfare during the experimentation process.

In aiming to reduce the stress suffered by these animals, while at the same time attempting to recreate their natural environments, one common problem was found. This problem was detected in social behavior experiments and it was the lack of enriched environments for the animals under experiment. However, non-naturalistic lab environments have been in place for many other reasons, e.g. the logistical complications of space and cost in animal facilities and the comparative lack of attention paid to ethological conditions. One of this problems is caused by the use of video/camera tracking systems in the behavioral experiments because it constrains the space for the experiment.

Up to now, it has not been possible to carry out animal tracking experiments without using cameras, and their use constrains the environments where the animals are being recorded. For example, it is not possible to enrich these environments because adding plants, burrows or a large number of subjects causes several occlusions to camera vision systems. If these occlusions occur, the result could be data loss and position errors. Moreover, *how are we to understand the social behavior of animals in their natural habitat if we cannot observe them behaving as they would in these habitats?*

Continuing with the “R” of *Refinement*, when animals are analyzed using certain procedures, e.g. Magnetic Resonance Imaging (MRI), they tend to suffer from particular problems, which humans do not. This causes alterations in their normal state and creates a bias that affects the results of the experiment. E.g., when a small animal is anesthetized and put inside an MR scanner, it is likely to suffer from hypothermia. This will directly affect the animal and the results of the experiment.

Another of the three Rs is the “R” of *Replacement*. This involves the replacement of live animals with other methods that use previous studies and computer models, among others. Sometimes it is difficult to understand/learn something if it is not physically tangible with our hands, even though it is illustrated in the literature. However, nowadays there are non-invasive techniques such as MRI that can extract information from animals without sacrificing them. Moreover, data from these techniques can be obtained and shown in 3D on the computer. But, what if we could create a rat brain, which is 3D printed and scaled up? In the first instance, this would certainly help students and researchers to understand the anatomy of this complex organ.

The last of the three Rs is the “R” of *Reduction*. It is mandatory to keep to a minimum the number of animals used for experimental purposes. So, *how can we optimize the information that is extracted from one experiment in order to minimize the number of animals used?* One obvious answer would be “*by improving current methodologies*”. In order to overcome this issue and based on the field of histology, a lack in the commercial vibratomes/vibroslicers was found. This lack corresponds to the inability of the devices to cut tissue in a 3D plane in order to extract long-haul neuronal tracts.

The final challenge is to apply all of the skills and knowledge acquired during the development of this thesis to different fields. This, and in collaboration with the Instituto Valenciano de Oncología, led to the motivation of attempting to reduce the number of radiotherapy doses that patients receive. All of the issues stated in section 1.3 will be properly explained and referenced in each of the corresponding thesis chapters.

1.4 Objectives

The overall objective of this thesis is to improve existing and develop new tools for neuroscientific research in order to facilitate the expansion of knowledge in this field. Five specific objectives were defined as follows:

- The creation of tracking tools that capture the trajectories and paths that animals and humans follow in indoor spaces in order to conduct behavioral experiments.
- The development of a device that increases the accuracy of fMRI images acquisition in preclinical experiments, frees up the technician and preserve the animal in normal physiological conditions.
- The creation of a tangible model of the rat brain that will provide more physical information to students and researchers in order to facilitate understanding of this organ.
- The creation of an accessory for commercial vibratomes in order to improve current slicing methodologies.
- The application of all of the knowledge acquired during the development of this thesis to a different field to create a device that simulates the movement of a lung tumor during the breathing cycle.

1.5 Thesis Structure

This thesis contains in 9 chapters. Chapter 1 presents a summary of neuroscience field and the general and specific objectives of the thesis. Chapters 2 to 7 present the experimental projects performed. Chapters 8 to 9 present the final overall conclusions reached in the development of the thesis and the publications issued in journals and conferences in the context of this thesis.

A summary of the important chapters of this thesis, which are self-contained and can be read independently, is introduced below:

Chapter 1, focuses on the motivation behind this thesis and summarizes the current neuroscience field and animal experimentation. Additionally, this introductory chapter establishes the specific objectives addressed in the thesis, as well as the resulting contributions to the field of network neuroscience.

Chapter 2, presents an RFID Assisted Tracking Tile (RATT), a tracking system based on passive RFID technology in the high-frequency band according to ISO/IEC 15693. This device is able to track multiple animals in a customized large surface without the use of cameras. It can be used for tracking small animals and can perform several types of behavioral experiments. This project was developed in extremely close collaboration with the Neuroscience Institute - Spanish National Research Council - Miguel Hernández University (Instituto de Neurociencias - Consejo Superior de Investigaciones Científicas - Universidad Miguel Hernández), San Juan de Alicante, Spain.

Chapter 3, presents Hive Tracker, a novel alternative to traditional tracking systems. It is a light and small wireless device that piggybacks on current commercial solutions to provide affordable, scalable, and highly accurate positional tracking. This device can be used to track small and precise human movements, to easily embed custom objects inside a Virtual Reality (VR) system, and to track freely moving subjects for research purposes. This project was developed in close collaboration with the Kampff Lab - Sainsbury Wellcome Centre for Neural Circuits and Behaviour, University College London during a research visit.

Chapter 4, this chapter provides a solution for controlling mouse temperature inside of a Magnetic Resonance scanner. In order to avoid hypothermia in anesthetized rodents an Open-Source automatic temperature control It is an automatic temperature control system, which reduces temperature fluctuations, thus providing robust conditions in which to perform fMRI experiments. Furthermore, this device frees up the technician to focus solely on monitoring the MRI sequences. This project was developed in extremely close collaboration with the Neuroscience Institute - Spanish National Research Council - Miguel Hernández University (Instituto de Neurociencias - Consejo Superior de Investigaciones Científicas - Universidad Miguel Hernández), San Juan de Alicante, Spain.

Chapter 5, this chapter presents an anatomical 3D printed rat brain with educative purposes. Hand manipulation of the structure, facilitated by the scaled up of its dimensions, and the ability to dismantle the '*brain*' into some of its constituent parts, facilitates the understanding of the 3D organization of the nervous system. This is an alternative method for teaching students in general and biologists in particular the rat brain anatomy. This work presents a methodology that could be expanded to almost any field of clinical and pre-clinical research, and moreover it avoids the need of dissect animals in order to teach brain anatomy. This project was developed in extremely close collaboration with the Neuroscience Institute and the Institute of Design for Manufacturing and Automated Production, Universitat Politècnica de València, Spain.

Chapter 6, This chapter presents an automatic positioning device for a three-dimensional cut in living or fixed tissue samples, which can be applied mainly in histology, anatomy, biochemistry and pharmacology. This device paves the way for researchers to make cuts in the sample tissue along different planes and in different directions by maximizing the surface of the tract that appears in a slice. This project was developed in close collaboration with the Neuroscience Institute and the Institute of Design for Manufacturing and Automated Production.

Chapter 7, This chapter presents a custom electromechanical system that follows the movement of a lung tumor. The developed device helps the verification of individualized radiation treatment plans and permits the improvement of radiotherapy quality assurance procedures. This project was developed in extremely close collaboration with the Department of Radiophysics, Fundación Instituto Valenciano de Oncología, Valencia, Spain.

Chapter 8 provides an overall conclusion and future prospects.

Finally, this manuscript ends with a brief CV and a listing of references.

Chapter 2

RATT: RFID Assisted Tracking Tile.

This chapter presents RATT, a tracking system based on passive RFID technology in the high-frequency band. The RATT system is composed of electronic tiles, each of which has nine active RFID antennas attached; in addition, A RATT tile contains several overlapping passive coils, which improve the magnetic field characteristics. By using several tiles, a large surface can be built on where rodents can move freely, allowing identification and tracking of their movements. This system, can also be combined with a visual tracking system and recharge electrophysiology and optogenetics implants wirelessly.

2.1 Introduction

Mental diseases, such as schizophrenia and autism are characterized by severe social anomalies and have a substantial genetic heritability. However, the complexity of human genetics and clinical heterogeneity have interfered with the understanding of the neuroscientists of the neurobiological basis of socially-related disorders [25].

Experiments in neuroscience typically employ small animals, such as fish or rodents, in order to improve the understanding of the nervous system and its pathology [26]. Furthermore, experimentation with animals, or in vivo testing, involves the use of these model organisms as substitutes for humans [27], [28] (section 1.2). Indeed, carrying out these experiments in humans is contrary to bioethics. For this reason, a model organism is used to study specific biological phenomena that can be extrapolated to other species [29], [30].

In the case of neuroscience research, rats and mice are the most frequently used model organisms. This is because of their high rate of reproduction, their ease of handling and the great number of physiological similarities that they share with human beings. Therefore, the experimental conditions must be adapted to the size and characteristics of these animals [31].

Mice are a social animals engaging in high level of social interaction [27], [32]–[34]. Furthermore, genetically modified mice are now commonly generated and used, making them a valuable tool to study the links between genes and behavior[25], [35], and thus to understand the neurobiological basis of social abnormalities in psychiatric disorders.

The predominant issue in the analysis of complex social behaviors is the reliable and objective investigation of specific behavioral parameters, which might last for extended periods. In such investigations, a manual or semi-automatic counting of the number of social interactions is still the main experimental constraint [36], [37]. Indeed, manual counting of social interaction suffers from several limitations, e.g. low reproducibility and lack of standardization.

Moreover, it is extremely challenging and time-consuming to visually follow subtle and composite social behaviors, especially when multiple animals are

involved. As a consequence, more detailed long-lasting and large-scale studies are not affordable. Hence, unless technological innovation is introduced in order to facilitate analysis, our ability to understand complex social behaviors in mice will remain limited, which in turn will limit the translational advances in psychiatric medicine.

2.1.1 Behavior Experiments

The increasing use of animal models in biomedical research has led to new demands for automated methods capable of testing complex behaviors [31]. Accurately tracking the positions of animals in a given space is fundamental to recording several social behaviors in rodents [38]. Some systems have been developed to robustly track large groups of small laboratory animals, see e.g. [39]–[43]. However, most of these systems are limited to tracking a center of mass by using video cameras. In the main, these methods rely on simple image processing (e.g., background subtraction) in order to extract the contour of a particular body, before computing a medial axis transform.

A large number of studies rely on animals moving freely within a controlled environment [26], [31], [44]; for instance, those related to behavioral or memory research [26], [41], [44], [45]. The configuration of the environment may vary according to the needs of the experiment [42], [46]–[48]. Also, they may contain devices that react to the presence or the actions of the subjects.

A significant drawback of such methods is their inability to discriminate between the front and rear ends of the bodies of the animals, forcing researchers to rely on simple heuristics instead [49] (e.g., by computing the direction of movement and assuming that the animal moves forward). Also, background subtraction tends to be sensitive to changes in illumination and often yields inaccurate estimates. In the context of biomedical research, these inaccuracies need to be detected either automatically [49] or manually in order to exclude the corresponding frames from the further behavioral analysis. A position estimation may lead to significant biases in behavioral analysis, especially if these system failures tend to co-occur more frequently with specific behaviors (e.g., for those behaviors that yield significant occlusion among subjects, such as social interactions in rodents)[50]. Overall, existing approaches are not robust enough to

allow for the thorough behavioral analysis needed for modern biomedical research applications.

Knowing the individual positions of animals within the space is essential. However, it is difficult for current visual tracking systems to locate the animals when they are in tight groups or when they are inside a burrow.

Hence, there is an increasing interest in the development of systems for developing automated behavior studies. Aiming at the abovementioned issues, this work proposes a novel system, which is capable of tracking several mice simultaneously. Plus, it provides a wireless recharging area for electrophysiology active implants, which can enhance the current experimentation methodologies.

2.1.2 Computer Vision Tracking Systems

Computer vision systems (see Figure 2.1) are based on recordings made by digital cameras and their processing, both in real time and a posteriori, by specialized algorithms that allow the differentiation of elements within the images [39], [45]. This type of technology has recently achieved widespread use because existing computer systems have the computing power necessary to perform this type of operation, something that was challenging to achieve years ago. One of the

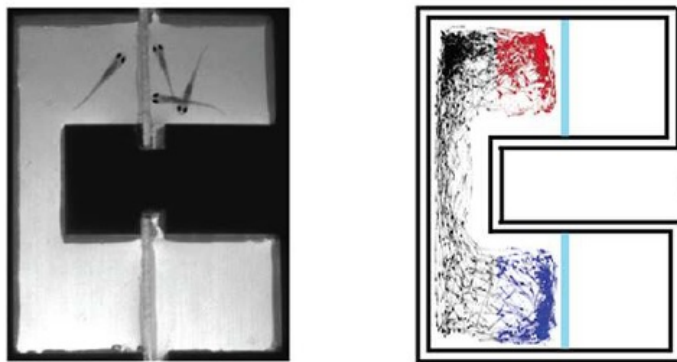


Figure 2.1. Zebrafish camera tracking. [51]

advantages offered by this type of system is the ease of implementation, as all that

is required is enough cameras within the space to be controlled and a sufficiently powerful computer system to analyze the images coming from them. Another notable advantage is the high-resolution, both spatial and temporal, that they are able to obtain, which is limited only by the pixel density of the cameras and the frame per second rate.

The main disadvantage of camera tracking is its inability to track animals that are in areas which are covered or are out of their reach. Another disadvantage is the computing power required for the processing of the images. However, camera tracking methods could be inadequate if real-time tracking is needed, while a large number of animals are tracked in a large area. The final disadvantage is the limitations of computer vision algorithms which, although they are able to locate individual animals with ease, they have difficulty when it comes to distinguishing them. This means that they are able to give detailed information about where the animals are at any time but, they are unable to locate one specific individual. This problem can be aggravated in situations in which several subjects cluster at the same point.

Hence, in this type of problem, there are commonly two main hurdles to be overcome: the tracking of multiple animals over a long period of time and the automatic behavior recording.

The first is frequently overcome using a tracking solution based on particle filter modeling, extended to multiple targets. An example of this type is the algorithm that was applied to mice by exploiting their slowly changing contour by recording the cage through a side view [52], [53]. A particle filtering approach, with a variation on the observation model in order to track multiple mice from above, was adopted by Pistori et al. [54]. However, the system was evaluated using white mice on a black background, and with a coarse position estimate (see Figure 2.2). Hence, these systems do not work sufficiently well in enriched environments in which the study of rodent behavior occurs.

The second hurdle is the automatic analysis of mouse behavior. In the computer vision literature, many methods are proposed for the recognition of human action/activity. In this context, several general purpose space-time descriptions were introduced for activity recognition tasks, such as HOG3D [55], eSURF [56] and hierarchical space-time features [57], to name a few. Some of

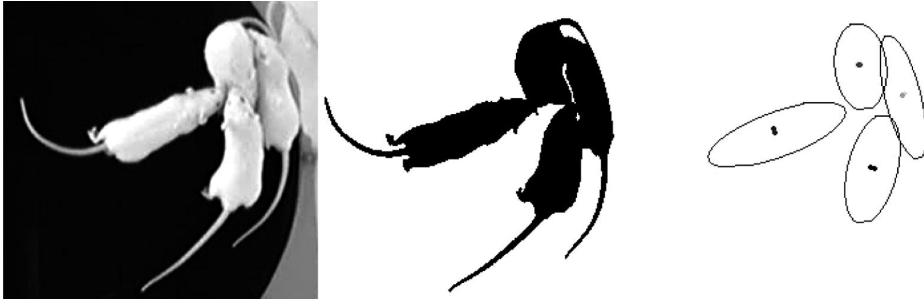


Figure 2.2. Particle filtering approach example. Original image (left), segmented image using background subtraction (center) and the results of the k-means clustering procedure with results shown in ellipses (right). [54]

these descriptors were applied as the initial coding step for the analysis of the behavior of a single mouse in the home cages [58], [59] followed by a classification stage or for more complex behaviors [60]. However, they were limited to the processing of a single mouse, which makes them inapplicable for the analysis of multifaceted social disorders [31].









Behaviour	Priority	Type	Behaviour	Priority	Type
 Nose2Body	1	Social	 Following	5	Social
 Nose2Nose	2	Social	 StandTogether	6	Undefined
 Nose2Genitals	3	Social	 StandAlone	7	Non-Social
 Above	4	Social	 WalkAlone	8	Non-Social

Figure 2.3. Behavior priorities employed to combine all pairwise classifiers in order to describe the behavior of a mouse with a single class [25]

While current visual tracking systems are useful, having an automatic tracking system [41], [51], [61], which facilitates data collection by filtering events of interest to the researcher, would provide greater accuracy. The *RFID Assisted Tracking Tile (RATT)* system we present in this work allows tracking of a large number of subjects, enabling easy identification of each one, at each moment.

Moreover, it overcomes the drawback of losing the positions of the animals when they are in places where the camera cannot satisfactorily record. Thus, combining current visual tracking systems with the RATT system will improve the quality of the results of behavior research studies.

2.1.3 Radio Frequency Tracking Systems

In this type of system, the subjects to be detected carry external or surgical implants. These implants are signal transmitters in different radio-frequency bands, each one emitting a unique serial code. At the same time, the experimental space contains several strategically located receptors capable of receiving these signals. By analyzing parameters, such as the difference in the strength of the signal received by each receiver or the different arrival times of the signals, it is possible to calculate the position of each of the transmitters, using the serial number to differentiate the subjects [61]–[70]. The technology used in these sorts of system is known as RFID, and it will be explained in detail at subsection 2.1.5.

2.1.4 Mixed Tracking Systems

Although each of the methods on its own suffers limitations, it is possible to combine the technologies in order to obtain a transmission system that offers the benefits of both technologies. In this way, visual tracking would be used to obtain high-resolution tracking information, while a parallel radio-frequency device would provide the identification of each animal. Both technologies combined would allow a high-resolution tracking system in an enriched environment [46], [71], [72].

A further advantage of combining the technologies is the improvement in the reliability of the system. For example, it is still possible to locate animals that are out of visual range, such as those inside a burrow, using radio-frequency devices. However, a failure of the RFID tracking, due to external electromagnetic interferences (e.g. phone signals), could easily be corrected by the continuity offered by the camera tracking.

2.1.5 Radio Frequency Identification (RFID)

The optimal solution would be the storage of data on a silicon chip. The most common form of electronic data transport device in use in everyday life is the chip card based on a contact field (e.g. SIM cards, credit cards, RFID Tags). However, the mechanical contact used in the chip card is not practical. A non-contact data transfer between the data transport device and its reader is much more flexible. The power required to operate the chip would also be transferred from the reader using contactless technology. Hence, because of the procedures used for the transfer of energy and data, the non-contact identification systems are called Radio Frequency IDentification (RFID) systems.

In RFID systems, data is stored on an electronic data-carrying device - the transponder (a.k.a. Tag). Power is supplied to both the data-carrying device (Tag) and to the reader using magnetic or electromagnetic fields by means of inductive coupling. Because of the advantages RFID systems have over other identification systems, RFID is the ideal technology for developing a computer-vision-free system to track rodents.

In RFID systems data is stored on an electronic data-carrying device - the transponder. The power supply to the data-carrying device (Tag) and the reader are achieved using magnetic or electromagnetic fields by means of inductive coupling. The underlying technical procedure is drawn from the fields of radio and radar engineering. Due to the advantages of RFID systems compared with other identification systems, RFID is the ideal technology for developing a computer-vision-free system to track rodents [73].

2.1.5.1 Inductive Coupling

Inductive coupling comprises an electronic data transport device (a Tag) and a large coil that functions as an antenna (see Figure 2.4). Inductively coupled transponders almost always operate passively. This means that all the energy necessary for the operation of the microchip must be provided by the reader (Antenna). For this purpose, the antenna coil generates a strong high-frequency electromagnetic field that penetrates the cross-section of the coil area. Due to the wavelength of the frequency range used (13.56 MHz: 22.1 m), the theoretical

distance is several times greater than the distance between the antenna and the transponder. Hence, the electromagnetic field can be treated as a simple alternating magnetic field concerning the distance between the transponder and the antenna. [73].

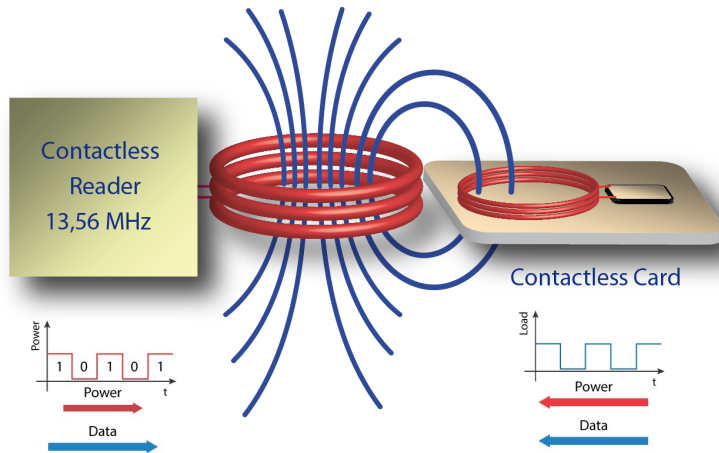


Figure 2.4. Inductive coupled RFID-System

A small part of the emitted magnetic field penetrates the antenna coil of the RFID tag, which is at some distance from the reader coil. By induction, a voltage is generated in the antenna coil of the transponder. This voltage is rectified and serves as a power source for the data transport device (the microchip). A parallel capacitor is connected with the antenna coil of the reader, whose capacitance is selected to be combined with the inductance of the antenna coil to form a parallel resonant circuit, with a resonance frequency that corresponds to the frequency of transmission of the antenna of the reader. High currents are generated in the resonance reader antenna coil, which can be used to generate the field strengths required for the operation of the remote transponder (the Tag).

2.1.5.2 Differentiation Features of RFID Systems

The power supply to the transponder (Tag) is a critical feature of RFID systems. Passive transponders do not have their own battery; hence, all of the power required for the activation of a passive transponder must be provided from the (electrical/magnetic) field of the reader. However, active transponders incorporate a battery, which supplies all or part of the power for the operation of a microchip [73].

The operating frequency is a critical characteristic of RFID systems and it modifies the resulting range of the system. The operating frequency of an RFID system is the frequency at which the reader transmits (see Table 2.1). In most cases the transmission frequency of the transponder is the same as the transmission frequency of the reader (load modulation, backscatter). However, the “transmitting power” of the transponders may be set several powers of ten lower than that of the reader [73].

The different transmission frequencies are classified into the three basic ranges: Low Frequency (30-300 kHz) (LF); High Frequency/Radio Frequency (RF) (3-30 MHz) (HF); and Ultra High Frequency (300 MHz-3 GHz) (UHF). (see Table 2.1)

Band	Regulations	Range	Data speed	Remarks
120-150 kHz (LF)	Unregulated	10 cm	Low	Animal identification, factory data collection
13.56 MHz (HF)	ISM bandworldwide	10 cm - 1 m	Low to moderate	Smart cards (ISO/IEC 15693, ISO/IEC 14443 A, B).
433 MHz (UHF)	Short range devices	1 - 100 m	Moderate	Defense applications, with active tags
865-868 MHz (Europe)	ISM band	1 - 12 m	Moderate to high	EAN, various standards; used by railroads
2450-5800 MHz (microwave)	ISM band	1 - 2 m	High	802.11 WLAN, Bluetooth standards
3.1-10 GHz (microwave)	Ultra wide band	Up to 200 m	High	Requires semi-active or active tags

Table 2.1. RFID Bands, regulations and specifications

2.1.5.3 Tag Construction Formats

There is a considerable variety of tag construction formats, but those most relevant to the present work are Coin Tags and Glass Housing Tags.

- **Disks and Coins:** The most common construction format is commonly known as disk (or coin), a transponder in a circular Acrylonitrile butadiene styrene (ABS) injection molded casing, with diameters ranging from a few millimeters to 10 cm (Figure 2.5). There is typically a hole for a fastening screw in the center. As an alternative to ABS injection molding, polystyrol, or epoxy resin, may be used to achieve a wider operating temperature range.



Figure 2.5. RF-HDT-DVBB-N2 Texas Instruments Coin Tag

- **Glass Housing:** Glass transponders are tags that can be injected under the skin of an animal for identification purposes. Glass tubes of lengths of just 12-32 mm contain microchips mounted upon a carrier (Printed circuit board (PCB)) and a chip capacitor to smooth the supply current obtained. The transponder coil incorporates wire of just 0.03 mm thickness, which is wound onto a ferrite core. The internal components are embedded in a soft adhesive in order to achieve mechanical stability (see Figure 2.6).

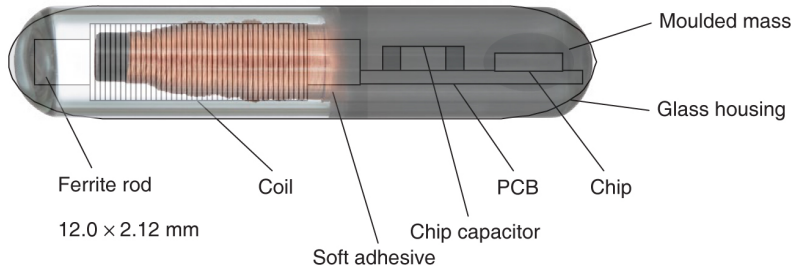


Figure 2.6. Mechanical layout of a glass transponder

2.1.6 RATT Features

Data from basic and pre-clinical in vitro electrophysiology experiments have helped to develop treatments for disorders ranging from schizophrenia to Parkinson’s disease, epilepsy and depression [74]. These experiments on animals that are awake and on their behavior usually use cables to transfer energy and neuronal data from instruments connected to the body of the animals (see Figure 2.7). As a result, the recording area is restricted to relatively small spaces and enriched environments, such as tunnels or burrows, are limited. [29].

Environmental enrichment has received strong support as a means to improve the quality of the data generated by these experiments [30], and there is a large body of research indicating that it leads to greater brain learning and plasticity [26], [31], [41], [42], [45], [46], [51]. In addition, cables prohibit experiments involving the registration of more than one animal at a time in the same arena.

In an attempt to overcome these issues, several battery-powered neural record systems have been developed [75]–[79]. However, these configurations are not suitable for longitudinal studies due to the limited life of the batteries and to the necessary handling of the animal subjects in order to replace or recharge the batteries. Batteries also add considerable weight to the animal, which can bias the behavior of the subjects when creating an impoverished environment.

All the constraints mentioned above make the current tracking systems inefficient, and they constrain the creation of enriched environments for animal behavior experimentation. For these reasons, RATT is presented in order to overcome these limitations and to pave the way to further behavioral experiments.

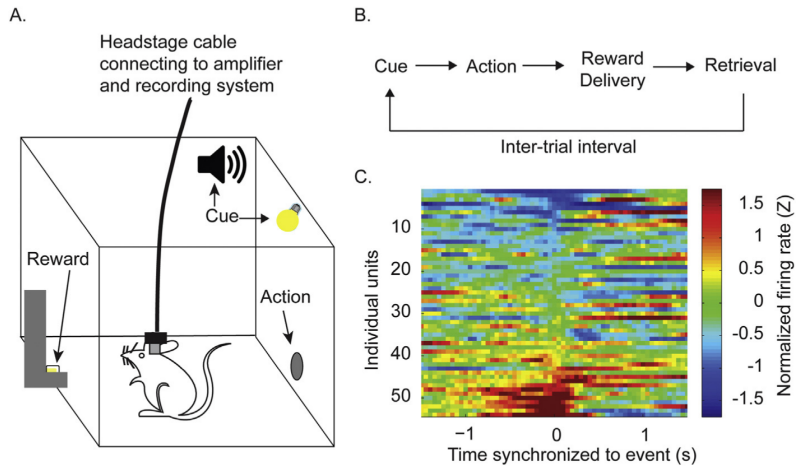


Figure 2.7. (A) Single unit electrophysiology performed with awake-behaving adolescent and adult rats during reward-related behavior. Rats implanted with microwire arrays and placed into an operant chamber equipped with a nose poke port, food trough that delivered sugar pellet rewards, and a cue light used to signal reward availability. (B) The instrumental tasks (C) This heat plot shows sample data demonstrating the typical response of individual neurons to a reward-associated event. [80]

The most significant advantage offered by the RATT system is the possibility of tracking individual animals, even in situations where they are in enclosed spaces, such as burrows. Another advantage is the immediate identification of each of the animals, information which is derived from the same signal that is used to track them. The RATT system requires the implantation of a biocompatible glass tag in each of the individuals.

The achievable spatial resolution (i.e. the minimum position change that the RATT system is capable of detecting) is limited as the parameters that are used to track the animal are based on a Received Signal Strength Indicator (RSSI). This signal has small variations, but, this small variations are enough for triangulate positions with the sufficient resolution to track small rodents (especially rats).

2.2 Materials and Methods

2.2.1 RATT System Concept

A RATT Tile is composed of more than 1200 elements (Integrated Circuits, discrete semiconductors, connectors, cables, etc) but it can be shown as a general block diagram, which is shown in Figure 2.8). The RATT system works in an High

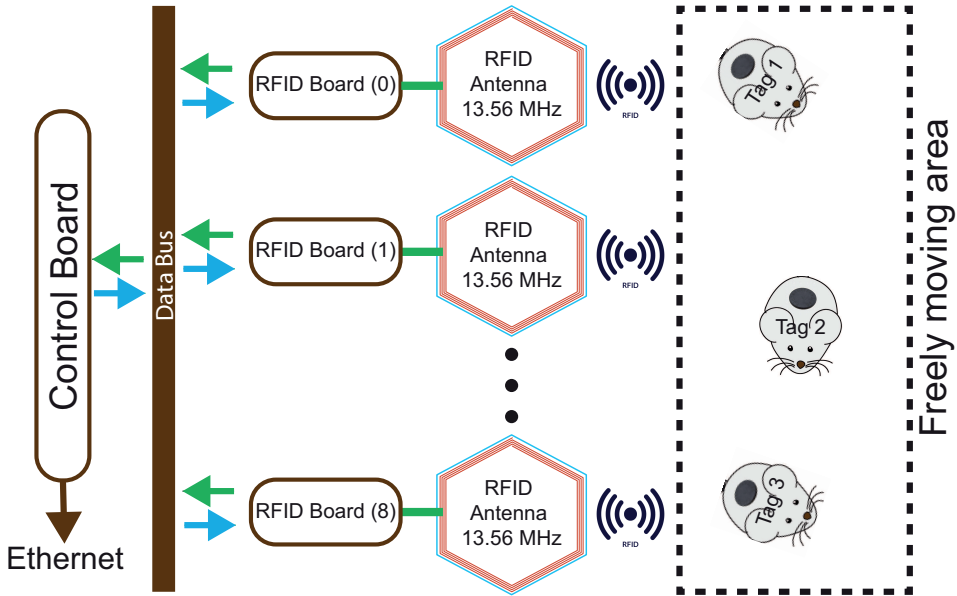


Figure 2.8. RATT simplified diagram block.

A RATT is composed of all the macro elements that are shown in this figure. The main control board is capable of managing up to 9 RF boards. Each RF board sends signals through one antenna in order to communicate with the Tags.

Frequency/RF (3-30 MHz) (HF) range based on the characteristics of (Table 2.1. Although the possibility of reducing the number of readers through the use of Ultra High Frequency (300 MHz-3 GHz) (UHF) was evaluated. Working on this frequency has two deficiencies: firstly, given that the tag will be implanted subcutaneously, the attenuation caused by the skin in UHF band could be significant, thus hindering its use. Secondly, having few antennas implies that

each one has to locate a greater number of animals. This, coupled with the fact that the available bandwidth, although high in relation to other RFID technologies, is limited, could cause problems in areas where there is a high density of subjects. Because of these two drawbacks, and due to the greater ease of obtaining resolutions of centimeters in a high-density antenna environment, the HF technology of 13.56 MHz was finally chosen. s that each one of them has to locate a greater number of animals.

The control of the RATT tile is centralized on the **Control board**. It has all the necessary communication buses and connectors and also has room for the microprocessor. Through the communication bus (brown line) it sends orders and receives data from the slave boards, which are called **RF boards**. In the whole system, there is a total of nine slave boards, each of which manages one antenna per board.

Each antenna can communicate with an unlimited number of RFID Tags, which are implanted in the rodents.

2.2.2 Software

- **MATLAB** (The MathWorks Inc. Massachusetts, USA) is a mathematical software tool that offers an Integrated Development Environment (IDE) with its own programming language (M language). Among its features are: the manipulation of matrices, the representation of data and functions, the implementation of algorithms, the creation of user interfaces (Graphical User Interface (GUI)) and communication with other hardware devices. The data acquisition from the RATT tile is performed through MATLAB. In addition, these data are represented using a GUI designed for this purpose (subsection 2.3.7).
- **SmithChart** (Bern University, Bern, Switzerland) is a simulation software to simulate the Smith chart (for more details read subsection 2.2.6). It helps visually to understand the designing and the tuning process of the RFID antennas (subsection 2.3.4).
- **CST MICROWAVE STUDIO (CST MWS)** (Dassault Systèmes, France, EU) specializes in providing an accurate 3D electromagnetic

simulation of HF problems. The software offers users shorter development cycles through virtual prototyping before physical trials. It was worth it to simulate the magnetic field that the RFID antennas provide before manufacturing them (subsection 2.3.5).

- **Siemens NX** (Siemens AG, Germany, EU) software is a flexible and powerful integrated solution that helps to develop products. NX is a Computer-Aided Design (CAD) software capable of 3D design, 3D simulation, and manufacturing solutions. In order to design, test and prepare to manufacture the supporting structure, this software was used (subsection 2.3.6).
- **Eagle PCB** (Autodesk Inc., California, USA) is software for diagrams and PCB design for electronic projects. It was used to design the electronic schemes as well as to design the PCB routing (subsection 2.3.2).
- **Bonsai** is a visual programming language that allows a modular, high-performance, open-source visual programming framework for the acquisition and online processing of data streams. It permits real-time data acquisition and processing among several interfaces [44], [81], [82]. This software has been used to develop a Camera tracking algorithm in order to have feedback from the tracking positions given by the RATT system (subsection 2.3.8).

2.2.3 *System Core: LPC4088-ARM cortex*

In order to control the entire system, an LPC4088 board(see Figure 2.9) from Embedded artists (Davidshallsgatan, Malmö, Sweden) was used. It has an Advanced Reduced Instruction Set Computing (RISC) Machine (ARM) Cortex-M4F at a frequency of 120MHz, with 96KB of RAM and 512KB of FLASH integrated into the chip. It also has Serial Peripheral Interface (SPI), Universal Asynchronous Receiver-Transmitter (UART) and Inter-Integrated Circuit (I²C) buses. This board contains Universal Serial Bus (USB) and Ethernet ports, providing the necessary entire physical layer. The power is limited to 5.5 V, and the output regulator is shared, allowing external devices to be connected (see Table 2.2).

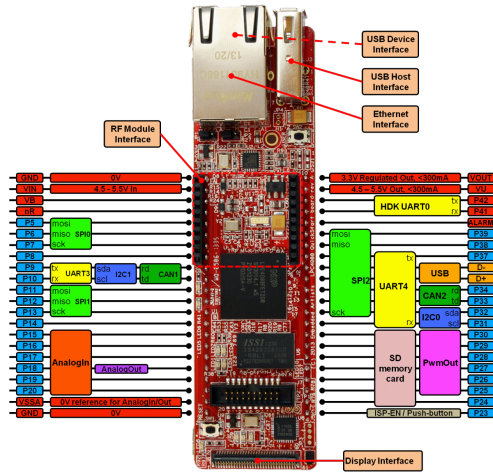


Figure 2.9. ARM Cortex M4F LPC4088 (Extracted from [83])

Characteristic	
Processor	Cortex-M4 LPC4088 (120 MHz)
Program Flash	8 MB QSPI + 512 KB on-chip
Data Memory	32 MB SDRAM 96 KB on-chip SRAM 4 KB on-chip E2PROM
Clock Crystals	12.000 MHz main 32.768 kHz RTC crystals
Interfaces / Connectors	2x22 pin edge pins 10/100Mbps Ethernet (RJ45) USB-A (USB Host interface) USB-micro B (USB Device interface) USB-micro B (mbed HDG debug interface)
Dimensions	101 x 28 mm (104 x 28 mm with connectors)
Power	4.5 - 5.5V
Other	CMSIS-DAP Interface On-board Supported by the mbed SDK and online tools Industrial temperature specified (-40 to +85°C)

Table 2.2. LPC4088 board features

2.2.4 RFID Tags

RF-HDT-DVBB tags from Texas Instruments were used for development and testing. These transponders are compatible with the International Organization for Standardization (ISO)/International Electrotechnical Commission (IEC) 15693 standard requiring a field of 112dBA/m for activation and are encapsulated in the form of a 3 cm diameter coin. Because of this, they cannot be located inside the bodies of the animals. However, this problem was solved with standard units enclosed in biocompatible glass as shown in Figure 2.10.



Figure 2.10. Biocompatible Crystal RFID Tags

2.2.5 ISO/IEC 15693

In the design of the prototype, as well as the already existing commercial tags, an existing protocol was used. Among the available protocols for 13.56 MHz, there are two that are commonly used. The “proximity cards”, which have a higher transmission speed and a limited range and the “neighborhood cards”, which have a greater range and lower bandwidth. For this project a protocol of “neighborhood cards” was chosen, which corresponds to the ISO/IEC 15693. The maximum theoretical scope of this protocol is 1.5 meters and the maximum transmission speed is 26.48 Kb/s. Almost all of the chips that work with this technology offer a measure of RSSI that can be used to measure the distance between tags and readers.

2.2.6 Smith Chart

The Smith table, invented by Phillip H. Smith (1905-1987), [84] is a graphic aid or nomogram, designed for electrical and electronic engineers, who specialize in radio frequency (RF) engineering, to help solve problems with lines of transmission and matching circuits. The Smith diagram can be used to simultaneously display

multiple parameters, including impedances, admittances, reflection coefficients, among others [85]. The Smith table is most often used in or within the region of the unitary radius.

While the use of physical Smith Chart tables to solve the complex mathematics involved in comparing problems has mainly been replaced by software-based methods, Smith's screen remains the preferred method of showing how RF parameters behave in one or more frequencies, an alternative to using tabular information. Therefore, most RF circuit analysis software includes a Smith chart option for displaying results and all, except the simplest impedance measuring instruments, can show the results measured on a Smith chart screen.

2.2.7 Connectors

Samtec (Santa Clara, CA, USA) Connectors TFM-115-01-L-D-WT were chosen to interconnect the PCB boards. This rugged Tiger Eye terminal strip features a multi-finger, copper contact system designed for high reliability and high cycle applications with surface mount or through-hole tails. Vertical or right-angle orientations for parallel, perpendicular and coplanar mating increase design flexibility, along with optional alignment pin, locking clip, dual screw down or weld tab for more rugged applications.

2.2.8 The TRF7960A

The TRF7960A is an integrated Analog Front End (AFE) and a multiprotocol data framing device for a 13.56 MHz RFID reader/writer system compatible with ISO/IEC 14443 A and B, Sony FeliCa and ISO/IEC 15693. Built-in programming options make it suitable for a wide range of applications for proximity and proximity identification systems. The TRF7960A must be configured by selecting the desired protocol in the control registers. Moreover, SPI or parallel interface can be used for communication.

The TRF7960A device supports a wide supply voltage range of 2.7 V to 5.5 V and data communication levels from 1.8 V to 5.5 V for the MicroController Unit (MCU) I/O interface.

The transmitter has output power levels of 100 mW (+20 dBm) or 200 mW (+23 dBm) equivalent into a 50 Ω load when using a 5-V supply. This power level is insufficient for the antennas that are used in the RATT environment; hence an external Class E 4W amplifier was used. This amplifier was designed based on the *application note* [86] given by Texas Instruments (Dallas, Texas, USA). This amplifier is typically able to read a range of 47 cm (18.5 inches) using a credit card size tag.

2.2.9 UDP Communication

User Datagram Protocol (UDP) is a protocol of the level of transport based on the exchange of datagrams (Encapsulation of layer 4 or Transport of the Model OSI). It allows the sending of datagrams through the network without having previously established a connection, since the datagram itself incorporates enough addressing information in its header. However, it has no confirmation or flow control, so that packages can get ahead of each other; and it is not known if the packages has arrived correctly, since there is no confirmation of delivery or reception. Its main use is for protocols such as Dynamic Host Configuration Protocol (DHCP), Bootstrap Protocol (BOOTP) and Domain Name System (DNS).

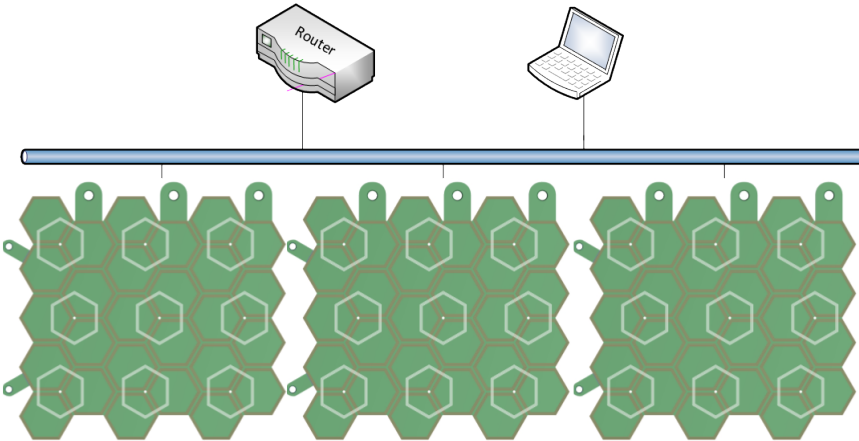


Figure 2.11. RATT tiles interconnection. The UDP interconnection between different tiles, a computer and a router are shown here.

Each electronic tile uses the Ethernet (Figure 2.11) connection to connect to a control computer; this receives the information from the different tiles to perform the necessary triangulation calculations and provides control and synchronization functions.

2.3 Results

In order to investigate animals under controlled conditions, an automated experimentation environment was created as shown in Figure 2.12. This modular environment recreates the natural conditions of the animals in order to collect data that are impossible to observe in currently closed environments [70]. One RATT environment is formed using at least one RATT tile, which makes the experimentation environment modular and extensible.

2.3.1 *RATT Tile Virtual Concept*

A virtual RATT tile environment was designed to give a first perspective of what is the the aim of the project. This is to create a space where small animals are able to move freely and behave as they usually would do in nature, while at the same time are being tracked. This environment could be enriched with sand, vegetation or other elements. In Figure 2.12 it is possible to see a virtual reconstruction of a RATT environment, formed by four RATT tiles, which support an arena where the animals are moving.

The RATT tiles have several objectives and requirements. The RATT tile by itself has to be capable of tracking several rodents, of providing energy to electrophysiology implants and of being easily interconnectable with more RATT tiles. In addition, the electronics inherent in the project cannot make noise or dissipate a lot of heat. Hence, low consumption electronics were used in order to avoid the need for cooling fans.

As was mentioned in subsection 2.2.1, a RATT tile is composed of several components. However, there are macro components such as the Control Board and the RF board that are interconnected by communication buses, clock signals, etc. The detailed interconnection among these components is shown in Figure 2.13. For instance, the system has a parallel 8 bit bus to communicate

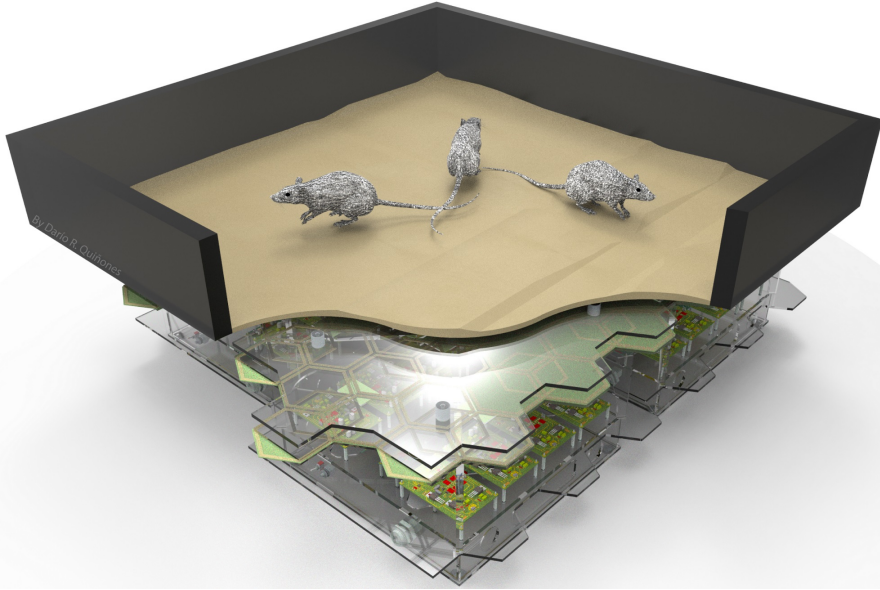


Figure 2.12. Three-Dimensional (3D) rendering of the RATT environment, where beneath the sandbox are four RATT tiles.

with each of the TRFs located on each of the RF boards. In addition, the system has an I²C bus to control a digital potentiometer on each RF board, which gives the option of increasing or decreasing the emission power.

2.3.2 Control Board

The Control board was designed in order to allocate the LPC4088, connectors and communication buses as shown in Figure 2.14. It functions in the system as the “motherboard” for the other boards. The Control board has 5 V power supply, which provides 3.5 A, for the electronic components in the Control board and RF board. The Control board has an I²C bus, integrated from the LPC4088 board to the Samtec connectors, which allows communication with the digital potentiometers, which are in the RF board. Communication with the nine RF boards is made through a parallel data bus with chip select control lines, so that the RFID transceivers on each board can be controlled independently.

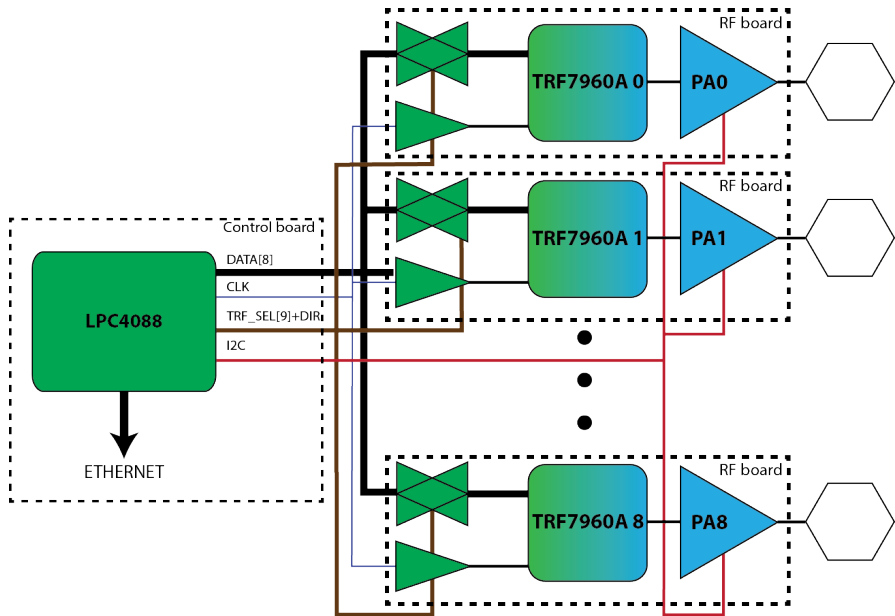


Figure 2.13. RATT detailed diagram block. Each RATT tile consists of one main Control board and nine RF Boards. The Control board is the core of the whole system, and it has the function of controlling the nine Power amplifier (PA), which are in the RF boards, and provides the UDP communication protocol.

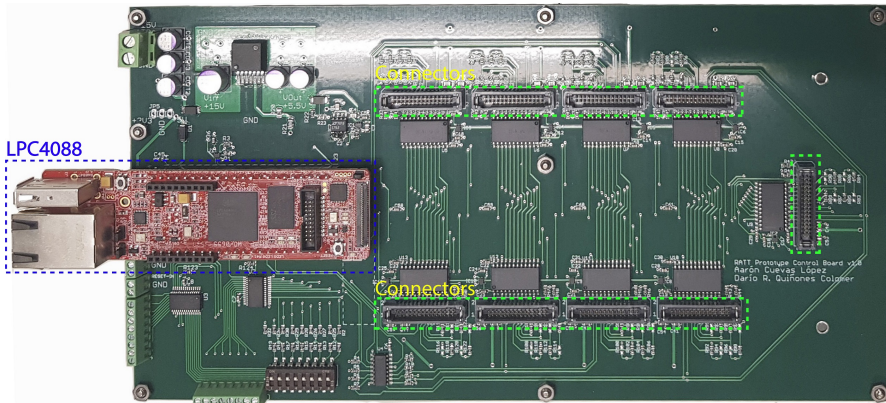


Figure 2.14. Control Board. The manufactured and assembled Control board is shown in the image, where it is possible to observe the LPC4088 and the nine Samtec connectors.

Additionally, an I²C bus allows control of auxiliary features, such as general purpose digital outputs and emission power control (see Figure 2.13).

In order to attach nine RF Boards to the Control Board, nine Samtec connectors (subsection 2.2.7) with one plug position were used. This ensures that the RF Boards are connected properly through the appropriate cables. Moreover, to prevent malfunction, a power indicator line was created. This power indicator line turns off all of the systems in case the external power supply is disconnected, thus protecting the LPC4088 and the computer.

2.3.3 RF Board

One RATT Tile is composed of nine RF boards in order to follow a modular structure. This modular idea of design was chosen based on different points. First of all, to manufacture several PCBs of a small size is cheaper than to manufacture one large PCB with all the RFID amplifiers and transceivers. Secondly, in the event of damage, repairing the system is easier; e.g. if one amplifier is damaged, it can be fixed by replacing the small RF board. Finally, this modular design facilitates the design of a compact structure. The RF boards (Figure 2.15) feature a digitally controlled RFID transceiver and a radio-frequency power amplifier. This transceiver is a TRF7960A (Multi-Protocol Fully Integrated 13.56-MHz RFID Reader/Writer) from Texas Instruments (subsection 2.2.8). The power amplifier is based on that featured in an application note from the transceiver manufacturer. It is a 4W class E amplifier connected with impedance-matching circuits to a 50 Ω antenna.

2.3.4 RFID Antenna Design

Antennas are the most important part of the project. If the antennas are not properly tuned there is no possibility of tag detection. In order to calculate and optimize the design of the Antennas, a bibliographical review was conducted [73], [87]–[97].

First, to determine the radius of the antennas, it is known [88] that the optimum radius “ R ”, which minimizes the number of ampere-turns necessary, of a circular coil for a range “ d ” is $R = d\sqrt{2}$. For the purposes of this project,

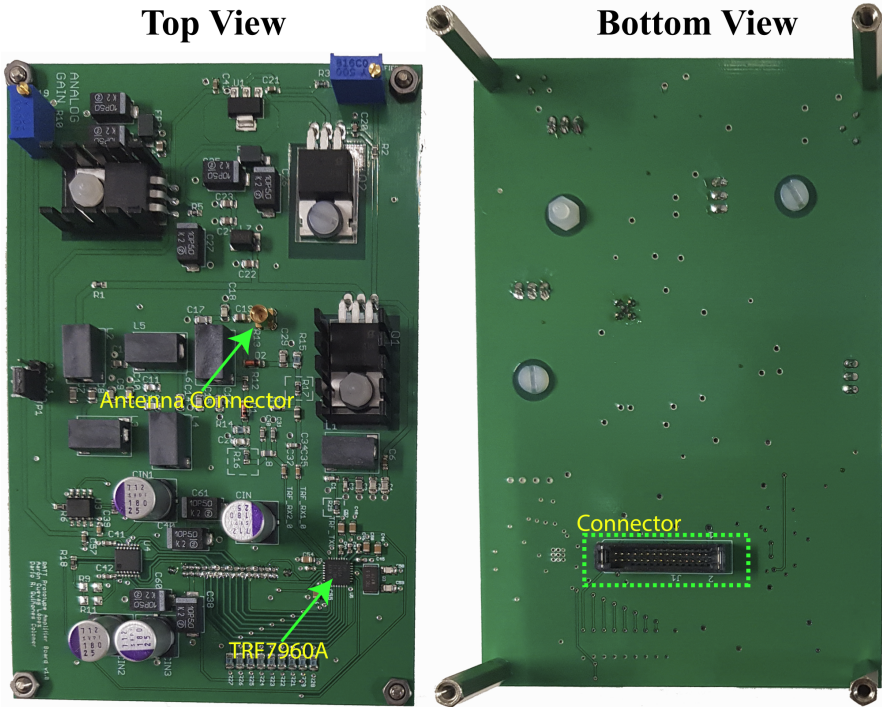


Figure 2.15. RF board. The manufactured and assembled RF board is shown in this image, where it is possible to observe the different components and the Samtec connector.

it was preferred to first obtain good functionality in terms of resolution, rather than to be able to read Tags at further distances. Hence, a radius of 5 cm was selected, which provides an optimal reading distance of 3.5 cm. This does not mean, however, that a greater distance cannot be achieved by increasing the transmitter power (or the number of turns). It was possible to calculate the total ampere-turns that were needed to feed a tag located coaxially to the antenna at a distance “ d ” using the formula [88]:

$$NI = \frac{2H(R^2 + d^2)^{\frac{3}{2}}}{R^2} \quad (2.1)$$

In the case of the transponders “ H ” is $112\text{db}\mu\text{A}/\text{m}$ or $0.398\text{A}/\text{m}$, with “ H ” being the necessary field for the Tags activation (subsection 2.2.4). Calculating the values at different distances (Figure 2.16), it is not hard to reach values up to ten

centimeters. The drawback is shown in Figure 2.17, which shows how the field

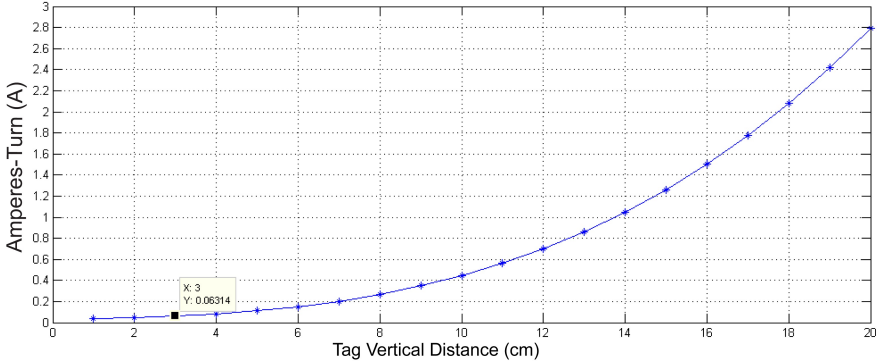


Figure 2.16. The Relationship between vertical distance and ampere-turns for a 5 cm radius antenna.

strength decays rapidly as the tag moves horizontally. This will force the use of high powers to achieve horizontal reach.

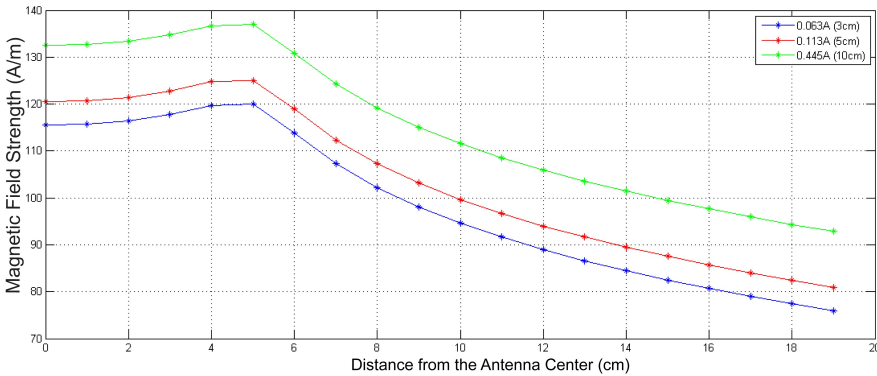


Figure 2.17. Magnetic field strength on the horizontal axis of a 5 cm antenna. The ampere-turns shown correspond to those that are necessary to feed the transponder used at vertical distances of 3, 5 and 10 cm, while the tag is coaxial to the antenna. Equation extracted from [89], [98].

Based on the abovementioned constraints, and following the work developed by Cuevas *et al.* [89] and simulated with the SmithChart simulator [99], the chosen characteristics for the antenna were: Hexagonal Shape, four turns and a quality factor $Q = 14$. The Hexagonally shaped antennas were developed for the RFID tags detection as shown in Figure 2.18. This shape was chosen to optimize the space between antennas and the magnetic field distribution.

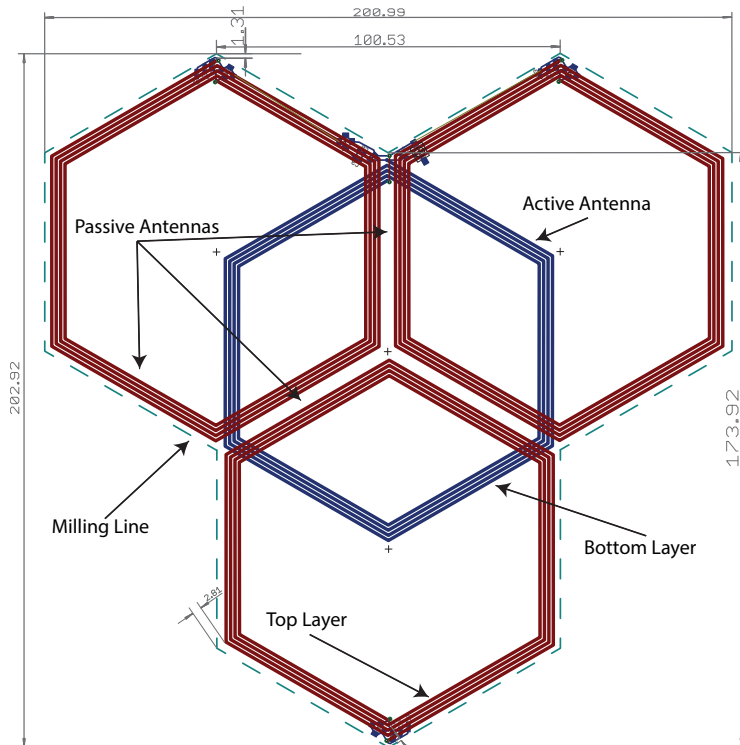


Figure 2.18. Antenna PCB footprint is shown where is possible to see both layers of the PCB. The top layer, where the passive antennas are, is shown in red, while in the bottom layer is the active antenna, shown in blue. The milling line, which represents the cutting marks, is shown with a dashed line.

In order to design the antennas, a PCBs footprint designer was needed. Utilizing Eagle PCB, the hexagonal shaped antennas were designed according to the theoretic specifications calculated before. As was mentioned, the antennas

were designed with a central active antenna and three surrounding passive antennas (see Figure 2.18).

2.3.5 RFID Antenna Simulation

In order to test the antennas before manufacture them, several simulations were performed. It is difficult to simulate an antenna and its magnetic field because of the enormous computational cost required. In the present work, these simulations were performed first in MATLAB and later in a specific antenna-simulation software (CST Microwave).

The first simulation was performed through MATLAB using a specific antenna toolbox. As a result, a non-detailed simulation was achieved, as shown in Figure 2.19. A second simulation was performed CST Microwave (see Figure 2.20)

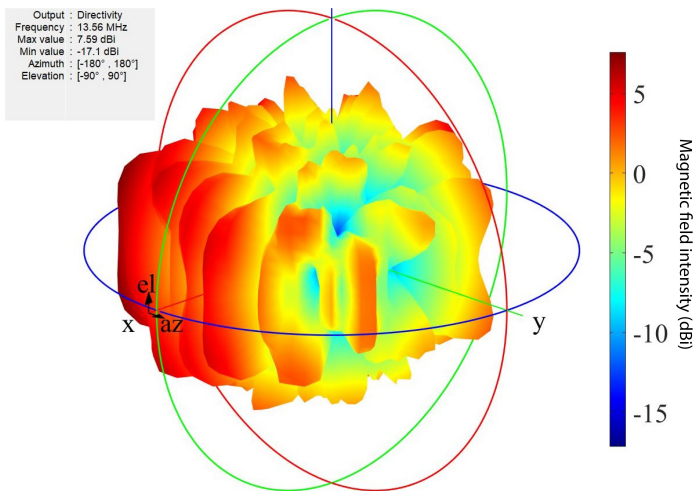


Figure 2.19. Antenna Simulation with Matlab. The figure shows the first Antenna simulation where it is possible to see that the magnetic field covers the whole area of the Antenna. This simulation was performed without taking into account the dielectric material, which conforms the PCB.

and this demonstrates that the magnetic field of the antenna covers its entire surface. However, this magnetic field is enough to cover a limited area only.

Following the above simulations, a third simulation, with the three passive

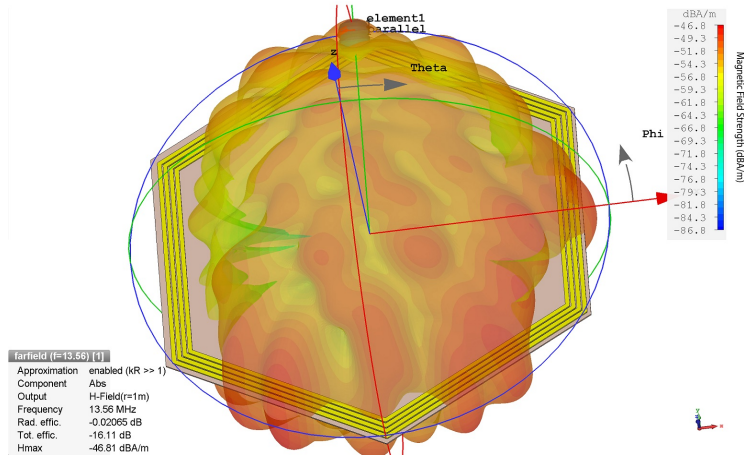


Figure 2.20. Antenna Simulation through CST. It is shown that the magnetic field covers all the antenna surface, however, this field is limited to the inner radius of the antenna.

antennas, as well as the active antenna, was done. It also has the dielectric (FR-4) that gives a more accurate simulation. As is possible to see in Figure 2.21, the passive antennas expand the magnetic field horizontally and permit to coverage of a larger surface with only one “*TriAntenna*”. Hence, the design that is shown in Figure 2.21 is the final design for the RATT tile. This allows to have magnetic field among *TriAntennas*, even when there is not an active antenna located beneath the tag.

2.3.6 Structure

In order to support all of the electronic parts that are needed for the RATT system, as well as to support the arena where the rodents will be placed, a methacrylate structure was designed (see Figure 2.22), manufactured and assembled (see Figure 2.23).

This structure was designed to attach the nine RFID boards and the Control board properly. The RF boards are positioned on a second level in the structure

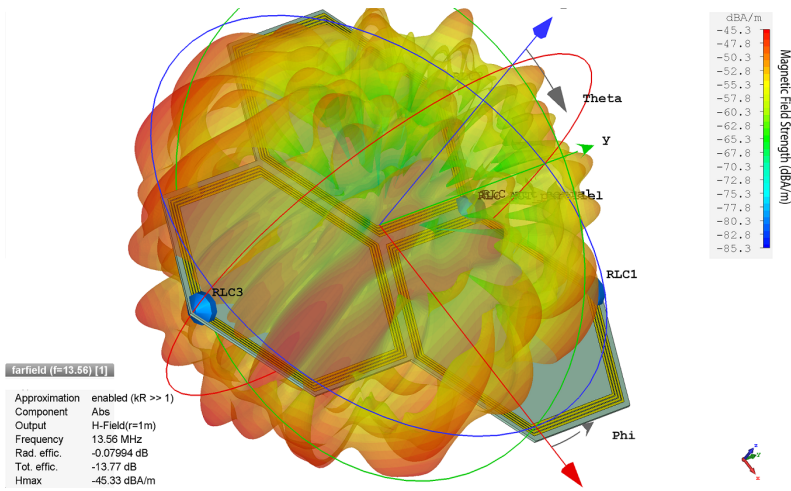


Figure 2.21. Antenna Simulation with passive coils through CST. This simulation shows that it is possible to expand the magnetic field by adding three tuned passive antennas.

and spaced 15 cm from the RFID antennas. This spacing was defined in order to avoid interferences between the antennas and the RF board. The Control board is attached to the lower level of the structure where all of the connectors and switches are located. In this lower level there is one Ethernet connector, one power stitch, one reset button and one DC plug-in. (see Figure 2.22).

The structure which is shown in Figure 2.23 was designed in order to facilitate the boards and antennas holding. However, the purpose of the structure is not simply to hold the different components. It also has to support at least 10 kg of weight because the sandbox, animals and burrows among others will be placed on the structure. For these reasons, two additional arcs were added between the antenna’s floor and the RF board’s floor. In addition, several reinforcements were added to specific points of the structure.

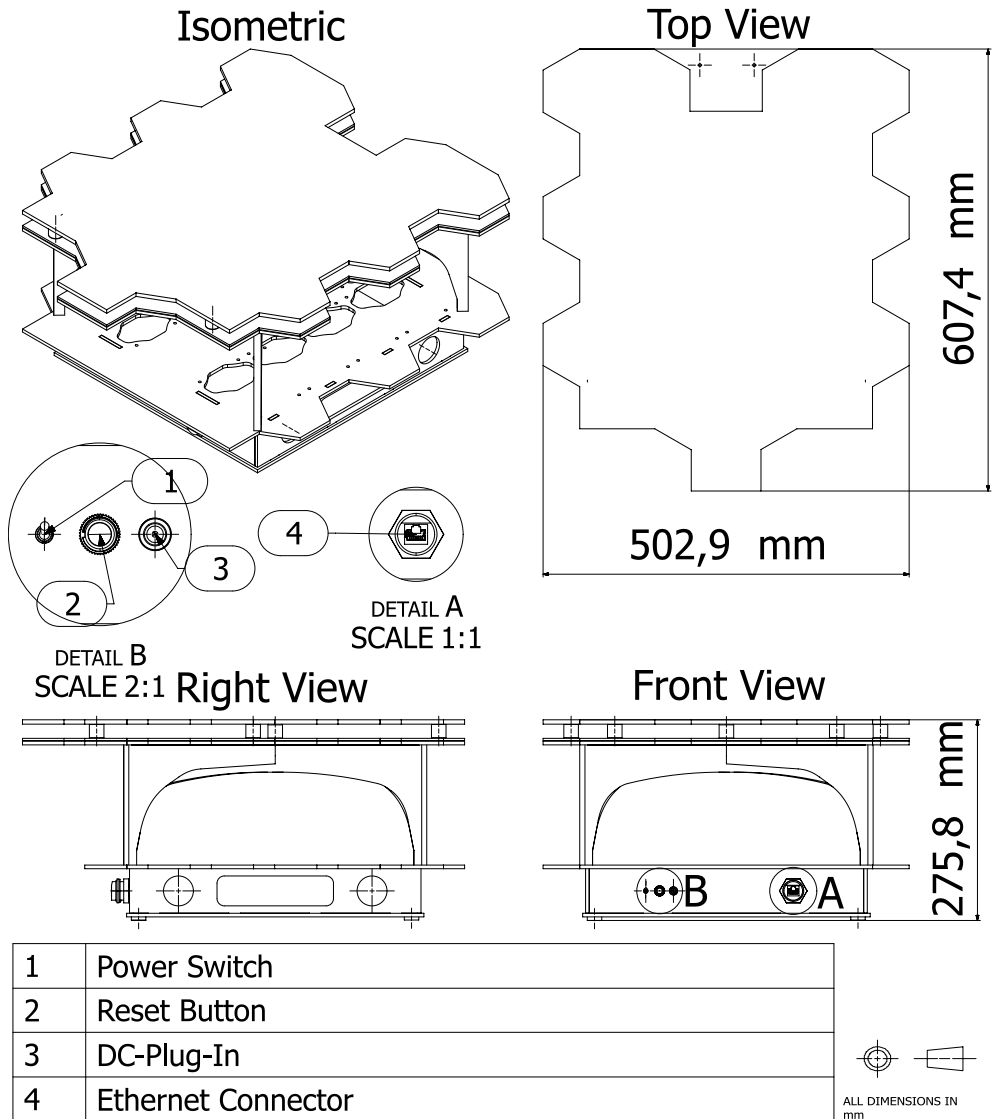


Figure 2.22. Two-Dimensional (2D) CAD of the structure. The dimensions of the structure are indicated on the figure. Detail A and B show the different connectors and switches that the structure has.

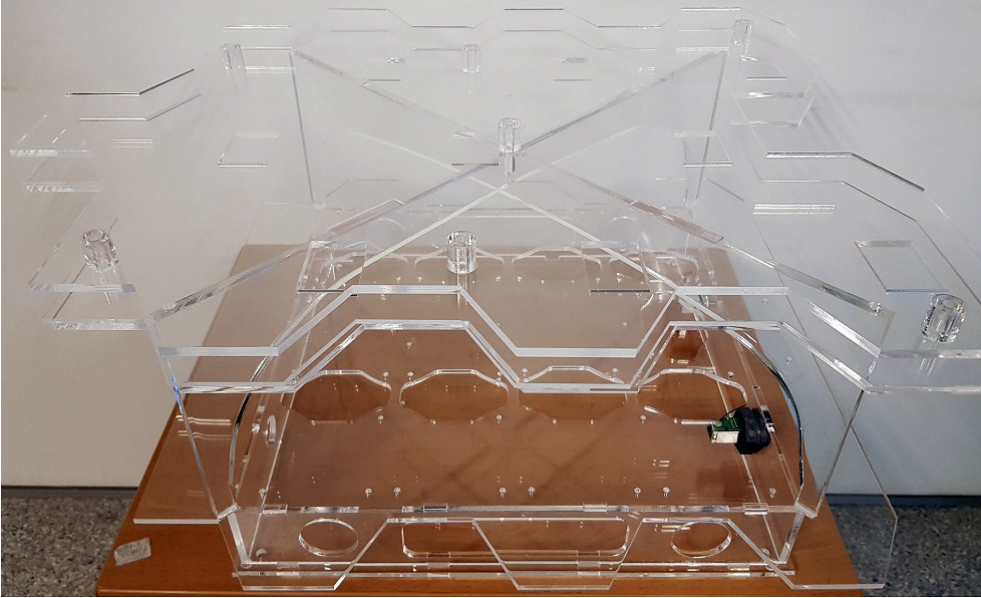


Figure 2.23. Photo of the assembled structure, which is manufactured with Poly(methyl methacrylate) (PMMA), also known as acrylic.

2.3.7 Triangulation Algorithm

In order to analyze and transform all data acquired by the RATT tile into 2D positions a triangulation algorithm was created. This algorithm is capable of transforming the RSSI received from each of the antennas into 2D coordinates of the corresponding Tag. In order to calculate the coordinates of each tag the Equation 2.2, Equation 2.3 and Equation 2.4 were implemented in MATLAB. These equations estimate the current position of the tags based on the RSSI signals and the previous position of the tag. This creates a smooth position path avoiding “jumps” between detection events.

In order to easily represent the data in an understandable way, a GUI was created as shown in Figure 2.27. It displays a map of the tile, the position of each detected tag and an RSSI map. In addition, the image is refreshed periodically,

each time a new set of positional data are received.

$$P_T(n) = \left[(1 - F_E) \sum_{a=1}^9 P_a \cdot R_A(n) \cdot F_{D_A}(n-1) \right] \cdot P_E(n) \cdot F_E(n) \quad (2.2)$$

$$F_{D_A}(n) = \max \left(\frac{dBase^{e^{-dRate \cdot (|P_a - P_T(n)|)}}}{dBase^{e^{-dRate \cdot dOffset}}} \right) \quad (2.3)$$

$$F_E(n) = \frac{MF}{e^{nRecs-1}} \quad (2.4)$$

Variable	Description	Variable	Description
P_T :	Tag Position	F_{D_A} :	Antenna Factor
F_E :	Estimation Factor	MF:	Max Trust Factor
P_E :	Estimated Position	nRecs:	ID of the antenna that detected a Tag
P_a :	Antenna Position	dBase:	Sort of attenuation (base 2 or exp)
R_a :	RSSI	dRate:	Attenuation weight that give more relevancy to the closest antennas

Table 2.3. Equation 2.2, 2.3 and 2.4 variables

2.3.8 Artificial Vision

In order to have visual feedback of the whole system while it is tracking animals, and for debugging purposes, a camera tracking system was created. This camera tracking system is composed of a Camera *Logitech C920*, which is capable of recording at 1080p (30 Frames Per Second (FPS)), attached by a mechanical arm to the RATT tile. This Camera tracking system uses an algorithm that was created as Bonsai workflow (subsection 2.2.2). The workflow has three main objectives.

The first is to track the two Aruco [81], [82] markers that are positioned over the RATT tile. These Aruco markers are tracked with an algorithm and they are used to determine the spatial reference for the camera; the marker at the corner (Figure 2.25) is used to track the rotation of the tile in respect to the camera. The center marker is a reference to correlate the center of the image with the center of

the tracking positions from the RATT tile. Moreover, all of the Tags positioned over the tile have an Aruco mark attached, which the Bonsai algorithm uses to track each of the simulated subjects (see Figure 2.25).

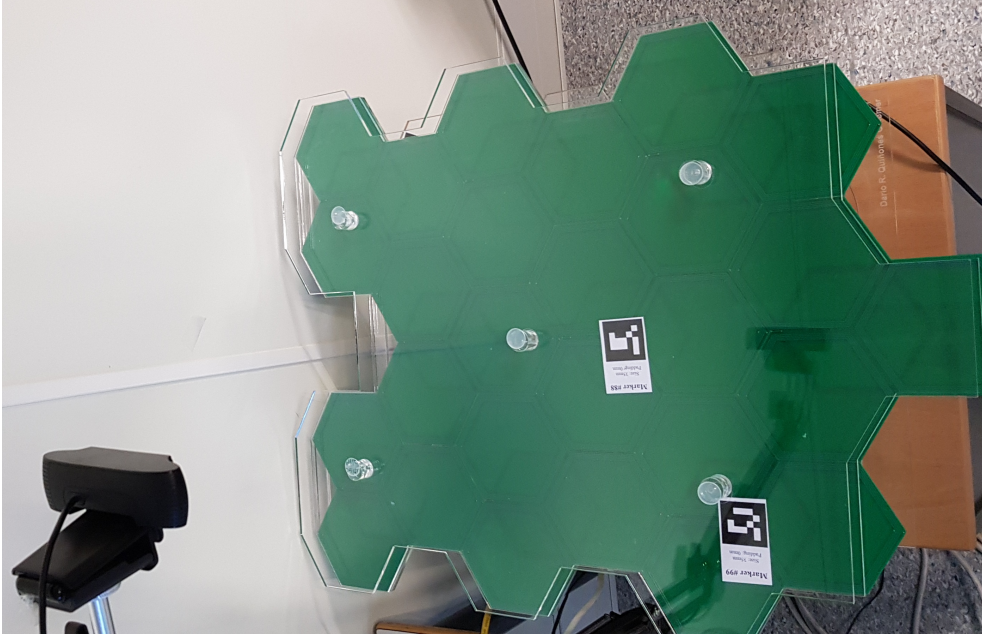


Figure 2.24. Co-tracking Setup. One RATT tile with the camera tracking setup is presented. It is possible to see the fixed Aruco markers that are used to establish the camera coordinate system.

The second aim of the Bonsai workflow is to DataLog and VideoLog all the events that happen in front of the camera focus. All the positions of the RFID tags are logged in a CSV file, which contains the position of the tags, a timestamp, and the markers ID. Moreover, the workflow makes a 10 FPS video recording of the screen. This video was made to show at the same time, the camera tracking and the RFID tracking as is shown in Figure 2.29.

The third aim of the Bonsai workflow is to give fast-visual feedback of whether or not the camera is detecting the marks. When a marker is detected by the

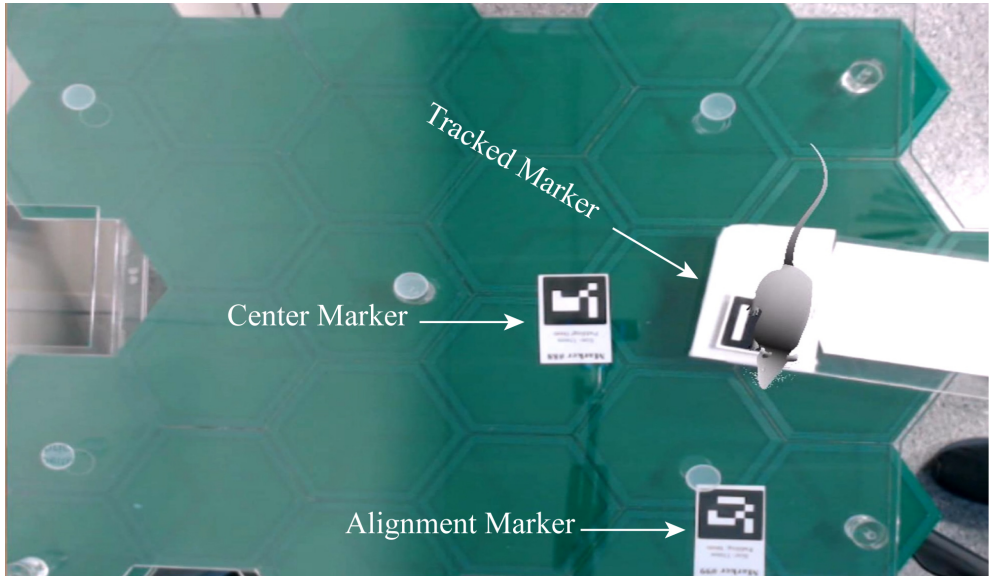


Figure 2.25. Camera tracking with Aruco Markers.

camera, it automatically overlaps a 3D rat over it. This function is especially useful for debugging and testing the whole system.

2.3.9 Data Acquisition

The data acquisition was performed with MATLAB. A script was created in order to read the data packages received through the UDP connection. These packages contain the RSSI of each tag in reference to each antenna of the tile. A GUI was created in order to visually interpret all of this information while the data are being acquired, as is shown in Figure 2.26. All of the data received from the RATT tile is analyzed in order to create an RSSI map (see Figure 2.27). This map is generated through the interpolation of the Received Signal Strength Indicator (RSSI) of each antenna. It allows the visual representation of which antenna is detecting each tag and how much RSSI has each one.

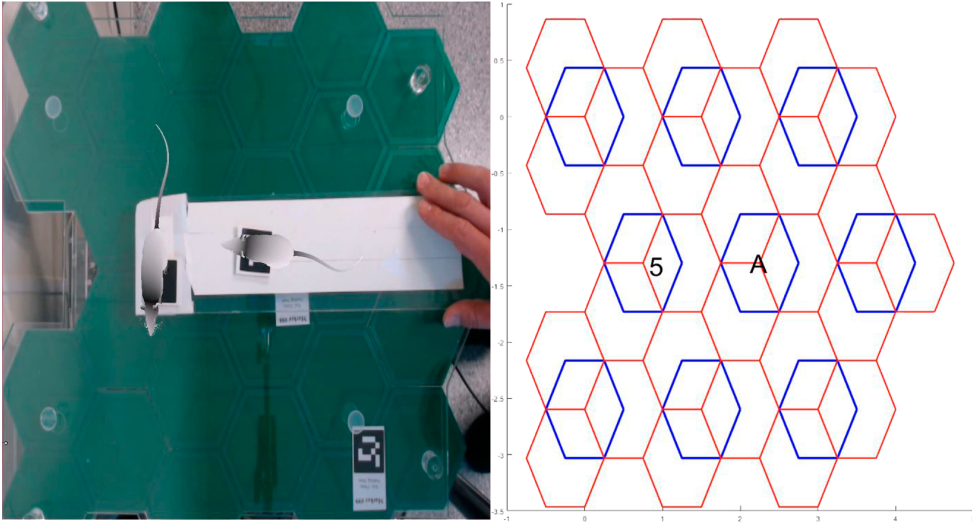


Figure 2.26. Co-tracking multiple tags. Multiple tags are tracked simultaneously by the RATT system and the Camera tracking system where it is possible to observe that both systems represent the spatial location correctly. In order to perform this test, the tags were attached coaxially to each Aruco mark.

2.3.10 Overall

By using the RFID Assisted Tracking Tile (RATT) a simultaneous localization of multiple RFID tags was achieved. It was possible to obtain readings as shown in Figure 2.29, which show the relationship between the various real positions of the tags and those measured by the system. An interesting result is the existence of an inductive interaction between tags when they are close together. This creates variations in RSSI readings. In this way, and with the current Tags, three zones can be identified:

- Tags distant from each other (>10 cm): This case offers the best resolution, with a maximum positioning error of 3 cm.
- Medium distance tags (5-10 cm): In this case, the positioning error increases up to 5 cm, maintaining the relative positions of the tags.
- Short distance tags (<5 cm): When the tags are so close, the error is still 5 cm, but the relative positions are not maintained.

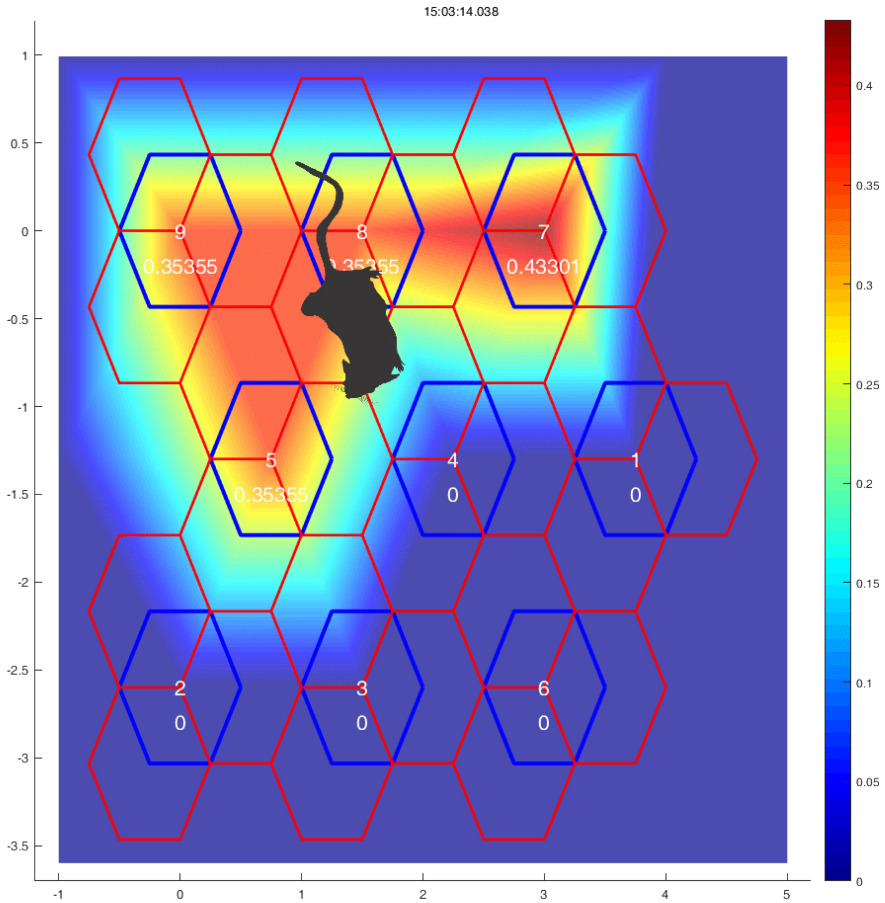


Figure 2.27. Received Signal Strength Indicator (RSSI) interpolation map. The interpolation gives a perspective of how the magnetic field detects different Tags. All these RSSI are useful in calculating the position of each tag. It is possible to observe that when an animal is among different antennas it is detected by multiple antennas and this facilitates the triangulation of the animal position. The color bar on right side refers to the percentage of RSSI received by each antenna (being 1 the maximum and 0 no tag detection.)

The strongest points of the system are its robustness against occlusions, the possibility of adding burrows and enriched environment and the possibility of having larger tracking surfaces. But, there is one even more interesting capability of the system. This is that the absolute position error does not increase when a large tracking area is set up. This is because, even though it is possible to perform

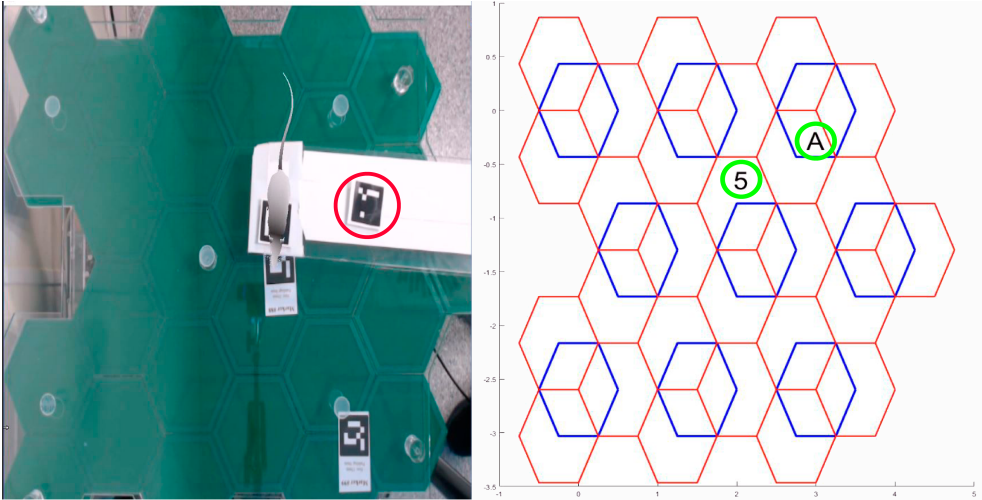


Figure 2.28. RATT against Camera tracking mistakes. It is shown a simultaneous tracking with the RATT system and the Camera tracking. On the right side of the image, it is possible to appreciate that the RATT tile is detecting two tags. Meanwhile, the camera has lost track of one Aruco marker (This is represented by the absence of a virtual Rat.)

tracking experiments in a large area, which will be formed by several tiles, the position error of the system remains the same in absolute value (5 cm) but it decreases in relative value. Hence, if the tracking area is one square meter and the absolute position error is 5 cm, then relative error is 5% (of the total surface). However, if the tracking area is $10m^2$, the absolute position error will still be 5 cm, which means that the relative error will be 0.5% (of the total surface). Hence, the larger the tracking area, the lower is the relative error. This is due to the fact that the triangulation algorithm calculates the Tag position based on the RSSI of the neighboring antennas (usually 3 or 4 antennas).

These tests were performed with the 3 cm RFID coin tags. When testing with the biocompatible crystal tags the quality of the RSSI varied depending on the dimensions of the tags. While the 22 mm tags were easily detected and properly positioned by the system, it was hard to detect the 12 mm tags in most cases. The discrepancies in signal strength between different tags are due to the different induction coefficient their internal antennas have. A close matching between the reader antenna and the tags is needed in order to achieve maximum

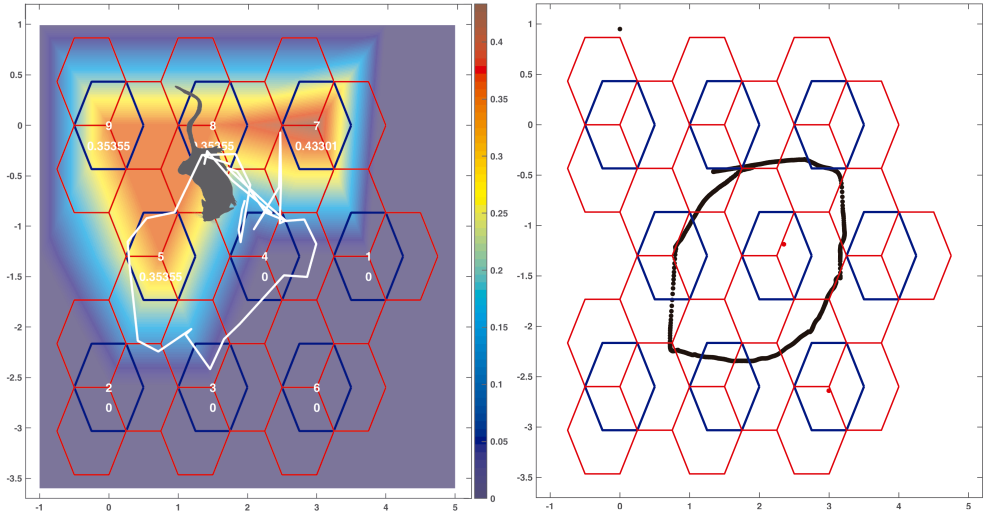


Figure 2.29. Camera tracking versus RATT tracking. It is possible to observe that the camera tracking is much more accurate than the RATT system (1-3 cm of position error). Nevertheless, the objective of the RATT system is to have continuous tracking in difficult situations, e.g., when the animals are inside burrows or are in a crowd. The most positive point is that both systems can work simultaneously, giving a high robustness tracking system.

signal transmission. This will be solved in future revisions by redesigning the geometry of the antennas with a smaller diameter and higher turn count.

2.3.11 MultiRATT Tile

The RATT tiles were designed to interconnect as many tiles as the users require. The tiles were designed with a “*puzzle philosophy*”, i.e. that any tile could be interconnected with any other tile. This paves the way for researchers to create a custom environment as large as the user wants and whatever shape the user wants. In Figure 2.30 it is possible to observe a squared shape setup. However, *L* shape (see Figure 2.31) and Linear shapes are also possible. This permits the creation of custom and enriched environments, including those without occlusions during the recording/tracking process.

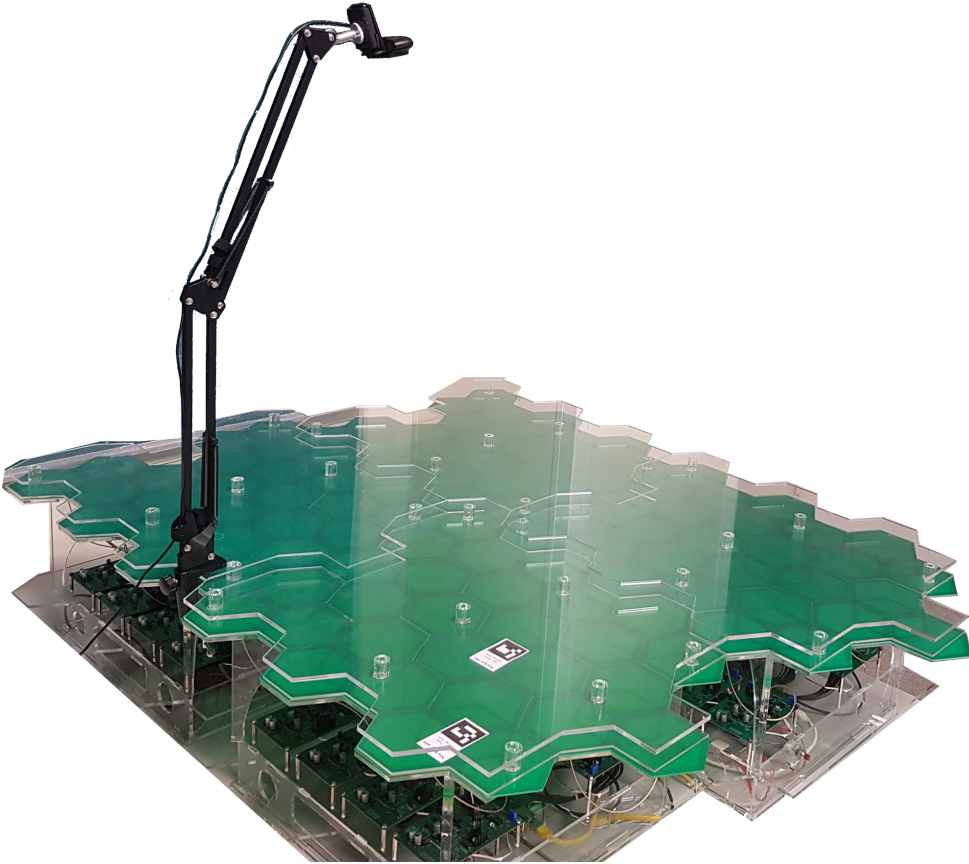


Figure 2.30. The figure shows Four RATT tiles together. It is possible to observe how the RATT tiles are physically interconnected, as well as the mechanical structure which supports the camera.

2.4 Conclusions

In order to complement current visual tracking systems, a radio frequency tracking system, which overcomes their limitations, was developed. The challenge was to create a RFID tracking system, which could be combined with existing visual tracking systems, in order to improve the location and identification of laboratory animals in controlled environments.

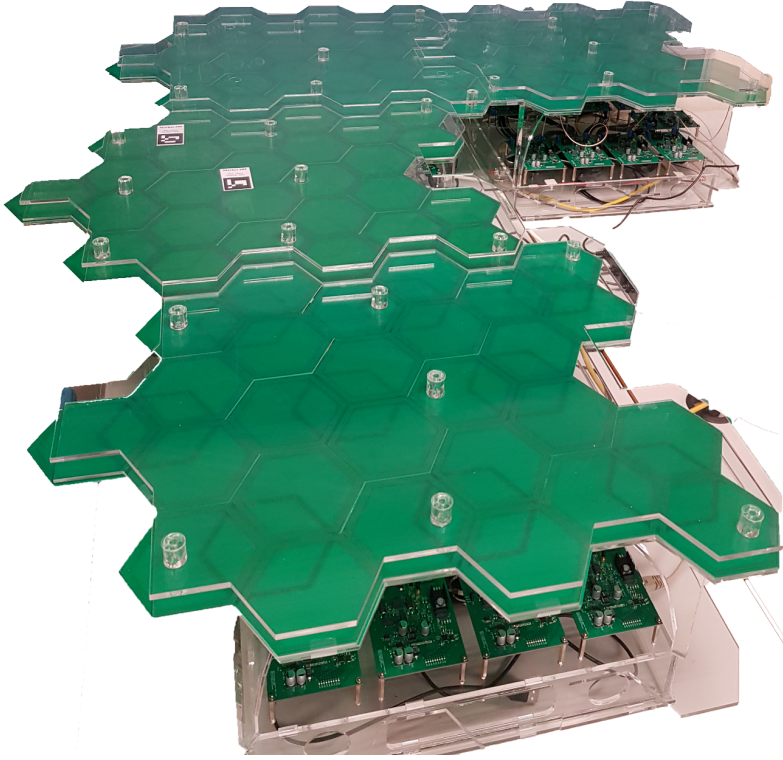


Figure 2.31. The figure shows Four RATT tiles together in an L shape distribution.

This system works such a “X-Ray” camera, it is capable of tracking animals in the absence of light and even when the top surface of the tile is covered with sand or any object.

The RFID Assisted Tracking Tile (RATT) system was designed to take into account the difficulties of experimenting with movement of small animals. This system is composed of electronic tiles, which have RFID antennas, to improve the tracking and the identification of the animals. It was designed in a modular fashion in order to be adaptable and easily maintained. The RATT system, as well as providing identification functions, gives coverage in places where visual tracking is not possible. This vastly improves the quality of the results of behavior research studies.

Chapter 3

HIVE Tracker: a tiny and scalable device for 3D tracking.

Positional tracking systems could hugely benefit a number of niches, including performance art, athletics, neuroscience, and medicine. Commercial solutions can precisely track a human inside a room with millimetric precision. However, these systems can track only a few objects at a time; are too expensive to be easily accessible; and their trackers are too large and inaccurate for research or clinical use. A light and small wireless device is presented that piggybacks on current commercial solutions to provide affordable, scalable, and highly accurate positional tracking. This device can be used to track human movements or to track freely moving subjects for research purposes.

The content presented in this chapter has been adapted from the following publication:

D. R. Quiñones, G. Lopes, D. Kim, C. Honnet, D. Moratal, and A. Kampff, “HIVE Tracker”, *Proceedings of the 9th Augmented Human International Conference on - AH '18*, vol. Part F1344, New York, New York, USA: ACM Press, 2018, pp. 1–8. DOI: 10.1145/3174910.3174935

3.1 Introduction

Humans and animals use bodies as our primary interface with the outer world, and as a powerful tool for expressing our inner worlds [101]–[104]. Movement is therefore a phenomenon of interest to many, such as neuroscientists, surgeons, engineers, makers and artists. Though we have long appreciated movement on a macro scale, it has become increasingly clear that much could be gained from studying movement in greater detail and with higher precision.

3.1.1 *Applications in Performing Arts and Athletics*

Two areas with long-standing interests in the precise study of human movement are the performing arts and athletics. In the 1920s, Rudolf Laban, a dance artist and theorist, developed with his colleagues a written notation system to precisely and accurately describe movement in terms of body parts, actions, floor plans, temporal patterns, and a three-dimensional use of space [105]. This has evolved into the modern-day Labanotation, or Kinetography Laban. However, many movement artists find Labanotation too complex and cumbersome for easy daily use. These days it is much more common to use videos to record, analyze, and teach the specific movements of performing artists and athletes. The increased prevalence of cheap video recording devices, especially phone cameras, has increased the use of this technique. But even high quality, state-of-the-art video recording technology struggles to capture the movements of aerial artists, acrobats, and other circus performers; the finer details of object manipulations performed by jugglers and athletes (e.g. finger placement and movements for optimal archery technique); and the tiny, fast movements of smaller body parts often found in hip-hop and modern dance.

3.1.2 Applications in Neuroscience and Medicine

The fields of neuroscience and medicine are also interested in precisely recording and analyzing movement, both for research and for clinical applications. A fundamental question in neuroscience is how nervous systems generate and execute movement goals. Historically, neuroscientists have prioritized the collection of cellular signals when answering research questions, so experiments are designed around the need to keep an electrode, or other data collecting device, stuck in the head of the animal. This means that most neuroscience experiments study animals that are either held in place (“head-fixed”) or tethered to a wire. However, a growing body of evidence supports the idea that cellular activity in the brain is significantly different when an animal is actively and freely moving in three dimensions through complex physical spaces, as opposed to when it is head-fixed or tethered to a wire. [106]–[111]. Studies of the development and degeneration of nervous systems in humans also show that nervous systems are profoundly affected by the movements and physical contexts of their bodies [112]–[114]. Better systems for precise positional tracking in humans and animals would significantly impact the scientific questions that neuroscientists and clinical researchers could ask.

3.1.3 Current State-of-the-art in Positional Tracking

All of these areas would benefit hugely from having greater access to precise movement tracking. Motion capture systems, or mo-cap for short, are the current state-of-the-art for recording the movements of people and objects. However, current motion capture technologies require multiple specialized cameras, in addition to a whole slew of accessories, which unfortunately make these systems inaccessibly expensive and bulky. Industry standards for mo-cap, such as VICON and OptiTrack [115], [116], require a minimum investment of 10-15 thousand USD in order to assemble a viable system. Another option out on the market are inertial measurement units, or IMUs, which combine accelerometers, gyroscopes and magnetometers to track small and fast movements [117]–[120]. Despite their sensitivity and speed, such IMUs do not measure absolute position, only relative motion. This means that to recover absolute position one must integrate the measured motion over time. Even small measurement errors will accumulate during this integration process, a phenomenon referred to as “drift”. This makes

IMUs inadequate for precise, continuous tracking of natural movement sequences. Another currently available alternative (at the time of writing) for motion tracking is Microsoft's Kinect, a consumer level 3D motion-sensing camera device for video game consoles. Using depth information and machine learning, the Kinect can infer in real-time the pose (position and orientation) of a human body located in front of the camera. However, a single Kinect cannot track motion in 360 degrees, as it was originally designed to track the movements of gamers facing a video game display. Some motion tracking systems combine Kinects and IMUs in an attempt to supplement one technology's weaknesses with the strengths of the other [121], but IMUs will always drift, and multiple Kinects will always be required to gain 360 degree tracking. While all these systems have found a niche, and are of great use to the military and entertainment industry, they are neither affordable to most artists, athletes, researchers, or clinicians, nor accurate enough for use in research or clinical settings [122].

3.1.4 Affordable, Smaller, and more Scalable

Simpler solutions are already coming out of artistic research, wearable applications and even implant experimentations [123]–[125]. Building upon this line of work, an affordable, compact, and scalable positional tracking device called “Hive Tracker” is presented, which can measure movement with sub-millimetric precision along six degrees of freedom; allows for untethered movement within a $5 \times 5 \times 5 \text{ m}^3$ space; connects easily and simply to virtual reality; and can scale up to as many devices as desired. This approach would allow the niches described above to take advantage of precise positional tracking technology, and opens the door to a plethora of new human augmentation applications.

3.2 Materials and Methods

Here the details of the multi-component system, composed of commercial products as well as custom devices and software are presented (see Figure 3.1). First a small proof-of-concept of the system using an off-the-shelf microcontroller board described in subsection 3.2.2.2 was developed and benchmarked. Below some of this benchmarking data is presented, which was used to constrain the subsequent design of the first Hive tracker prototype, described in section 3.4.

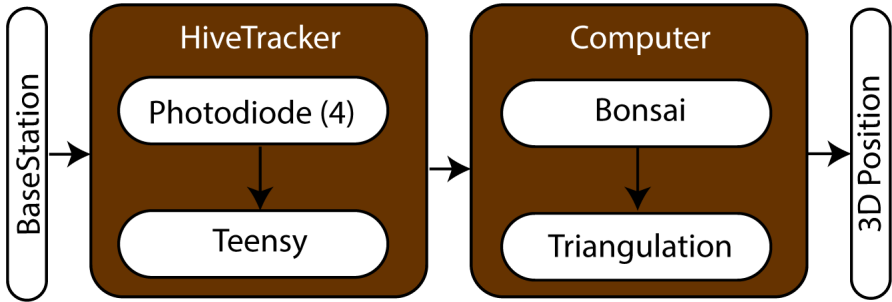


Figure 3.1. Overall HiveTracker system overview. An overview of the complete signal processing pipeline is shown, which is described in the following subsection.

3.2.1 Valve Tracking System

The Hive Tracker is a data-collection device that piggybacks on a commercial virtual reality system developed by Valve (HTC VIVE). The commercial system (see Figure 3.2) consists of a headset, two hand controllers, and two light-emitting devices (“lighthouses” or “base stations”). Each lighthouse contains an LED

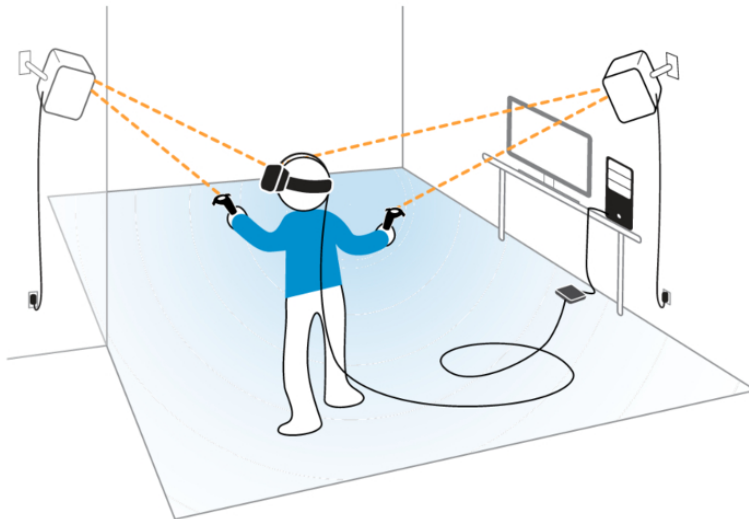


Figure 3.2. Valve tracking system (from Valve Corp. , WA, USA).

matrix and two mirrors mounted on high precision rotors. In order to achieve sub-millimetric precision, this system needs to be set up in a space no larger than a 5x5x5 meter cube. The communication protocol between the lighthouses and the commercial devices was reverse-engineered in order to replace the commercial devices with custom devices optimized to fit our needs.

The signal from the lighthouses is composed of four components (Table 3.1), which enable the system to synchronize the two lighthouses and to track devices within the VR space (Figure 3.3). When the system initializes, the lighthouses are automatically assigned as lighthouse A and B. To synchronize the two lighthouses, lighthouse A first emits a flash of light with known pulse length. Soon after, lighthouse B emits a similar flash of light, as described in Table 1. The length of the flash determines which lighthouse will start the laser plane sweep, and whether that sweep will be horizontal or vertical (see Figure 3.4).

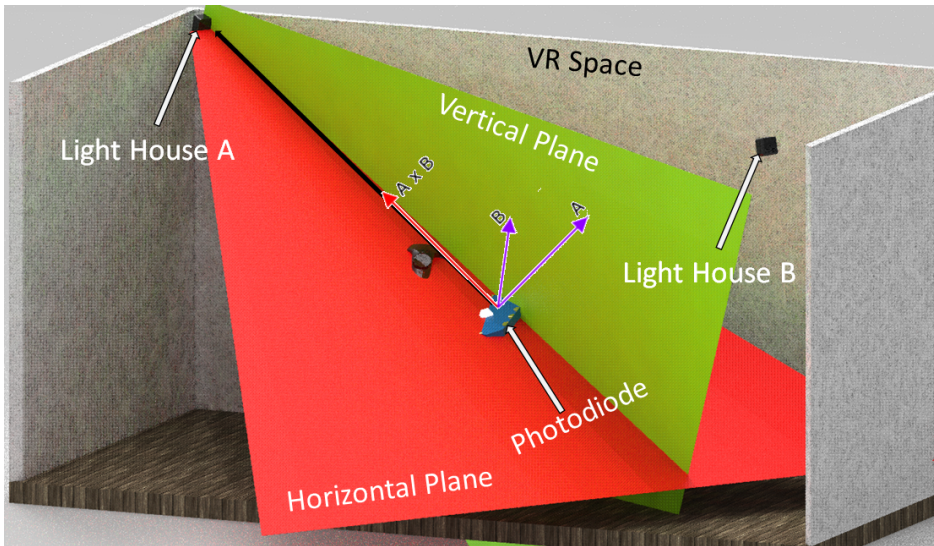


Figure 3.3. Picture represents how two intersected planes represent a 3D line pointing to each base station.

3.2.2 Signal Processing

3.2.2.1 Photodiode circuit

In both our proof-of-concept and our first PCB prototype, the Chiclet was used, which is a sensor processing development board made by Triad Semiconductors (Winston-Salem, NC, USA). The first-generation of the Chiclet uses the TS3633 Integrated Circuit (IC). The IC converts a weak and noisy analog signal (obtained with the photodiode) to a digital signal which is simpler to use with a microcontroller. It provides both high-gain noise filtering and envelope detection of pulsed InfraRed (IR) light that is incident on the photodiode.

Pulse start, μs	Pulse length μs	Source station	Meaning
0	65 - 135	A	Sync pulse
400	65 - 135	B	Sync pulse
1222 - 6777	~ 10	A or B	Laser plane sweep
8333	1556		End of cycle

Table 3.1. Activation Timings

3.2.2.2 Acquisition Hardware: Teensy

The Hive Tracker proof-of-concept was developed on a Teensy 3.2 (PJRC.COM, LLC., Sherwood, Oregon, USA). This 35x17mm microcontroller uses an ARM cortex M4 processor overclocked at 120MHz to reduce interrupt handling latency. The Teensy timestamps the digital signals coming from the TS3633 and sends them to a computer to be converted into angles (subsubsection 3.2.2.3).

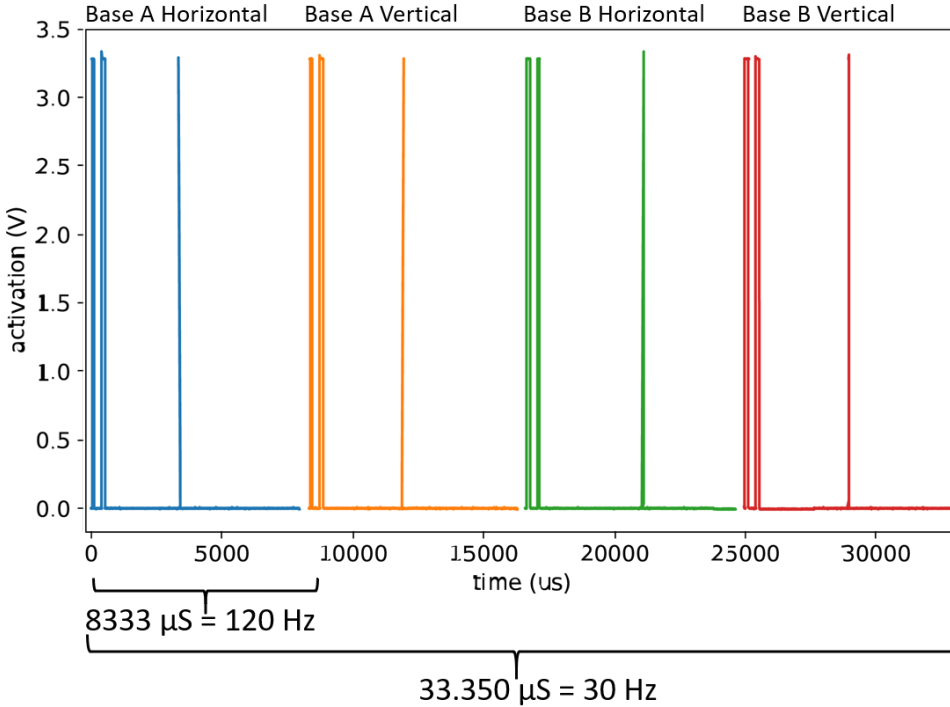


Figure 3.4. Light signal sequences (4 are shown): wide pulses are base station flashes and short pulses are laser plane scans.

3.2.2.3 Acquisition Software: BONSAI

For data collection, integration, and online visualization, the Bonsai visual programming language [44] was used. Photodiode activation timestamps were collected and serialized into UDP packets via the Open Sound Control (OSC) protocol [126]. These packets were streamed wirelessly into the host computer using Wi-Fi. In order to reconstruct the position and orientation of each HiveTracker, the VR package of the Bonsai programming language was used to access the estimated 6 DOF (degrees of freedom) location of each lighthouse in parallel with the OSC messages.

3.2.2.4 *Triangulation Algorithm*

For each light signal sequence (Table 3.1), each lighthouse will first flash, then scan a beam of light either horizontally or vertically [127]. Every photodiode gets hit by both the flash and the scans, but the light hits each photodiode at different times. Each lighthouse sweeps at 120Hz. The “incident plane” is the plane defined by the angle between a photodiode and a lighthouse (Figure 3.3). The cross product of the normals of the horizontal and vertical incident planes defines a vector (“incident line”) between the tracking device and the lighthouse. The absolute position and orientation of each lighthouse is given by the commercial system, which allows us to project the incident lines from each lighthouse into the global coordinate system. The closest pair of points between these two incident lines defines the absolute location of a tracking device [128], which can be determined at 30 Hz (Table 3.1).

3.3 Results and Discussion

3.3.1 *Tracking: inside an ideal room*

The Hive Tracker proof-of-concept was first compared against the hand-held controllers of the commercial Valve tracking system in an ideal room. A non-regular hexagonal shape was taped on the floor of the testing room, then traced this shape by hand with both devices, recording the devices’ positions using Bonsai. The acquired trajectories were overlapped to compare the accuracy of the commercial controller (32 photodiodes) against that of the first Hive Tracker proof-of-concept (1 photodiode). In this comparison, the commercial device was used as our baseline “ground truth”. Since the tracing movements were parallel to the floor plane, only the sensors’ X and Y axes were used for this benchmark (Figure 3.5).

In order to quantify the comparison, a polygon shape was fit to the tracking data from the commercial device. Then, this trajectory was compared to the average traces from the Hive Tracker by calculating the average distance of each point in the tracker trajectory to the fitted hexagon. The results of this comparison are shown in Figure 3.5. The Hive Tracker proof-of-concept, which

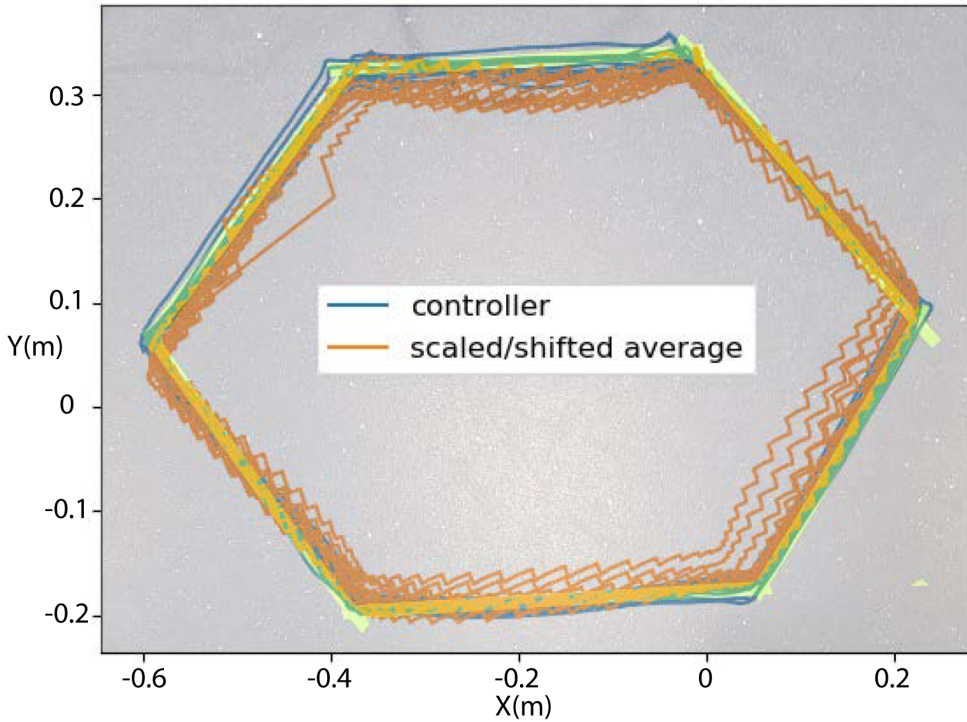


Figure 3.5. Accuracy comparison between a commercial controller and Hive Tracker proof-of-concept in an ideal room. Traces from both devices are superimposed over a photo of a polygon taped to the floor. Blue = commercial controller, Orange = Hive Tracker, Green = tape on the floor.

uses only one photodiode, had an average error on the order of 10 mm more than the average error of a commercial tracker.

3.3.2 Tracking: in a non ideal room

The Hive tracker proof-of-concept has been tested in the worst possible scenario: in a $1.2 \times 1 \times 1.5 \text{ m}^3$ space with a glass floor. In this situation the proof-of-concept was not able to achieve good accuracy, due to the short distances between the lighthouses and the reflection of the laser light on the glass floor (Figure 3.6).

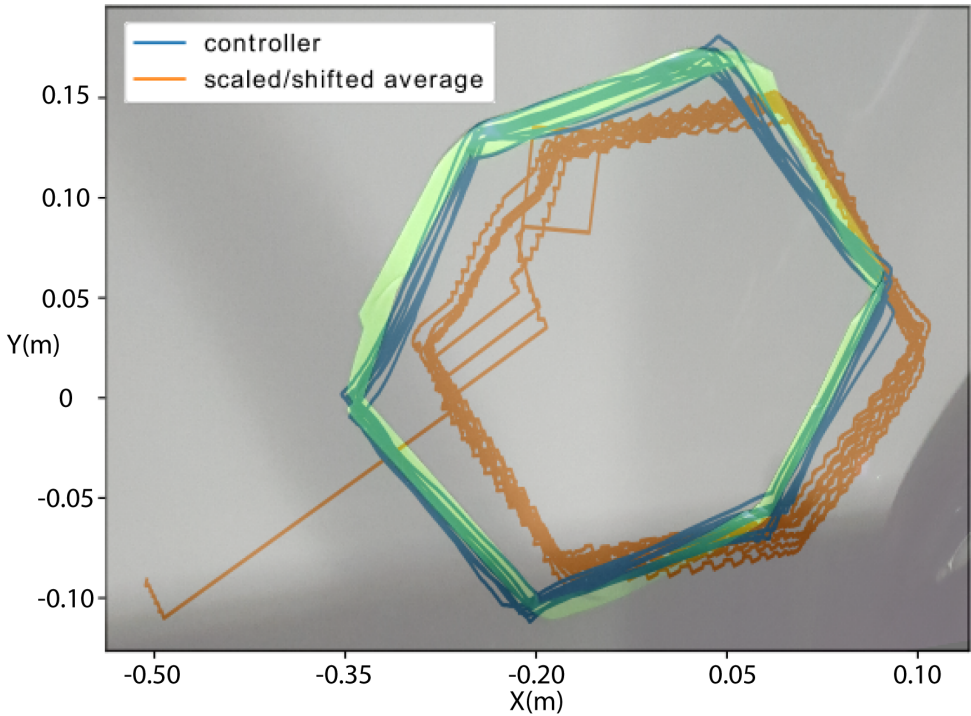


Figure 3.6. Accuracy comparison between commercial controller and Hive Tracker proof-of-concept in a non-ideal room. Traces from both devices are superimposed over a photo of a polygon taped to the floor. Blue = commercial controller, Orange = Hive Tracker, Green = tape on the floor.

3.3.3 Light Reflections

Light reflections are a potential source of errors in this setup. As the laser plane (see Table 3.1) sweeps across the VR space, it is possible for light to bounce off a wall (or any shiny surface) and hit a photodiode sensor. Figure 3.7 shows false detections in the photodiode signal. This issue has been addressed in the first PCB prototype by adding extra photodiode sensors for more redundancy in the system. One can further shield the photodiodes from non-direct hits by embedding them in a shallow depression.

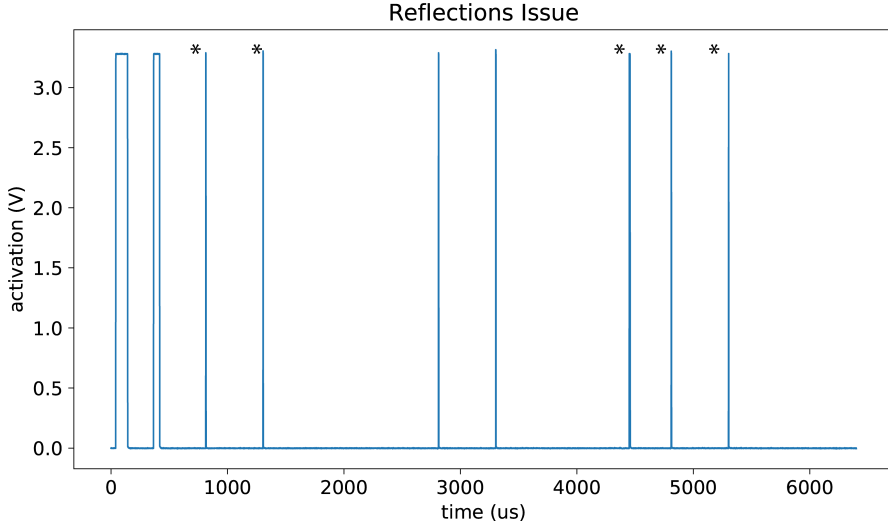


Figure 3.7. Reflections off the walls cause undesired pulses (asterisk) in the photodiode signal (compare to Figure 3.4).

3.3.4 Tracking Refresh Rate

Another limitation of the proof-of-concept was the refresh rate of positional measurements. In order to find the closest pair of points between the two incident lines from the lighthouses using only one photodiode, it is needed to collect light data for at least four full cycles from each lighthouse. This means that the Hive Tracker proof-of-concept updates positional tracking measures at 30 Hz (See Figure 3.4). This limitation can be addressed by using multiple photodiodes placed in a known geometric configuration relative to each other. In this way, the sequence of incident lines hitting each of the photodiodes in a single sweep can be used to constrain estimations of the absolute position and orientation of the Hive Tracker. This situation can be framed as a “Perspective-n-Point” problem, or the more general problem of estimating the position and orientation of a calibrated camera based on the projection of 3D points in the world onto that 2D camera image. Given this framing, it is possible to consider each lighthouse as an ideal pinhole camera where the 2D-to-3D point correspondences are known exactly. Efficient algorithms to solve this problem for 3 or more points have been introduced by the computer vision community. [129]

The reconstruction can further be constrained by using inertial motion measurements to estimate motion over time. This makes it possible to reconstruct the position and orientation of an entire Hive Tracker device from single sweeps at 120Hz. These insights motivated the development of the first Hive Tracker PCB prototype described in the next subsection.

3.4 PCB Prototype

Our tests with the Hive Tracker proof-of-concept confirmed our initial suspicions, namely that we would need to use more photodiode sensors. However, this also increases the computational load on the microcontroller processing system, as multiple photodiode sensors may be hit simultaneously. To address this, our first PCB prototype includes a dedicated system for processing in parallel the photodiode signals.

3.4.1 Hardware

Increasing the number of photosensors increases the computational load on the system's processing units. The most common way to deal with this is to use Field-Programmable Gate Array (FPGA) processors, which enable true hardware parallel processing. However, a simpler approach was found in order to achieve the necessary parallelization while maintaining an extra-compact board, such that the device does not hamper free movement. The nRF52 by Nordic Semiconductors (Oslo, Norway) was chosen, a "System on Chip" (SoC) that replaces the functionality of the FPGA with a Programmable Peripheral Interconnect (PPI). The nRF52 also includes a Bluetooth Low-Energy (BLE) (Bluetooth Low Energy) and an ARM cortex M4 core.

Figure 3.8 shows the design of the first custom board, with 5 Chiclet connectors. On the top side of the board, shown on the right of the figure, the largest component (labeled "MCU" for Micro Controller Unit) is the ISP1507 by Insight SIP (Sophia Antipolis, France). This $8 \times 8 \text{ mm}^2$ system-on-package (SoP) includes the nRF52, its necessary passives, a high accuracy crystal resonator to define the radio communication speed, and a low power oscillator, which enables the microcontroller to save power while in deep sleep. The rectangular chip above

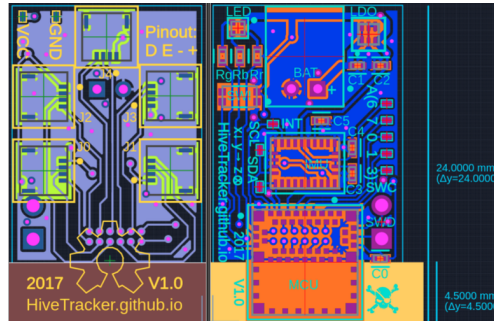


Figure 3.8. PCB design (left: bottom layer, with the photodiode connectors - right: top layer includes MCU, BLE, Integrated Motion Unit (IMU), battery connector, button, LEDs, etc.)

the MCU is the Bosch BNO055 (Reutlingen, Germany), an IMU SoC with a 3D accelerometer, a 3D gyroscope, a 3D magnetometer, and an ARM cortex M0 to perform sensor fusion. The other parts are the battery connector to connect LiPo batteries, a regulator, an RGB LED, a button, and 5 analog inputs that can behave as any General Purpose Input/Output (GPIO) - to connect other MCU, sensors, etc.). This first custom miniaturization prototype is far from cost-optimal, as the Chiclets are quite expensive. However, we have kept them in our design because their reliability is proven, and the cables connecting them to our PCB give us greater flexibility when placing the photodiodes. The next iteration of the Hive Tracker will not use Chiclets; instead, it will use the TS4231, a new IC by Triad Semi, and through-hole photodiodes that can accommodate custom orientations.

3.4.2 Firmware

The embedded software (firmware) configures the Triad Semi IC, processes the signal, merges it with the IMU data, and then sends it to a computer or a smartphone over BLE. This firmware fulfills the same function as the Teensy on the first proof-of-concept. The Teensy measures timing differences using interrupts, but this method can degrade the positioning accuracy. In the time it takes to handle an interruption, other light signals may have occurred. As mentioned earlier, an FPGA would solve this problem, but would make the Hive Tracker bulkier. While trying to keep the PCB small, it was possible to validate

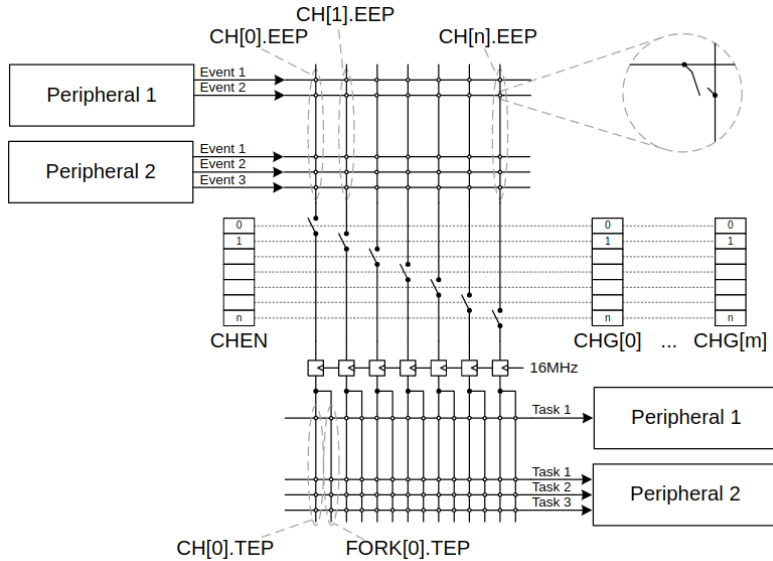


Figure 3.9. Programmable peripheral interconnect (PPI), ©Nordic Semiconductors [130]

that a rare feature of the MCU, the Programmable Peripheral Interconnect (PPI), could connect the edge detector and the capture register. This connection would normally need to happen via a CPU or FPGA, but using a PPI allows peripherals such as GPIOs and timers to interact autonomously with each other using tasks and events. The lack of interruptions makes it possible to simultaneously process up to 5 signals, which would improve robustness to potential occlusion. For a trackable object to detect IR signals in any 3D orientation, the geometric placement of at least 4 photodiodes must be on the vertices of a tetrahedron. Figure 3.9 shows how these peripherals are connected.

This embedded software is developed using the Software Development Kit (SDK) provided by Nordic Semiconductors, the MCU manufacturer, to allow optimal performances. It is also Arduino compatible, to allow the research community, makers, or artists to experiment openly and freely.

3.4.3 Size/Accuracy Trade-off



Figure 3.10. Size/weight comparison. Commercial tracker: $10 \times 10 \times 4.2 = 420\text{cm}^3$; 85g. Hive Tracker: $2.5 \times 1.5 \times 1.1 = 4.13\text{cm}^3$; 8g.

Our custom PCB prototype can fit into a bounding box volume about 100 times smaller than the one necessary to enclose a commercial tracking device, and our device weighs about 10 times less than the commercial tracker (Figure 3.10). These improvements in size and weight did cost some tracking precision (see section 3.3), but since our error calculations were made with the proof-of-concept, which used only one photodiode, we can treat those error measurements as a “worst-case scenario”. The increased number of photodiodes in our PCB prototype can only improve the precision of the proof-of-concept (Figure 3.11).

These reductions in size and weight make the Hive Tracker much more convenient to use in a wider variety of human applications. Because it is not only small but also quite flat, the Hive Tracker can be integrated into clothing, gloves, or shoes worn by circus performers, theater artists, and dancers to capture their movements in real-time without hindering them. The Hive Tracker can also be easily integrated into objects manipulated by jugglers and athletes, in order to track and capture the movements of their props in addition to their bodies.

For medical and neuroscience research, which primarily use rodent subjects, the size and weight reductions are crucial. In neuroscience research, ethical review boards generally find it acceptable to use implants that do not exceed 10% of the body weight of the animal to be implanted. The average adult laboratory rat weighs between 250 to 500 grams [131], and the average adult rat head measures

about 5 cm in length [131]. Given that the Hive Tracker measures 2.4 cm x 1.4 cm and weighs 8 grams, the Hive Tracker is already both small and light enough to be approved for use with rats, which are often implanted with devices that weigh 15 to 25 grams.

The accuracy of positional tracking that the Hive Tracker needs to achieve in order to be useful to medical and neuroscience research varies depending on the research question. Most research questions require a system that can precisely track the 3-dimensional movements of the whole body and the direction and orientation of the head. Current setups in neuroscience and medical research usually use video cameras to create a record of animal behavior, from which body trajectory and head movements are later extracted offline. This is both computationally and financially costly, and so many researchers simplify or ignore completely the behavioral validations required to thoroughly investigate their hypotheses. Even with the proof-of-concept’s “worst-case scenario” precision, the Hive Tracker would already greatly increase researchers’ ability to perform behavioral validations with a similar level of rigor as other controls currently used in neuroscience and medical research.

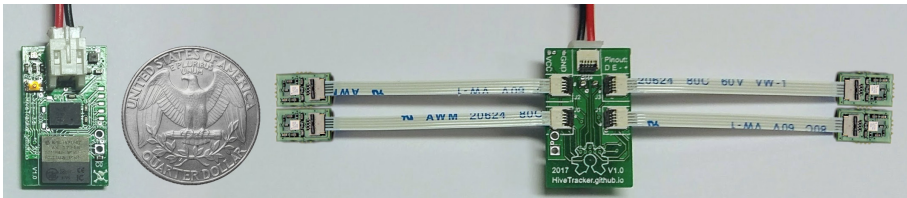


Figure 3.11. Hive Tracker prototype, with a US 25 cent coin for size comparison.

3.4.4 Cost

To produce the first 10 prototypes, the cost of the current version was about 75 USD, as opposed to 99 USD for the commercial tracker. This cost will be improved in our next version as the Chiclets will not be necessary anymore, so we can easily anticipate the cost of each Hive Tracker to be under 60 USD, especially if we produce them in larger quantities.

3.4.5 *Autonomy*

Various batteries can be used, but the one shown in Figure 3.10 has a capacity of about 100 mA. Given that our maximum power consumption is estimated to be about 40mA, this version of the Hive Tracker can run autonomously for at least 2 hours, depending on the usage. Embedded devices are in sleep mode most of the time, so the autonomy would greatly depend on the desired refresh rate. In addition, there is no need to process nor transmit data during periods of inactivity. For the applications mentioned in this project, the inactivity rate might range from 10% to 90%, so the Hive Tracker could potentially run autonomously for 20 hours.

3.5 Conclusion

This project showed an affordable and scalable custom positional tracking device that can integrate easily with a commercial consumer-level VR system. The Hive tracker is totally wireless and battery powered, which allows us to attach this small tracker to humans, animals, or even objects without interfering with natural movements and complex interactions. Furthermore, there is no limit to the number of trackers that can be used simultaneously. Based on the proof-of-concept presented here, we plan to use the Hive Tracker in a variety of applications, including neuroscience experiments of natural behavior; tracking and capturing object manipulations; 3D haptics in VR; and detailed and precise documentation of movements in artistic and clinical settings. These applications of the Hive Tracker can directly enhance our understanding of interactive movement and behaviour in humans and other animals. Thus, devices like the Hive Tracker are crucial to the kinds of research necessary for developing the next generation of human augmentation tools.

TherMouseDuino: A Temperature Control System for fMRI Experimentation with Mice

BOLD signal is based on vascular responses to neuronal activation and is extensively used in clinical and preclinical research studies. In preclinical settings, animals are usually anesthetized. However, anesthetics cause alterations, e.g. hypothermia, in the physiology of the animals and this has the potential to disrupt fMRI signals. In order to avoid hypothermia in anesthetized rodents TherMouseDuino is presented. It is an Open-Source automatic temperature control system that reduces temperature fluctuations, thus providing robust conditions in which to perform fMRI experiments.

The content presented in this chapter has been adapted from the following publication:

D. R. Quiñones, L. M. Fernández-Mollá, J. Pacheco-Torres, J. M. Caramés, S. Canals, and D. Moratal, “TherMouseDuino: An affordable Open-Source temperature control system for functional magnetic resonance imaging experimentation with mice”, *Magnetic Resonance Imaging*, vol. 58, p. 9, 2019. DOI: 10.1016/j.mri.2019.01.009

4.1 Introduction

Functional Magnetic Resonance Imaging (fMRI) is a non-invasive imaging technique that allows in vivo and longitudinal investigations of brain function. The Blood-Oxygen-Level Dependent (BOLD) signal is the most commonly used fMRI contrast to study brain activity [133], [134]. BOLD depends on a number of factors, including the different magnetic properties of oxygenated and deoxygenated hemoglobin, Cerebral Blood Volume (CBV) and Cerebral Blood Flow (CBF) [135]–[137].

Neuronal activity has an associated level of energy consumption [138], [139]. This energy is produced through chemical processes that require glucose and oxygen, the latter being transported in blood by the molecule hemoglobin. An increase in neuronal activity in an area of the brain immediately produces a higher ratio of oxygen extraction from the capillary network and therefore an increase in the concentration of deoxygenated hemoglobin. This initial blood deoxygenation is overcompensated by a vascular response increasing CBF and CBV around the activated brain area, a phenomenon known as neuro-vascular coupling and that represents the origin of the BOLD signal [133], [134]. Not surprisingly, the BOLD signal is influenced by a number of physiological parameters not directly related with neuronal signaling and cognitive processes, but directly coupled to vascular responses, such as temperature, blood pressure, CO_2 and O_2 concentration, pH and others. Nevertheless, a high correspondence between the BOLD signal and brain activity has been observed in well-controlled experiments [140]–[145].

Currently, preclinical research is a fundamental step preceding the translation of scientific findings to clinical application in humans. In most of these investigations, anesthetized animals are used to study cerebral function [146]–[148]

The main reason for the use of anesthetics is that brain imaging requires immobilization of the subject inside the magnet, to generate meaningful and high signal-to-noise datasets. Immobilization, however, is a well-known stressor that induces important physiological changes that can severely influence the experimental results [149]. Therefore, animals are usually sedated/anesthetized before immobilization in the MRI setup [143]–[147], [149], [150]. As a side effect, however, anesthesia has an effect on the animal’s physiology.

Mammals, such as laboratory mice, are endothermic animals, meaning that they are able to produce the heat necessary to regulate and maintain their body temperature (homeothermic) [151]. Temperature is therefore maintained within a stable range by physiological processes [152]. However, external agents, such as anesthetics, alter this physiological regulation in the animal [153] disrupting thermoregulation [154]–[159]. The high body surface to weight ratio of the mouse makes it especially susceptible to hypothermia [160]. During anesthesia, body temperature decreases and must therefore be kept stable and within the physiological range in order to provide robust and quantitative fMRI signals. [161]–[166].

fMRI data cannot be acquired without proper temperature control because the quantitative value of the measure would be lost. The reason is that vasodilation, and so the BOLD signal depends on body temperature [135]. Since most animal fMRI experiments are done under anesthesia, and since anesthesia affects temperature autoregulation [154], the animals must always be warmed to maintain a physiologic temperature. Therefore, what our development provides is an open-source, convenient and inexpensive way of controlling this vital parameter with high precision, instead of doing it manually.

For the reasons exposed above, a system to monitor and control the temperature of experimental animals is fundamental for fMRI experiments. Routinely, MRI setups are equipped with manual systems to control the temperature of the experimental animals (most often mice and rats) monitoring the temperature with an MRI-compatible rectal probe and adjusting the temperature of a water bath connected to the bed of the animal or an air-heating system with a thermostat [167]. In this paper, an affordable Open-Source temperature control system for pre-critical fMRI experimentation is presented. This automatic control device is designed for interconnecting and coordinating the necessary devices and

actions for regulating temperature of an animal while being scanned. Employed accessories and components for communication between the different laboratory equipment and the Arduino microcontroller are presented. The experimental identification of the system thermal behavior is also studied and mathematically modeled. It verifies the design of the Proportional-Integrative-Derivative (PID) controller and the application of a control algorithm to regulate the temperature in anesthetized mice.

4.2 Materials and Methods

4.2.1 Overview

A temperature control system for anesthetized animals in preclinical scenarios has been developed. For this purpose, different subsystems were employed (Figure 4.1).

The core of the whole system is based on an Arduino MEGA 2560 (Smart Projects, Turin, Italy & SparkFun Electronics, Boulder, CO USA) with different “*shields*” attached. These “*shields*” are modules or boards that can be plugged on top of the Arduino PCB for compact assembly. Currently, many platforms allow the users to develop their own microelectronic devices, with the Arduino (Smart Projects, Turin, Italy & SparkFun Electronics, Boulder, CO, USA) platform being one of the most renowned [168]. It is an open source hardware and software development platform whose basic principle is to facilitate a simple use of the hardware and software prototypes offer. Arduino has generated a large international community of users or makers (students, artists, programmers and professionals) who share their projects [169]–[171].

To warm up the anesthetized animal, a heated bath was employed. This bath allows control of the temperature of the fluid that warms the bed where the animal lies. An optical fiber sensor was used to measure body temperature due to its compatibility with the electromagnetic fields produced by the MR scanner. To set up the signal of the sensor, a signal conditioner with a serial communication port was employed.

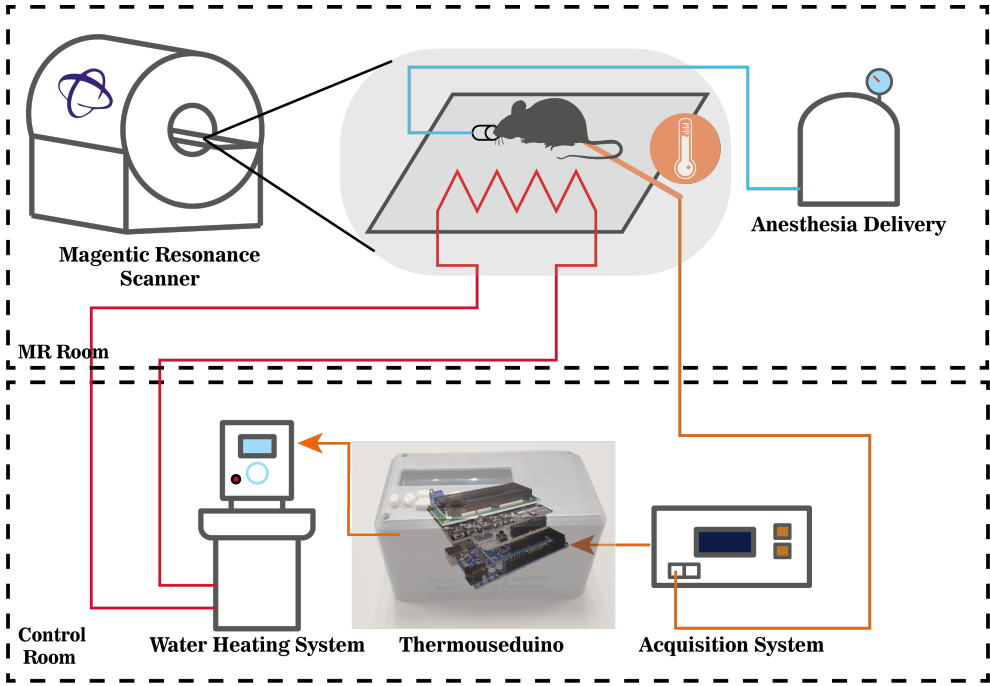


Figure 4.1. Schematic diagram of the connected devices. In the MRI room (upper part), the anesthetized animal is fixed to the MRI-bed, lying on a thermal water-pad connected to the water heating system (located in the Operator room). The optic-fiber temperature sensor is introduced into the rectum of the animal and connected to the OpSens Multisens signal conditioner and acquisition system in the Operator room. The TherMouseDuino interconnects the temperature acquisition system with the water heating device.

4.2.2 Heating System

Thermo Scientific STANDARD Series Thermostats SC150 (ThermoFisher Scientific, Waltham, Massachusetts, USA) were attached to a Thermo Scientific SAHARA Heated Bath Circulator S5P (ThermoFisher Scientific, Waltham, MA, USA) water bath, which pumps water through pipes to warm up the bed of the animal. Underneath this bed there is a pad, which is in direct contact with the animal. By modifying the reference temperature, it is possible to vary the temperature of the animal; however, these variations are neither linear nor immediate. Between the bath and the pad several thermal losses occur, due to

the length of the tubing connecting them. This causes the temperature of the pad to not be exactly equal to that of the bath, but a few degrees below it.

The bath consists of a thermal system that has its own time constant (a small reservoir in charge of storing the fluid and maintaining its temperature). The distance that the fluid must travel until it reaches the bed creates a delay between changes in the control action and the response of the actuator (the bath). In addition, the thermostat model has a protection system for high temperatures. This function is useful to prevent the animal from being burnt. Furthermore, it serves to protect the fluid conducting elements, which are not designed to conduct a fluid at very high temperatures. It also has a low-level liquid protection system, which stops pumping water when the liquid is below a threshold.

4.2.3 Acquisition Device

To obtain the body temperature of the animal an OTP-M Fiber Optic [172] high accuracy optical temperature sensor (Opsens Inc., Quebec, QC, Canada) is used together with the signal conditioner OpSens MultiSens signal conditioner (Opsens Inc., Quebec, QC, Canada). It consists of a sensor designed for medical applications approved by the FDA that offers high precision and resolution in temperatures measurement. The temperature sensor uses a glass specifically designed for this type of applications.

The fiber optic transducer contains a temperature-sensitive optical device. In this case, since it is not a distributed temperature sensor, the temperature-sensitive zone is located at the tip of the sensor. The other end of the sensor is connected to the signal conditioner. This device is responsible for generating the light that passes through the optical fiber and, at the same time, for processing the received modified light signal, in order to convert these physical changes into units of measured temperature.

The OTP-M measures changes in the birefringence of the crystal used by the sensor. For this reason, there are no moving parts that could cause progressive deterioration of the sensor. These types of sensors are characterized by their high precision.

Once the sensor is connected, configured and calibrated in the MultiSens signal conditioner, it is possible to visualize the temperature it measures. On the backside, it has a RS-232 connector for serial communication. Through this connection, it is possible to communicate externally with the MultiSens.

4.2.4 Microcontroller

The Arduino Mega 2560 development board is a printed circuit allowing the use of a microcontroller ATMEGA2560 (Figure 4.2A)[173]. Arduino is commonly used in a high variety of research fields due to its versatility and low cost [170], [174]–[176]. This microcontroller controls 54 digital Input/Output pins,

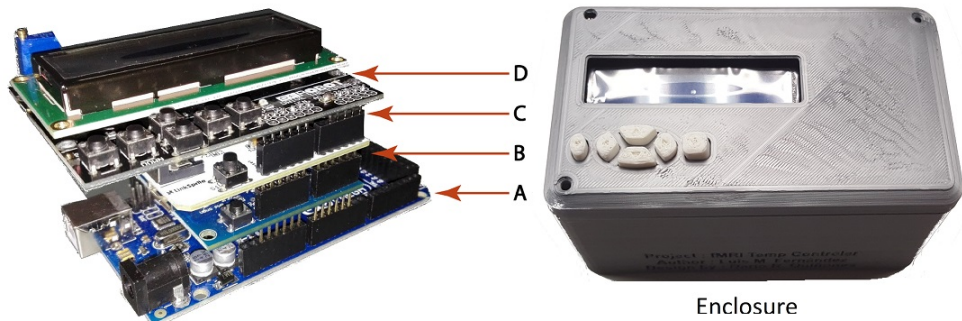


Figure 4.2. A) Arduino Mega 2560 development board. B) USB Host Shield V2.0 for USB communication with the ThermoScientific STANDARD Series Thermostat SC150. C) LinkSprite RS232 Shield V2 for RS-232 communication with the opSens Multisens signal conditioner. D) LCD Keypad Shield for the user interface.

15 pulse width modulation pins, 16 analog pins and is able to automate any system. Documentation and software are open source and available at the Arduino website. The programming software is based on the C/C++ language. Programs can be adapted to the evolution of the project. The power supply of this development board can be done through USB or main supply from 5V to 12V.

4.2.5 *USB Host Module*

For the communication of the Arduino with the thermostat SC150 the available USB port in the thermostat was used, meaning that, an additional USB port in the Arduino board was required. Using the USB Host Shield V2.0 for Arduino (Shenzhen KEYES DIY Robot co., Shen Zhen, China) (Figure 4.2B) it is possible to incorporate a standard type A USB port that allows communication with peripheral devices.

This module incorporates the integrated MAX3421E, which includes the digital logic and analog circuitry required to implement a USB port according to the USB design specifications in version 2.0. This operation is controlled by accessing a series of registers through an SPI interface. In this way, the Arduino MEGA 2560 microprocessor can incorporate a USB port using the connections of the SPI bus. This allows several peripheral devices to be simultaneously connected to the microcontroller.

Like the built-in module for RS-232 serial communication, the USB module allows direct connectivity with the Arduino, forming a compact multi-layer device.

4.2.6 *RS-232 Communication Module*

The above mentioned Arduino MEGA 2560 has only one USB port, used for communication with a personal computer and debugging, and a TTL UART interface. Nevertheless, to plug the signal acquisition device, a serial communication interface is needed. For this reason, an Arduino Shield with an RS-232 interface was attached to the Arduino Mega 2560. The LinkSprite RS232 Shield V2 (LinkSprite, Longmont, CO, USA) module for Arduino (Figure 4.2C) incorporates a DB9 port to the board. This module includes the integrated MAX232 and the necessary components to provide serial communication through the RS-232 standard. In addition, the RS232 Shield V2 design allows itself to be connected directly to Arduino, which improves their connection and permits a compact assembly.

4.2.7 LCD User Interface

To interact with the microcontroller, the LCD (Liquid Crystal Display) module Keypad Shield (DFRobot, Shanghai, China) for Arduino (Figure 4.2D) was added. This shield incorporates an LCD and a five-button keyboard and acts as a user interface with the Arduino.

This module provides a friendly user interface, permitting the user to move within the menus and to select the desired option. The screen consists of 2 rows and 16 columns. Furthermore, it also incorporates an additional microcontroller reset button. In the shield upper left corner, there is a potentiometer that allows the user to adjust the contrast of the LCD screen. This module provides the control of the temperature and it permits to display information (e.g. the selected reference temperature or the temperature of the animal).

4.2.8 Model Identification

Before designing the regulator, a mathematical approach to the system was obtained. The process of identifying a system model consists of finding mathematical equations that approach the behavior of the real system [177]. The model should be able to reproduce the outputs to different inputs. However, it should also be as simple as possible to achieve the objectives of the system quickly and without requiring a high computational demand. For this reason, it is necessary to reach a compromise between fidelity and computational cost.

The system processes comprising the biological regulation mechanisms of the animal have a high degree of complexity, and they cannot be easily approximated using mathematical equations [178], [179]. For this reason, experimental identification was considered the most appropriate modeling method [177].

Unitary Step Response was the experimental methodology employed [180] for model identification. By means of this test, it is possible to determine the dynamic characteristics of the system and the output gain. The steps that are carried out for this type of identification are:

1. Move the system to the operating point. The first step was to bring the temperature of the system near the operating temperature.

2. When the temperature became steady, a positive step was entered as an input to the system [180]. In this case, the positive step was 2°C.
3. When the new equilibrium was reached, the previous 2°C increment was retracted to return to the initial operating point. As in the previous steps, it was necessary to wait for the system to regain equilibrium.
4. Finally, a negative step was introduced at system input with the same amplitude as the positive one, followed by repetition of steps 2 and 3.

After performing the mentioned steps, a system model was implemented in MATLAB (The Mathworks Inc., Natick, MA, USA). With the *System Identification Toolbox*, different models were obtained and, based on the percentage of adjustment, a model was chosen.

4.2.9 PID Control

A PID controller is a feedback control mechanism widely used in industrial control systems. This mechanism calculates the deviation or error between a measured value and a desired value. The PID control algorithm consists of three different parameters: proportional, integral and derivative. The proportional value depends on current error. The integral depends on past errors and the derivative is a prediction of future errors, which is based on past error trends. The sum of these three actions is used to adjust the process by means of a control element such as the position of a control valve or the amount of power supplied to warm up a heater.

For unknown processes, it has historically been considered that the PID controller is the most suitable controller. By adjusting these three variables in the PID control algorithm, the controller can provide a control action designed for specific process requirements. The controller response can be described in terms of a control response to an error, the degree to which the controller exceeds the desired setpoint (overshoot), and the degree of oscillation of the system.

Some applications may only require one or two modes provided by this control system. PI controllers are particularly common because the derivative action is

very sensitive to noise, and the absence of the integral process can prevent it from reaching the desired value due to the control action [181], [182].

4.2.10 Animals and MRI Acquisition Protocol

Some functional MRI experiments were carried out in order to test the effectivity of the TherMouseDuino in controlling mouse's temperature and its impact over the evoked BOLD signal in real conditions. Experiments were carried out in a horizontal 7 T scanner with a 30 cm diameter bore (Biospec 70/30v, Bruker Medical, Ettlingen, Germany). The system has a 675 mT/m actively shielded gradient coil (Bruker, BGA 12-S) of 11.4 cm inner diameter. A 1H rat brain receive-only phase array coil with integrated combiner and preamplifier, no tune/no match, in combination with the actively detuned transmit-only resonator (BrukerBioSpin MRI GmbH, Germany) was employed. Data were acquired and processed with a Hewlett-Packard console running Paravision 5.1 software (Bruker Medical GmbH, Ettlingen, Germany) operating on a Linux platform. For the fMRI experiments, mice (n=3) were anesthetized with isoflurane (4% induction, 1-2% maintenance). Anesthetized animals were placed in a custom-made animal holder with adjustable bite and ear bars, and positioned on the magnet bed. The animals were constantly supplied with 0.8 L/m O₂ with. The heart rate, SpO₂, and breathing rate were monitored throughout the session (MouseOx, Starr Life Sciences, Oakmont, US). Temperature was controlled using the presented device.

4.2.11 Surgery for fMRI experiments

Mice were anaesthetized with urethane (1.4 g/kg) and fixed in a stereotaxic frame (Narishigue, Tokyo, Japan). We placed a custom made carbon fibre MRI-compatible electrode [148], [183] in the perforant pathway (-4.3 mm AP, -2.5 mm LM, +1.4 mm DV, 12° angle). Briefly, a bunch of 7 μm diameter carbon fibres (Goodfellow Cambridge Limited, Cambridge, UK) were introduced into a pulled double borosilicate capillary (WPI, ref. TST150-6") with $\cong 200\mu\text{m}$ tip diameter and electrical impedance of 40-65 k Ω . A wire connector was coupled to the carbon fibres using silver conductive epoxy resin (ref: 186-3616, RS components, Madrid, Spain) and isolated with rapid epoxy resin (Araldite, Basel, Switzerland). Pulled capillary tip was bent to form a 90° angle and then implanted into the perforant pathway. The carbon fibre electrode was secured to the skull with super-bond

C&B dental cement (Sun Medical Co. LTD, Moriyana, Shiga, Japan). Then the animals were carried to the fMRI facility and placed in a custom made animal holder with adjustable bite and ear bars and positioned into the horizontal 7-T scanner (Biospec 70/30, Bruker Medical, Ettlingen, Germany). Animals were constantly supplied with 0.8 L/min O_2 through a mask. Temperature was set at 37°C using the developed device.

All experiments were approved by our institution's Animal Care and Use Committee and complies with the Spanish (law 53/2013) and European regulations (EU directive 86/609, EU decree 2001-486 and EU recommendation 2007/526/EC).

4.2.12 fMRI data extraction

Functional images acquisition was performed in coronal slices using a GE-EPI protocol applying the following parameters: field of view (FOV) 25x25 mm, slice thickness, 1 mm; matrix, 96x96; segments, 1; FA 600; time echo (TE), 15 ms; time repetition (TR), 2000 ms. T2-weighted anatomical images were collected using a rapid acquisition relaxation enhanced sequence (RARE): FOV, 25x25 mm; 12 slices; slice thickness, 1mm; matrix, 192x192; TE_{eff}, 56 ms; TR, 2 s; RARE factor, 8. A 1H mouse brain received -only phased- array coil with integrated combiner and preamplifier, and no tune/no match, was employed in combination with the actively detuned transmit-only resonator (Bruker BioSpin MRI GmbH, Germany). Functional MRI data were analysed offline using our lab own software developed in Matlab, which included Statistical Parametric Mapping packages (SPM8, www.fil.ion.ucl.ac.uk/spm) and Analysis of Functional NeuroImages (AFNI, <http://afni.nimh.nih.gov/afni>). After linear detrending, temporal (0.015-0.2 Hz) and spatial filtering (3x3 gaussians kernel or 1.5 sigma) of voxel time series, a general linear model (GLM) was applied. Functional maps were generated from voxels that had a significance higher than $p < 0.01$.

4.3 Results and Discussion

4.3.1 Experimental Identification Results

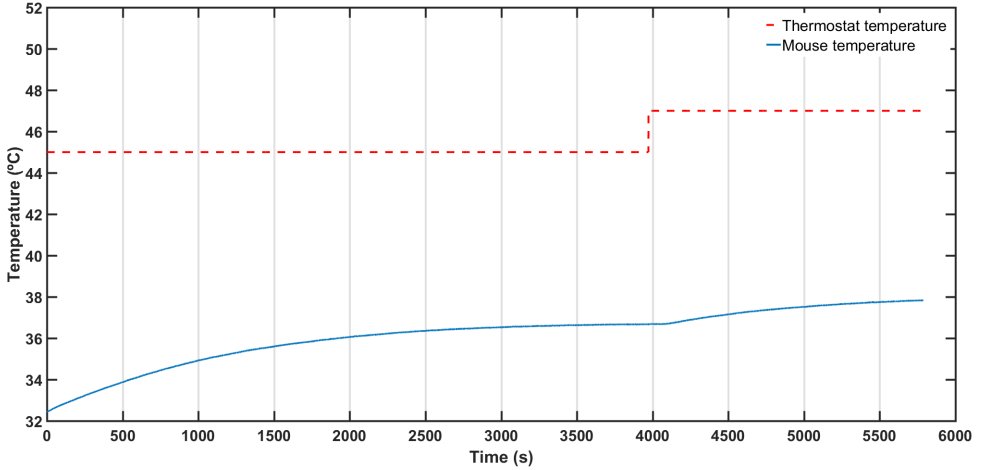


Figure 4.3. The data shown correspond to an fMRI experiment with a mouse. The dashed line shows a 2°C positive step in the bath. The continuous line represents the body temperature of the mouse during the experiment. It is possible to observe that mouse body temperature starts to be stable at 3500 seconds (1 hour approximately) after the unitary step. The figure shows how the positive step in the heating system affects body temperature.

Experimental identification of the model parameters was performed with a mouse in an fMRI experiment. First, the mouse was anesthetized and placed into the MR scanner. Due to the loss of thermoregulation induced by anesthesia, body temperature drops quickly below 33°C (Figure 4.3). Initially, the water bath temperature was set at 45°C . This temperature was selected to raise the body temperature of the mouse to the desired operating temperature ($37 \pm 0.5^{\circ}\text{C}$). When the temperature of the animal had stabilized at $36.5 \pm 0.3^{\circ}\text{C}$, a positive step of 2°C was applied, raising the bath temperature to 47°C . This generated a variation in the body temperature of the animal, which is taken as output.

To study the abovementioned output as a response to the input (positive step), a data preprocessing was performed. It consisted of normalizing the

data and selecting the necessary data window. (Figure 4.4). The output curve

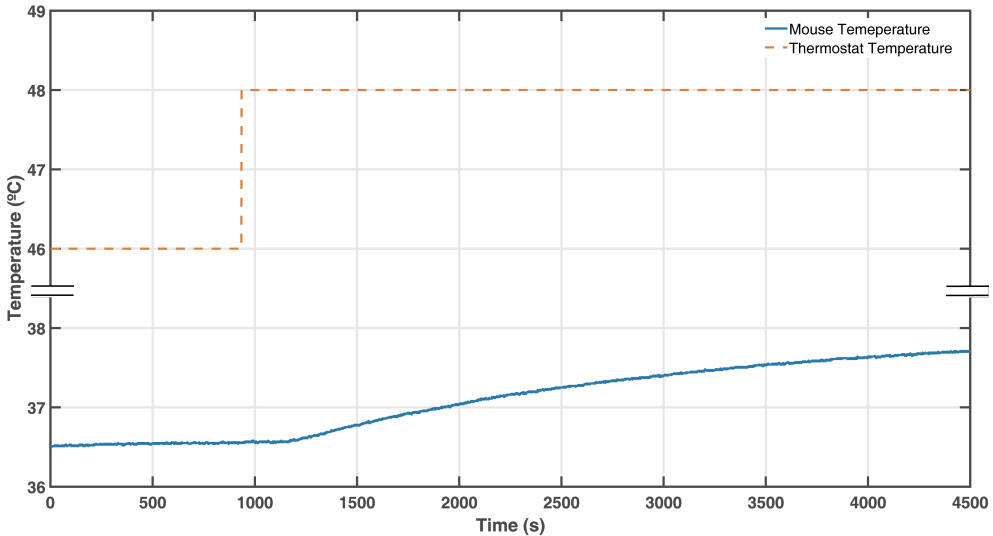


Figure 4.4. This graph displays the response of body temperature of the animal to a 2°C increase in the thermostat temperature. The selected and normalized data window was employed for the experimental identification. The dashed line shows the input temperature positive step applied to the system. The continuous line shows the body temperature of the mouse during the experiment

mimics the curve corresponding to a first-order system. However, there is a small delay between the input signal and the system response. This is due to a delay introduced by the dynamics of the actuators and the own physiology of the animal. When a new temperature is set in the bath thermostat, the fluid takes some time to reach that temperature.

Experimental identification must be a compromise between the complexity of the estimated model and the benefit that this complexity reports. A mathematical model was calculated from the above mentioned data as shown in Figure 4.5. This mathematical model has a small difference in the percentage of fit between a first-order model and greater order models. Therefore, the first-order model without delay ('TF (fit 91,49%)' in Figure 4.5) was selected. The estimated model for the mouse system is shown in Equation 4.1.

$$G(s) = \frac{K}{1 + \tau \cdot s} = \frac{0.6792}{1 + 952.38 \cdot s} \quad (4.1)$$

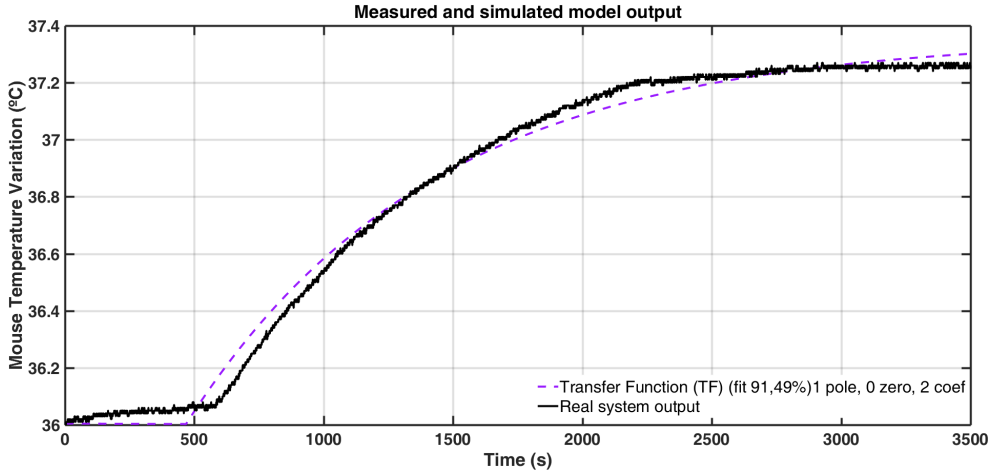


Figure 4.5. This image displays the output of the real system against a positive step input (continuous line) and, the simulated output of the final mathematical model (Transfer Function).

where the static gain of the system $K = 0.6792$ and the time constant $\tau = 952.38$ seconds ($\cong 16$ minutes).

4.3.2 Control System Design Results

Once an approximate model of the real system was obtained, the next step was to translate the specifications that the control system must meet to mathematical constraints. With reference to dynamic specifications, one of the requested conditions was establishment time (t_e). This condition was adjusted to experiment preparation time, that is, 30 to 45 minutes used in the placement of the animal, survey images, and adjustments for the homogeneity of the magnetic field. The regulator was required to be capable of reaching the reference temperature within that time range. Next, it was desired that the temperature in steady state were maintained at a physiological level of $37 \pm 0.5^\circ\text{C}$. Additionally, an

overshoot that not exceeds 37.5°C was required, in order to keep the physiological temperature.

In terms of steady error, this should be zero. However, this condition will be extremely demanding for a thermal system. Due to this fact, the acceptable error was established at $\pm 0.5^\circ\text{C}$. Finally, an oscillation in steady state was deemed undesirable. To avoid overheating or burning the skin of the animal, the control action was limited to 50°C. High control actions will not represent the real control system because the abovementioned limit will not allow them. These constraints limit the design of the control system.

These specifications were transferred to the MATLAB control systems design tool. Using the mentioned tool, the root locus of the system with all the constraints was calculated. This corresponds to a unit gain proportional controller (i.e. output is directly proportional to input). However, there is one main drawback, this system does not ensure a null error in the steady state. In order to solve this, an integral control action was introduced along with the proportional action to ensure the minimal stationary error. The PI regulator equation in zeros and poles form is shown in Equation 4.2.

$$PI(s) = \frac{K_R(s + b)}{s} \quad (4.2)$$

The tuning of the regulator consists of obtaining values of K_R and b that allow fulfillment of the specifications in closed loop. The PI regulator consists of a pole at the origin and a zero. The method used for tuning the regulator is the poles and zeros adjustment [177]. A zero is added to a tenth of the pole of the system ($b = 0.000105$). This zero was required to know the Integrative Time (T_i) as it is shown in Equation 4.3

$$T_i = \frac{1}{b} \quad (4.3)$$

The goal is not to overturn the root locus. This zero adjustment is called “the empirical criterion”. The last step is tuning the gain in order for the specifications to be achieved. We decided to select an energetic PI regulator with a $K=5$. This

can cause saturation of the control action, but it is necessary to accelerate the process as much as possible in order to meet the establishment time specification.

To eliminate the steady state error, the integral control action was increased. The steady state error was eliminated with an integer value of $Ki = 0.01$, but a small overshoot was introduced in the system response (Equation 4.4).

$$Ki = \frac{K}{Ti} \quad (4.4)$$

Nevertheless, this overshoot was acceptable with the required specifications, since it did not exceed the temperature of 37.5°C . The set-up time is around 2700 seconds (45 minutes), which is in conformity with the specifications. Finally, the accepted parameters for the PI controller and the results obtained are shown in Figure 4.6. An overshoot still appears at the system output, but we deem it to be within the acceptable range. This corresponds to one of the required specifications. In addition, the temperature oscillations around the reference were negligible. The regulator is responsible for maintaining this temperature with the smallest possible error. This allows reduction of the setup time necessary for image acquisition and provides automatically a stable temperature through the course of the fMRI experiment.

An example of fMRI experiment in mice can be seen in Figure 4.7A and Figure 4.7B. In this study we stimulate the perforant pathway, main input from the entorhinal cortex to the hippocampus, to investigate the global consequences of local synaptic plasticity (i.e. [183], [184]).

These experiments require long periods of brain imaging to monitor longitudinally the consequences of short- and long-term plasticity. During the complete recording time, the physiology of the animal needs to be exquisitely constant, in order to preserve the quantitative value of the BOLD signals [143], [148], [167]. Only a control experiment without induction of synaptic plasticity is shown in Figure 4.7C, to illustrate the high stability of the signal in time.

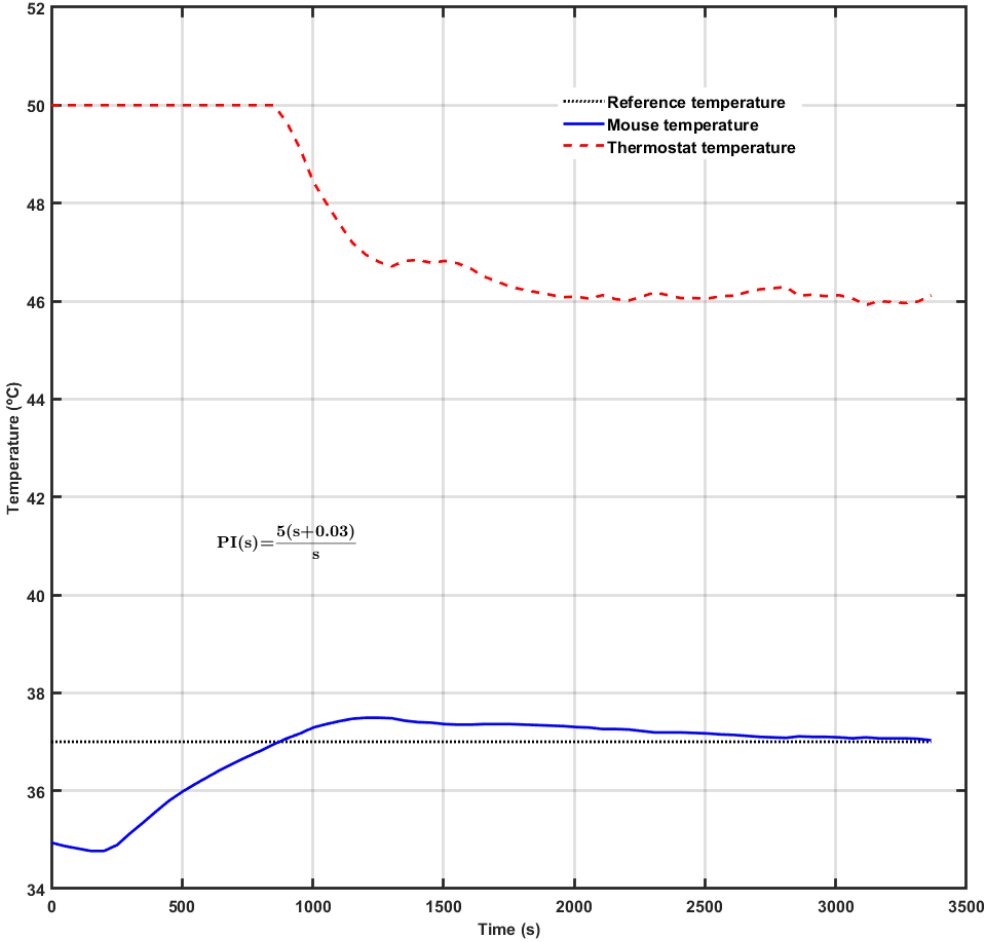


Figure 4.6. This figure shows the results for the final PI regulator meeting the required specifications. It shows the data output obtained in an fMRI experiment with an anesthetized mouse. The body temperature of the mouse (continuous line) and the thermostat temperature (dotted line) are shown.

4.4 Conclusion

Results obtained by fMRI based on the BOLD contrast are very sensitive to physiological changes. The use of anesthetics for experimentation with animals causes alterations in their temperature regulation system. This translates into important variations in the MRI images obtained. Commonly used systems to

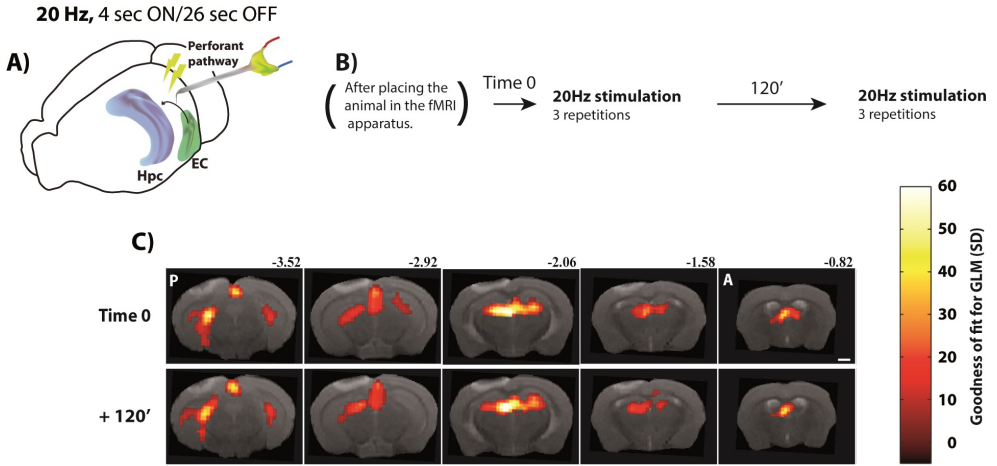


Figure 4.7. BOLD response for 20Hz electric stimulation in the perforant pathway. A) Scheme of the carbon fibre electrode implanted in the perforant pathway. B) Timing of the fMRI acquisitions in the experiment. C) Representative T2-weighted anatomy images with overlaid functional maps evoked during stimulation of the perforant pathway (20Hz, 0.8 mA). Scale indicates 1 mm. Colour-bar indicates the goodness of fit for the General Linear Model (GLM) applied, comparing activation during the 20 Hz stimulation train (ON period, 4 sec) vs. baseline (OFF period, 26 sec). Numbers above the images represent mm from bregma. P: posterior; A: anterior. Threshold for GLM significance set on $p < 0.01$.

maintain body temperature are manual, requiring continuous inspection by the researcher or the technician performing the experiment. By using an automatic control system based on Arduino we have developed an Open-Source temperature control device for fMRI experimentation in mice.

Model and experimental result demonstrate the viability of the system for maintaining the temperature of the anesthetized animal within the physiological range and meeting user specifications that assure its practical use. TherMouse-Duino can control both, increases and decreases in temp. It just needs to be coupled to the specific hardware (e.g. a cooler system).

TherMouseDuino therefore, provides an automatic, safe and precise control of body temperature for anesthetized mice. It was tested with strain C57 (inbred line) and ICR (outbred line) with the same satisfactory result in both cases. In addition, all the schematics, parts and firmware are available at <http://dmoratal.webs.upv.es/research.html>.

Chapter 5

A Tangible Educational 3D Printed Atlas of the Rat Brain

In biology and neuroscience courses, brain anatomy is usually explained using Magnetic Resonance (MR) images or histological sections of different orientations. These can show the most important macroscopic areas in an animals' brain. However, this method is neither dynamic nor intuitive. In this work, an anatomical 3D printed rat brain with educational purposes is presented. Hand manipulation of the structure, facilitated by the scaled up of its dimensions, and the ability to dismantle the 'brain' into some of its constituent parts, facilitates the understanding of the 3D organization of the nervous system. This is an alternative method for teaching students in general and biologists in particular the rat brain anatomy.

The content presented in this chapter has been adapted from the following publication:

D. R. Quiñones, J. Ferragud-Agulló, R. Pérez-Feito, J. García-Manrique, S. Canals, and D. Moratal, “A Tangible Educative 3D Printed Atlas of the Rat Brain”, *Materials*, vol. 11, no. 9, p. 1531, 2018. DOI: 10.3390/ma11091531

5.1 Introduction

Neuroimaging technologies, such as Computed Tomography (CT) and Magnetic Resonance Imaging (MRI), are indispensable tools for the diagnosis and treatment of central nervous system diseases [186]–[191]. Even though MRI and Computed Tomography (CT) techniques collect 3D data, clinicians typically view these data on 2D screens. 2D representations limit our appreciation of complex structures, such as brain convolutions, and 2D displays of these models on computer screens prevent us from interacting with a model of the physical brain. A tangible physical model based on MR images or digital templates would permit biologists, neuroscientists and students to complement information obtained by 2D and virtual 3D imaging. Furthermore, physical 3D models could be more advantageous for clinical education than computer-based 3D models [192]–[194]. Therefore, high-resolution multiscale and multimodal 3D models of the brain can be seen essential tools to understand its complex structure and organization [195].

The most widely used MRI template of a rat brain is that developed by Schwarz et al. [196]. It is co-registered with the stereotaxic co-ordinates of the Paxinos and Watson (1982) digital atlas [131]. The template set provides anatomical images as well as tissue class probability maps for brain parenchyma and CerebroSpinal Fluid (CSF). The use of this template paves the way for the use of standard fMRI software for tissue segmentation of rat brain data. This enables the atlas structure and the stereotaxic coordinates that correspond to a feature within a statistical map to be interactively reported, which facilitates the localization of functional effects. Furthermore, voxels, which are within selected brain structures, can be combined to define anatomically based 3D volumes of interest (VOIs) [196]. The use of standard functional MRI (fMRI) software for tissue segmentation of rat brain data is facilitated by the use of this template.

3D printing is rapidly becoming a source of novel biomedical applications, as well as a cost-effective mean of producing customized 3D objects [197]–[200], for example, printing organic tissue [201] or developing scaffolds for tissue engineering [202]. However, some of the most complex applications use high-end industrial printers that are too expensive for educative purposes or even for research centers with limited funds. Nonetheless, the progression of open source platforms has increased the capabilities and popularity of desktop 3D printers.

In this work, we describe a step-by-step, end-to-end easily replicable methodology to generate and scale a 3D printed model of a rat brain with the most important macroscopic regions. It is based on an MRI template of the rat brain co-localized with the Paxinos and Watson rat brain atlas, combined with 3D computer-aided design (CAD) tools and 3D prototyping technologies to obtain a didactic 3D printed brain. Furthermore, each 3D printed region of the brain is designed to be easily attached to or detached from the other parts.

This model could have a big impact on the way biologists and neuroscientists teach in the future. It makes more “tangible” the understanding of the relevant areas of the brain for teaching, while reduces the use of experimental animals for these purposes. In addition, the methodology can be extrapolated to different regions of the brain or even to other body regions.

5.2 Materials and Methods

The process of generating 3D objects from images generally follows these steps: (i) selection of the data, (ii) segmentation of the region of interest (ROI), (iii) transformation of the data from 2D ROIs to a 3D triangular mesh, (iv) editing the 3D mesh (in order to clean uneven areas, add support structures, etc.), (v) transferring the data to 3D printer software in order to create printing coordinates and (vi) sending it to production (Figure 5.1).

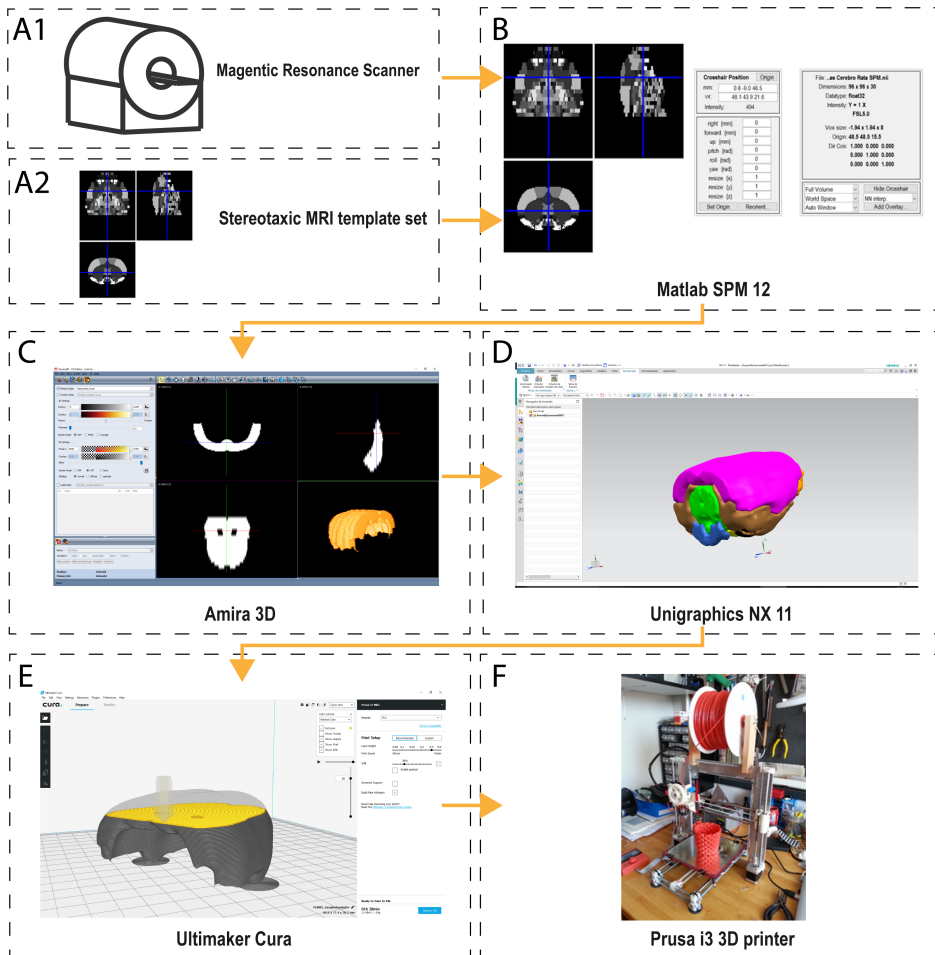


Figure 5.1. First, images from a CT or MRI scanner (A1) are colocalized with a stereotaxic template (A2). Next, these images are clustered in SPM (B) in order to create the Voxels of Interest (VOI). With this set of images, a 3D reconstruction is created in Amira 3D software (C). Then, the 3D surface, which was created in Amira, is opened in a 3D design tool, e.g. Unigraphics NX, (D) where 3D surfaces are converted into 3D solid bodies. These solid bodies are provided with joints and connectors to add detachable properties to the 3D printed body. Once this process is complete, the manufacturing process starts (E). This consists of transforming the 3D body into a physical set of coordinates, which the 3D printer can interpret. In this case, a Prusa i3 MK2 3D printer with Cura software was used (F).

5.2.1 Data Selection: The 8 Most Relevant Macroscopic Areas in the Rat Brain

The first step in creating 3D printed models from a digital atlas is the selection of the regions of interest. The image data choice is important; low-resolution images can result in a discrepancy between the generated model and actual anatomy. In this particular case we chose a stereotaxic MRI template set for the rat brain with tissue class distribution maps made by Schwarz et al, [196] and co-registered anatomical atlas “*The Rat Brain in Stereotaxic Coordinates*” from Paxinos and Watson (1982) [131]. This document shows sagittal and coronal cuts throughout the brain of a specimen rat. The atlas partially contains all the encephalon of a rat, but the brain is the main part which appears in the MRI atlas. However, the whole cerebellum, the medulla and the olfactory bulb are not included in the atlas.

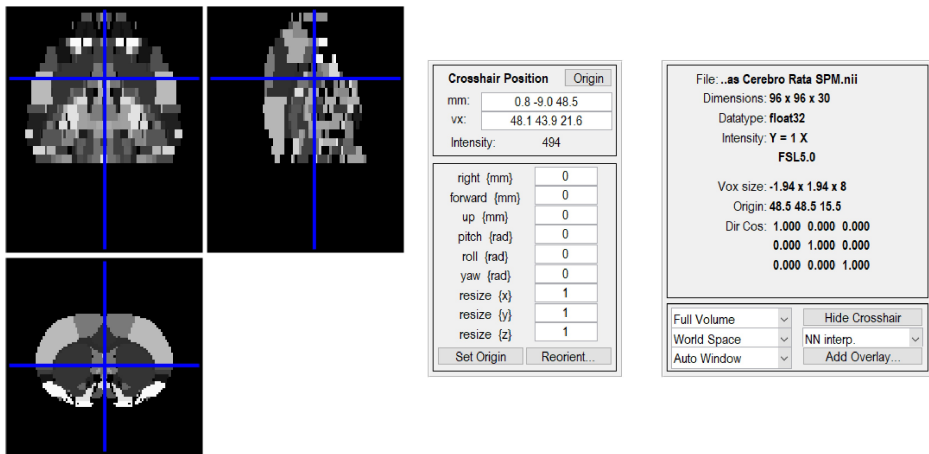


Figure 5.2. The image represents a slice of the employed digital atlas whereas the specific coordinates are shown in SPM 12.

The MRI template that was used is the one presented in [196]. Briefly, this template was created from multi-slice T2-weighted images of a rat brain acquired using a RARE sequence on a Bruker Avance 4.7-T MR scanner with the following acquisition parameters: RARE factor 8, matrix 256 X 256; FOV

40 mm, slice thickness 1 mm, 32 contiguous coronal slices; $T_{\text{Reff}} = 5500$ ms; $T_{\text{Eeff}} = 76$ ms. A 72-mm birdcage resonator was used for RF transmission and the Bruker quadrature FRat Brain_ coil was used for RF reception. The images were acquired in the coronal plane, centered 8 mm caudal from the posterior edge of the olfactory bulb [196]. Each region is marked with a different gray intensity. There are 466 brain regions that were clustered into 38 sub-regions and grouped into 8 regions with the participation of an experienced neurobiologist. These parts correspond to the eight pieces of the printed rat brain that is presented in this project (table 5.1).

Regions	Sub-region
Neocortex	Cortex Parietal Association, Cortex Retrosplenial, Cortex Temporal Association, Corpus Cortex Sensory, Cortex Motor, Cortex Insular, Cortex Frontal Association, Cortex Orbitofrontal, Cortex Medial Prefrontal, Cortex Cingulate, Collosum
Archicortex	Hippocampus, Cortex Entorhinal Piriform
Paleocortex	Olfactory Nuclei, Olfactory Tubercle
Basal Ganglia	Globus Pallidus, Amygdala, Diagonal Band, IPAC, BNST, Caudate Putamen, Ventral Pallidum, Substantia Innominata, Caudate Putamen
Basal telencephalon	Septum, Accumbens
Diencephalon	Hypothalamus, Thalamus, Medial Geniculate, Zona Incerta
Midbrain	Raphe, Mesencephalic Region, Substantia Nigra, Periaqueductal Grey, Superior Colliculus, Interpeduncular Nucleus, VTA (Ventral Tegmental Area)
Metencephalon	Pons

Table 5.1. Regions clustering.

In order to visualize and choose the desired areas from the stereotaxic MRI template set, a specific software was needed. In this case, Statistical Parametric Mapping 12 (SPM12) [203], which is designed as a MATLAB (Mathworks Inc., Massachusetts, United States) toolbox, was chosen (Figure 5.2), because it is the most suitable and open source software available for this purpose [204], [205]. SPM is an academic software toolkit for the analysis of functional imaging data for users familiar with the underlying statistical, mathematical and image processing concepts. SPM12 can be also executed on GNU/Octave [206], which is an Open-Source alternative to Matlab. Once the areas were chosen in the atlas and identified in the MRI template set, they were grouped in SPM and saved in different files in *NIFTI* format (.nii).

The *OBJ* file format is a simple data-format that represents 3D geometry. It gives the position of each vertex, the UV (coordinates for projecting 2D images to a 3D model) position of each texture coordinate vertex, vertex normals, and the faces that make each polygon defined as a list of vertices, and texture vertices. However, this format has a drawback: it is not easily editable because it only represents the surface of the 3D body with the necessary number of triangles. It does not represent the 3D object as 3D solid body. This means that the Boolean 3D operation (e.g. add, subtract, intersect) cannot be easily applied. In our specific case, it was necessary to edit the geometry of the resulting 3D faceted body, because the objective was to create an easily detachable 3D brain.

5.2.3 *Transforming the Facet Body into an Editable Solid Body*

In order to create a 3D brain with interlocking plastic parts it was necessary to edit the facet bodies that were previously generated, and then to add fastener joins. This process was performed with Unigraphics NX 11 (Siemens, Munich, Germany). This software, widely used in the industry, enables design, structural analysis, simulations and image study, among other things. Through a program of this type, it is possible to create 2D and 3D designs from scratch, or to modify files from other sources. FreeCAD (Blender Foundation, Amsterdam) can be used as Open-Source alternative to Unigraphics NX. Using these features, the *OBJ* files were imported and analyzed as a convergent body. Then each analyzed part was converted into an editable 3D solid body. However, as it is shown in Figure 5.4A, the resulting shape is not as smooth as could be expected. These uneven surfaces are due to the low resolution of the template. To correct this, a constrained smoothing process was applied to each of the 8 macroscopic regions. There are two methods of smoothing the surface of the 3D object. One, which is less computationally demanding, is using Amira 3D, but it has some drawbacks as shown in Figure 5.4B. This method creates a well-smoothed body, but it suppresses relevant details of the region. The other method is more computationally demanding and involves a tool of Unigraphics NX called “*surface smoothing*”, which allows smoothing of the surfaces without losing the relevant morphology of the region. This second method was chosen for all the bodies that were extracted from the template.

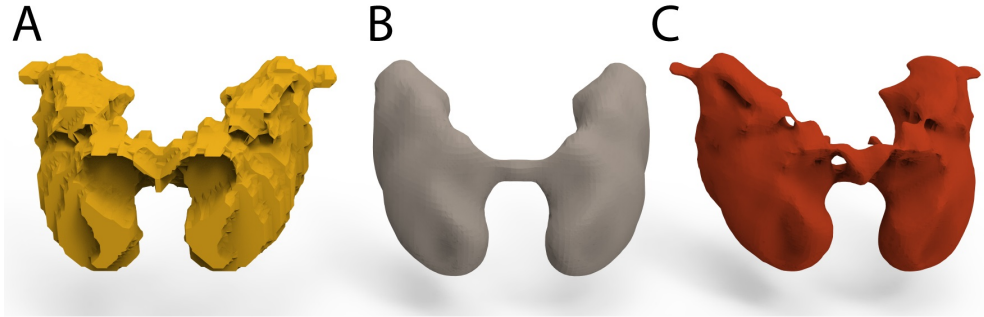


Figure 5.4. A. Basal ganglia before being smoothed. B. Smoothing process with Amira 3D software. C. Smoothing process with Unigraphics NX.

In order to create the joints for each component, the ideal position of the joint was studied for each part. According to the part dimension the position of the joint was determined as an extrusion (male) or a depression (female). Then each joint was added to the corresponding part in Unigraphics NX by converting the joint and the part into a unique 3D solid body.

The joints were added with a 5% tolerance to facilitate attach and detach parts after being 3D printed. As it is shown in Figure 5.5, each joint was created in a specific place and as specific shape in order to facilitate an interconnection between the parts. The Archicortex was further divided into 2 parts in order to make it easy to assemble and disassemble the inner parts of the brain.

5.2.4 Rapid Prototyping

Rapid prototyping can be defined as an approach or methodology used to quickly manufacture physical models using 3D CAD data. Rapid prototyping has also been referred to as solid free form, computer-automated or layered manufacturing. Rapid prototyping has its obvious use as a truly 3D method for visualization and better haptic interaction.

Nowadays, 3D home printers have become more accessible than industrial 3D printers, and this has increased the number of “Do It Yourself” (DIY) projects that are underway. The most affordable and common type of rapid prototyping is Fused Deposition Modelling (FDM) technology, also known as Fused Filament

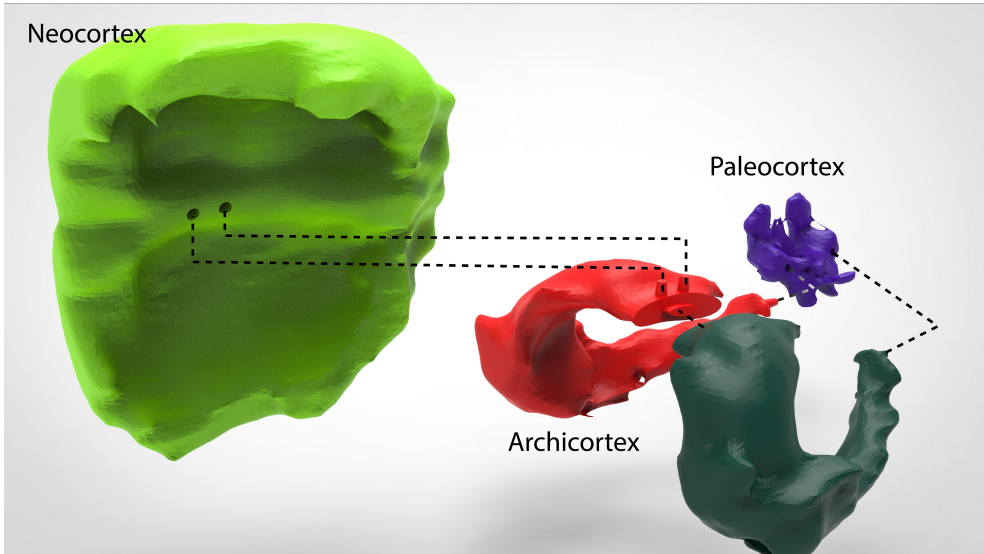


Figure 5.5. Figure shows the interconnecting joins among three parts of the brain 3D model. It is possible to appreciate that the Neocortex, as well as the Paleocortex, has two depressions. These depressions fit perfectly with the protuberances on the top of the Archicortex.

Fabrication (FFF). There are also more types of rapid prototyping, such as Stereolithography (SLA) or Selective Laser Sintering (SLS) [207], which are more accurate and detailed but which cost more[208]. FDM technology prints an object one layer at a time by extruding heated plastic through a nozzle, while moving around a flat hot surface (hot bed).

A Prusa i3 MK2 with a precision of 50 microns per layer height, and a printing surface of $10,500\text{ cm}^3$ (25 x 21 x 20 cm or 9.84 x 8.3 x 8 in) was used to print all of the parts. With these manufacturing constraints and the modified solid models with the joins, a scale of four times the actual size (4:1) was chosen in the printing software Ultimaker Cura (Geldermalsen, Netherlands).

5.3 Results

The final 3D printed model of the rat brain (Figure 5.6) is composed of the eight smoothed parts, all of which fit together perfectly. The scaled measures of each part are shown in table 5.2.

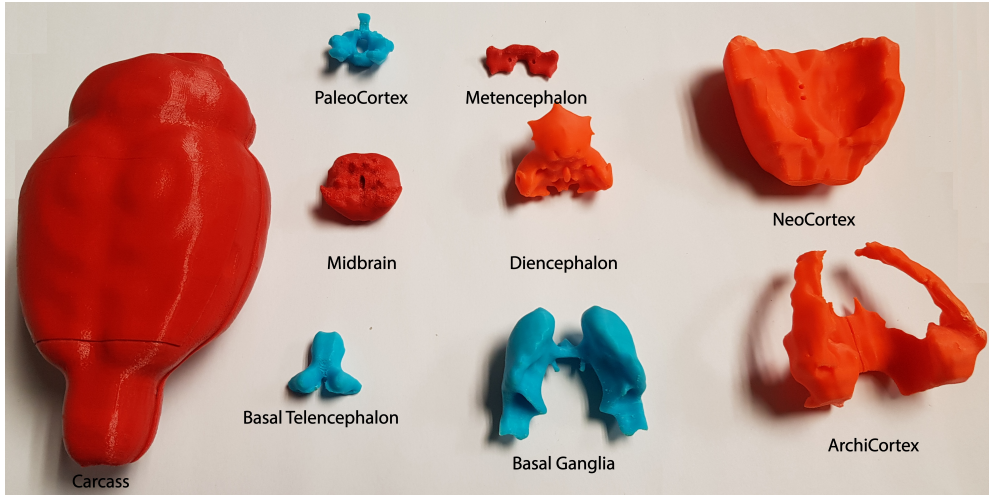


Figure 5.6. Final 3D model (disassembled) of the rat template.

Part	X (mm)	Y (mm)	Z (mm)	Part	X (mm)	Y (mm)	Z (mm)
Neocortex	59.60	28.94	54.40	Midbrain	26.72	24.90	15.10
Archicortex1	28.58	30.19	50.38	Metencephalon	26.43	12.48	6.02
Archicortex2	32.08	30.19	50.38	Bottom Cover	69.54	30.08	131.73
Paleocortex	24.00	17.94	18.69	Upper Cover	69.07	39.04	132.66
Basal ganglia	51.01	25.98	34.83	Small Cover	64.46	13.73	49.60
Basal Telencephalon	22.83	18.45	15.84	Total without cover	59.60	38.37	57.60
Diencephalon	33.02	24.35	30.35	Total with cover	69.54	52.34	132.66

Table 5.2. Measurements on X, Y, Z axes of each part, total assembly without container and total assembly with container.

An external container was made in order to accommodate the eight regions. This container was designed using the external contour of the brain in the template. It was then enlarged a little (4.2:1) in order to facilitate the accommodation of the other parts as well. In addition, the cover was divided in two in order to make it possible to open as shown in Figure 5.7.

Figure 5.6 shows the whole-brain model disassembled, all 8 parts plus the container that encloses them. Figure 5.7 shows that all of the parts fit perfectly together.

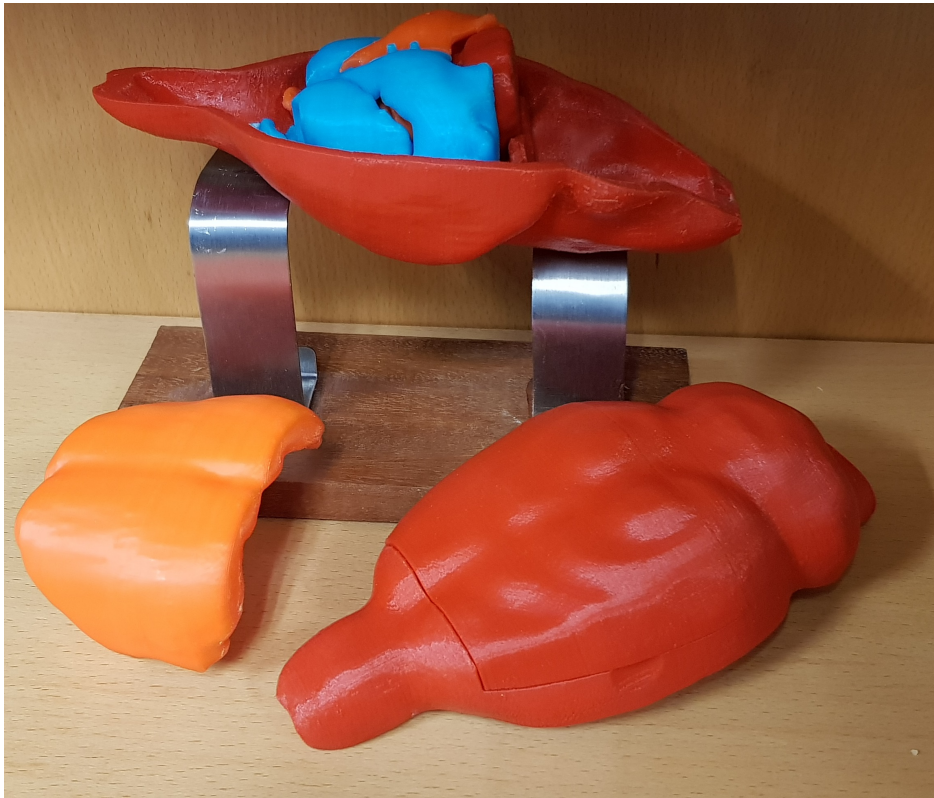


Figure 5.7. Final 3D model of the rat template.

In terms of material for the printing process, poly(lactic acid) (PLA) was chosen. This material is a thermoplastic polymer that is made from renewable

resources. It melts at 160 degrees Celsius and it is less rigid than Acrylonitrile butadiene styrene (ABS), another commonly used material in 3D printing. This is important for the 3D model because it makes the printed parts more elastic and shock-resistant.

5.4 Discussion

Rapid prototyping has grown beyond its initial use in industrial sectors, e.g. the automobile industry, and today can be regarded as one of the most promising techniques for use in medical imaging. Although medical applications are relatively recent, their enormous potential has already been demonstrated in several studies [209]–[211]. Rapid prototyping objects are useful for training surgeons, as they allow surgical procedures to be simulated in a realistic manner. Even though medical research has already benefitted from rapid prototyping [212], [213] and efforts have been made in the development of artificial organs and tissues [214], [215], the traditional approach of teaching anatomy remains the same. This approach focuses mainly on MRI, CT and dissections of real animals, without taking into consideration any variations and pathological changes. Currently, there is a well-known rat brain model called “C29 Rat Brain Comparative Anatomy”, which is interesting from an educational point of view, but is not detailed enough for scientific purposes. The 3D printed brain that is presented in this project could serve as the medium for bringing anatomical variations to pre-clinical studies in order to improve the understanding of anatomy [192] while preserving animal lives. In addition, by using other materials to adapt transparency or rigidity, certain aspects can be emphasized for the trainee and the student. In the scientific domain, adding the cranium of the subject to the 3D model, we envision applications of this approach in designing and probing brain implant prototypes, as recording chambers, electric and/or optogenetic stimulation holders, and designing coils for transcranial magnetic or direct current stimulation.

5.5 Conclusions

To obtain the necessary images to generate the 3D parts, a digital atlas, which was correlated with a stereotaxic anatomical atlas, was used. With the participation of an experienced biologist a total of 466 structures were extracted and clustered into eight different parts, which correspond to the eight pieces of the printed rat brain that is presented in this project. These parts are the Neocortex, the Archicortex, the Paleocortex, the Basal Ganglia, the Basal Telencephalon, the Diencephalon, the Mesencephalon, and the Metencephalons. Each part has joins in order to fasten together the different parts. Also, a housing formed by three additional pieces was created. This in turn performs the function of storing the rest of the pieces and serves as a spatial orientation for the assembly of the brain. In further researches, a complete rat brain with 38 sub-regions will be developed. This work presents a methodology that could be expanded to almost any field of clinical and pre-clinical research, and moreover it avoids the need of dissect animals in order to teach anatomy.

Automatic Positioning Device for Cutting 3D Tissue in Living or Fixed Samples.

The study of tissues has always been an important part of the subject in biology. Hence, obtaining samples of tissue has been vital to morphological and functionality research. The main tools used to obtain slices of tissue are microtomes and vibratomes, but it is impossible to obtain a full 3D structure of a tissue sample with these devices. This chapter presents an automatic positioning device for 3D cutting in living or fixed tissue samples. This device paves the way for researchers to make cuts in the sample tissue along different planes and in different directions by maximizing the tract that appears in a slice.

The content presented in this chapter has been adapted from the following publication:

D. R. Quinoñes, R. Perez-Feito, J. A. Garcia-Manrique, S. Canals, and D. Moratal, “Automatic positioning device for cutting three-dimensional tissue in living or fixed samples. Proof of concept”, *2017 39th Annual International Conference of the IEEE Engineering in Medicine and Biology Society (EMBC)*, Jeju Island, South Korea, South Korea: IEEE, 2017, pp. 1372–1375. DOI: 10.1109/EMBC.2017.8037088

6.1 Introduction

6.1.1 Histology

Histology is the science that studies the anatomy of the cells and tissues of plants and animals through microscopy. It is commonly studied with an optical microscope or electron microscope since the sample was sectioned, stained (not always) and mounted on a slide. Histological studies can be carried out using tissue cultures, where the cells of living animals are isolated and kept in vitro for several research projects. [217], [218].

6.1.2 Microtome and Vibratome

A microtome is a device used to cut slices through tissue, but it has a fixed blade (Figure 6.1). A vibratome, on the other hand, is similar to a microtome but has the advantage of a vibrating blade. The amplitude and speed of vibration, and the angle of the blade, can all be controlled in current models of vibratomes; however, the sample orientation cannot [219].

Vibratomes are mainly used in histology [220]–[222], anatomy [223], biochemistry [224]–[226] and pharmacology [227]. Furthermore, they are key in neuroscience [228], because they are useful tools which allow researchers to obtain fresh tissue slices.

In the last two decades the use of vibratomes has increased in neuroscience laboratories [229]–[231]. Vibratomes are used to obtain relatively thin subsections of tissue (hundreds of microns thick) without the need to process this tissue. As

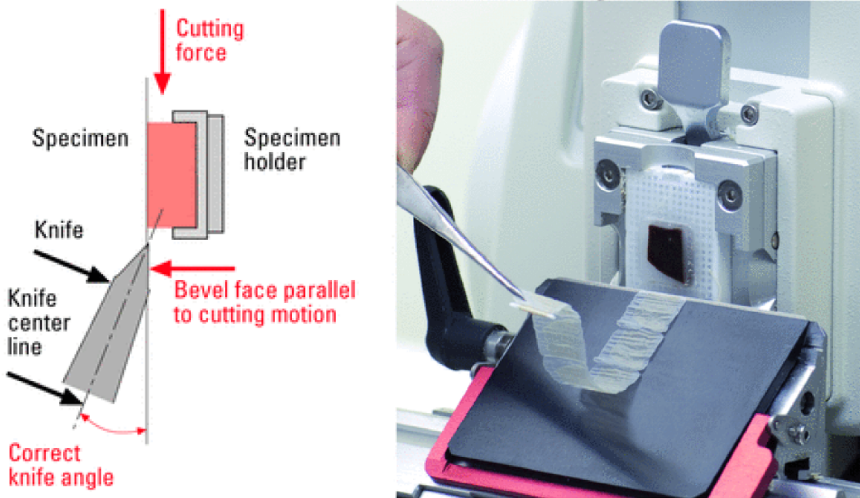


Figure 6.1. Microtome slicing process (from Leica Biosystems Nussloch GmbH, Germany, EU)

a result, they are used to simplify the 3D complexity of brain function and to investigate the anatomical connectivity of selected neuronal groups. Therefore, this equipment permits *in vitro* electrophysiological studies; for instance, the investigation of electrical and functional coupling between neuronal populations and the fine details of the structural connectivity.

The drawback with existing commercial vibratomes is that they only permit cuts in a single plane which is defined by the user [232] [233]. Moreover, once the cut has begun, the plane cannot be altered. In addition, these planes are subject to axial and longitudinal directions. Because of the 3D nature of the brain, it is impossible to study most of its information processing pathways. The most interesting tracts in the brain do not exist in a two-dimensional plane.

Physiological studies in local neuronal populations using conventional vibratomes are limited in the usefulness. This is in sharp contrast to the requirements of a 3D structure such as the brain. With our current 3D positioning device, the position and orientation of the sample can be changed while the vibratome is in use. Therefore, it is possible to perform a tomographic slice of any plane following a 3D curve path as shown in Figure 6.2. As a result, long

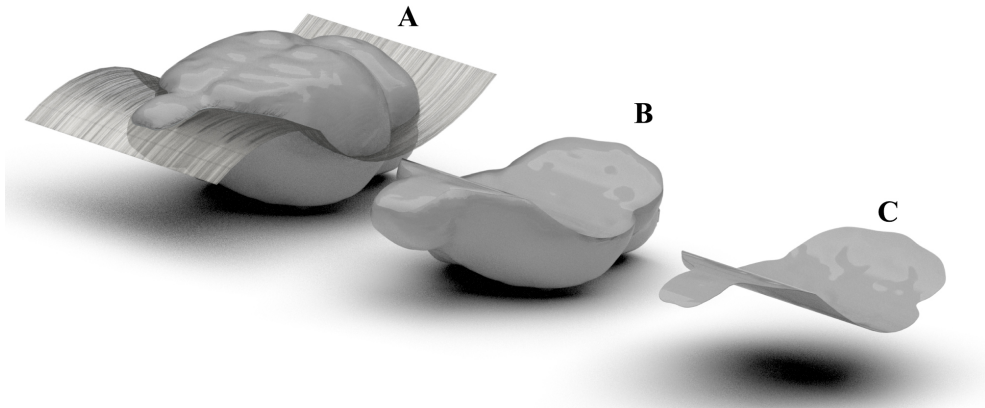


Figure 6.2. The figure shows a simulation process where the curved plane represents the path followed by the cutting blade. A) Tissue sample to be cut and cutting plane. B) The bottom part of the tissue sample after slicing. C) Resulting three-dimensional slice.

distance circuits can be dissected and studied *in vitro* for electrophysiological experiments.

6.2 Materials and Methods

6.2.1 System Concept

The automatic positioning device for cutting 3D tissue is based on a commercial vibratome. The original vibratome has two containers, which sit one inside the other. The outer container is used to keep ice close to the inner container and to maintain the temperature of the tissues. The outer container is made of plastic and the base is rectangular. It is 145 mm wide, 235 mm long and 40 mm high. The inner container is used to hold the sample and buffered liquid. It is 90 mm wide, 90 mm long and 35 mm high.

The automatic positioning device for cutting 3D tissue in living or fixed samples consists of two containers with dimensions approximately equal to those mentioned above. Moreover, it was redesigned to contain a mechanical system,

as it is shown in Figure 6.3. The mechanical system is composed of a pair of interconnected toothed gears, which allow the tissue samples platform to rotate.

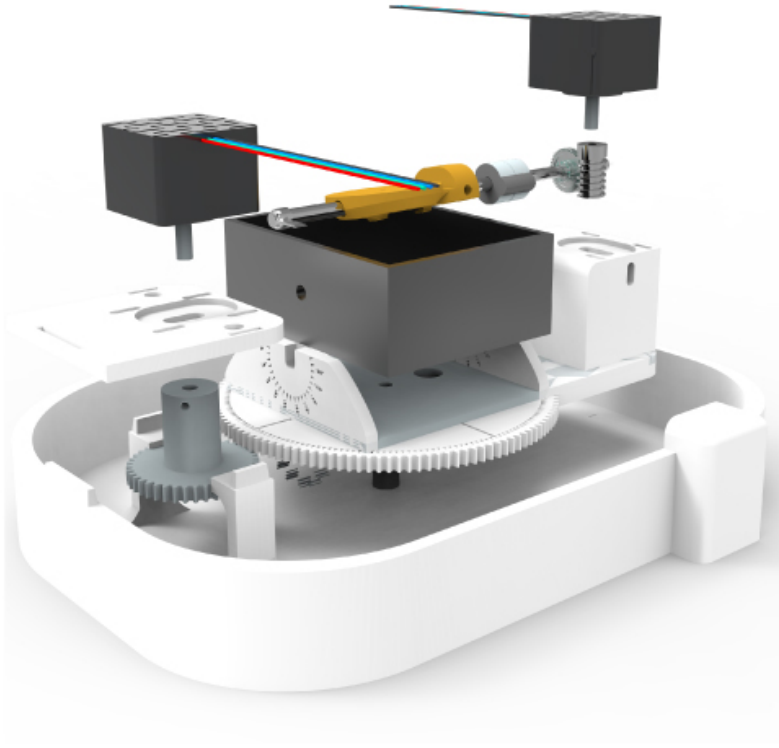


Figure 6.3. 3D model disassembled where is possible to visualize the different gears and platforms of the device.

Another mechanical system inside the Gearbox consists of a worm gear and a toothed gear. This gives the platform the ability to change the angle at which the microtome blade penetrates sample tissue. In addition to this flexibility, the device enables multi-directional histological subsections. All parts of this system were designed and modeled with Unigraphics NX 11 (Siemens PLM software, Plano, TX, USA) as shown in Figure 6.3.

The part of the system which controls the mechanics consists of an Arduino (Smart Projects, Turin, Italy & SparkFun Electronics, Boulder, CO) and a set of electronic drivers; these drivers control two stepper motors that move the gears described above. By combining these engines, the control system and the gears, the device was able to accomplish rotation and inclination movements. A specific firmware was designed to control and coordinate the whole system. The system was powered by a power supply of 12 V (2 A) which provides the necessary voltage range for the Arduino system and stepper motors.

6.2.2 System Parts

The automatic positioning device for cutting 3D tissue (Figure 6.4) contains the Samples platform on which tissue samples can be deposited. It was necessary for the design process to ensure that the platform was centered in the Inner container. The Ice container (Figure 6.4, Element 10) was made to contain the rotational mechanical system and dry ice. It has a central axis which was designed to be concentric with the Structural support in its center. The Inner container was made to be filled with buffered liquid. However, it was necessary to drill two holes at either end in order to allow the Shaft to pass through. Moreover, in order to prevent the liquid from leaking out through these holes, a pair of O-shaped rings were used. In order to ensure that the mechanical system (a worm gear and a toothed gear), which tilt the platform, was protected from the dry ice, it was placed inside the Gearbox.

In order to enable a rotational movement of the platform, an electromechanical system which consists of the Rotation engine, the Rotation power gear and the Rotation Gear was developed (Figure 6.4, Element 2, 4 and 5). To keep a simultaneous movement between the Rotation gear and the Structural support, both elements were fixed in a solid structure. The Rotation engine and the Angular engine have a minimum step angle of 1.8 degrees (200 steps/revolution). Each phase needs 280 mA to 7.4 V, allowing a torque of 650 g-cm (9 oz-in). In order to drive both engines, a pair of stepper controllers A4988 (Pololu Robotics and Electronics, Las Vegas, NV, USA) was used. In order to calculate the exact position of zero at inclination and rotation, a pair of Hall effect sensors was installed.

6.2.3 Manufacturing materials

The Inner container where the living tissue sample is deposited was built in Alumide; this is to achieve maximum thermal transfer. Alumide is a material of a metallic grey color, composed of aluminum-filled polyamide powder, which is characterized by its rigidity and metallic appearance [234]. The Ice container and the Structural support, described above, were composed of white plastic materials. It was finished with matte plastic (PA 2200). The Shaft that supports the platform was made with stainless steel 420 SS+.

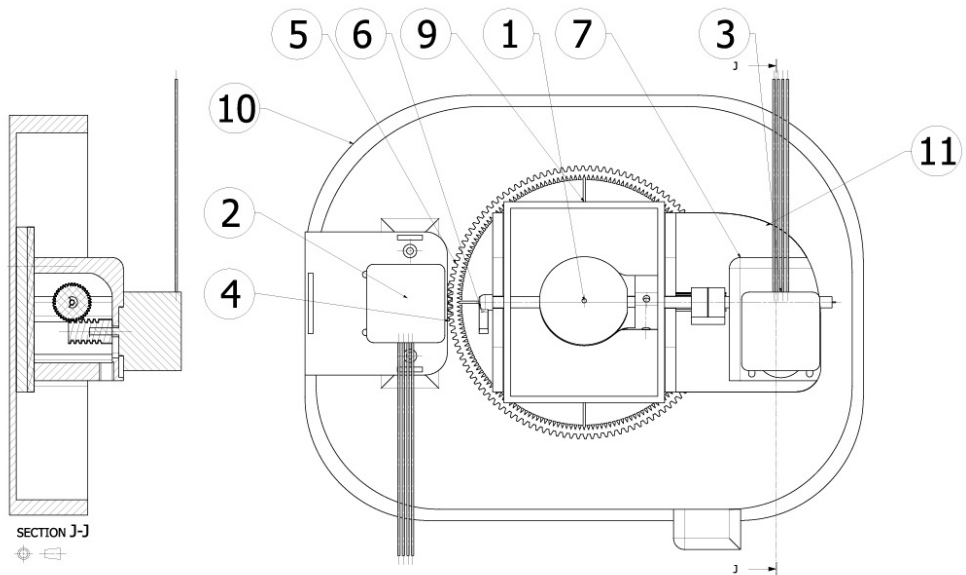


Figure 6.4. The figure on the left shows the top view of the plant and on the right a side view showing the cutting G is depicted. 1-Sample platform, 2-Rotation engine, 3-Angular engine, 4-Rotation power gear, 5-Rotation gear, 6-Shaft, 7-Gearbox, 9-Inner container, 10-Ice container, 11-Structural support.

6.2.4 Acquisition System

To validate the system, a motion-capturing sensor was placed inside of the Sample platform (see Figure 6.5). The more adaptable sensor was the Multiple Process Unit (MPU) 9150 manufactured by InvenSense (Sunnyvale, CA, USA), which is a Micro-Electro-Mechanical Systems (MEMS) embedded in a microchip. This contains an accelerometer, a gyroscope and magnetometer. It also includes a Digital Motion Processor (DMP), which enables the calculation process in the same MPU. Due to the limited Arduino computational power, the DMP is an

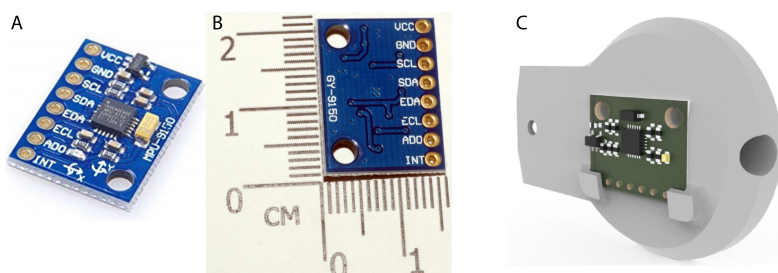


Figure 6.5. A) Motion-capturing sensor MPU 9150 (21 mm x 16 mm). B) Dimensions of MPU 9150. C) Samples platform with the MPU 9150.

excellent feature in order to preserve the main microprocessor managing the movements accurately instead of making position calculations. The MPU works at 200 Hz and the results are delivered to the main microcontroller through I²C and then transited to MATLAB.

6.3 Results and Discussion

6.3.1 Systems Specifications

In order to know the mechanical limits of the automatic positioning device, movements from zero to the end of the path were programmed in a debugging script. The orientation changes were quantified with MPU 9150 as it is shown in Figure 6.7.

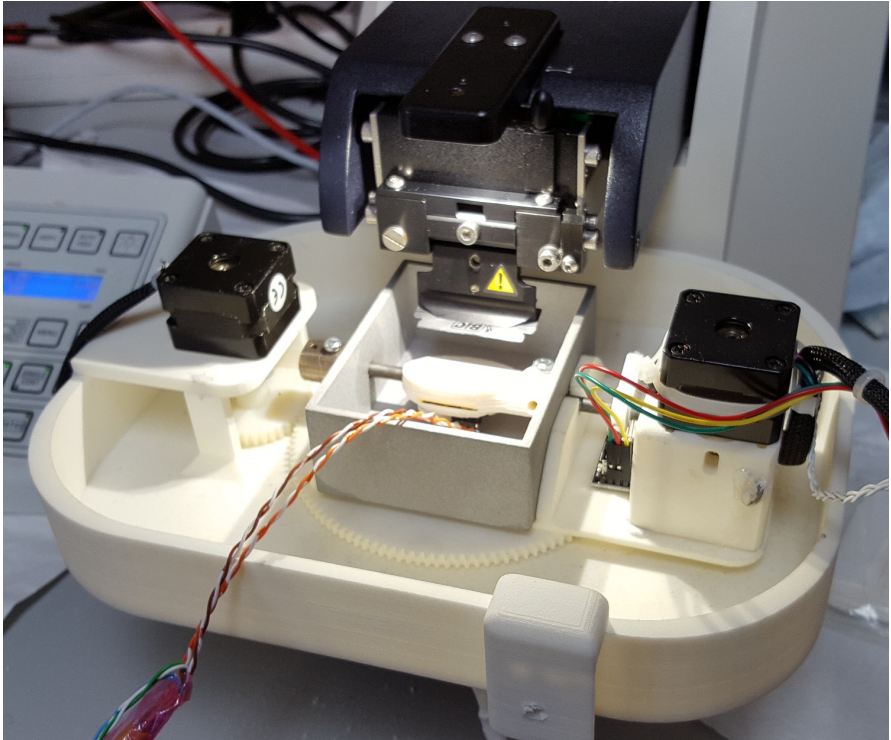


Figure 6.6. Real Automatic positioning device for cutting 3D tissue assembled with a commercial Vibratome Leica VT 1200 S. It is possible to observe the cables that connect the MPU, which is inside of the platform, to the Arduino.

The mechanical limits were defined as the maximum rotation or inclination angle that is possible to obtain. The maximum rotation range (pitch) was 70.01 degrees as shown in Figure 6.7A. The maximum inclination range (roll) was 67.20 degrees, between -33.6 and +33.6 degrees, as shown in Figure 6.7B.

The resolution of the system was defined as the minimum movement that is possible to do with the device. It was obtained by making a test with Arduino firmware and MATLAB. The test was started moving the engines gradually. When movement was detected by the MPU, the stop order was sent. Then, the number of engine steps divided the movement increment. As a result, the minimum rotation movement obtained was 0.66 degrees and minimum inclination movement was 0.08 degrees.

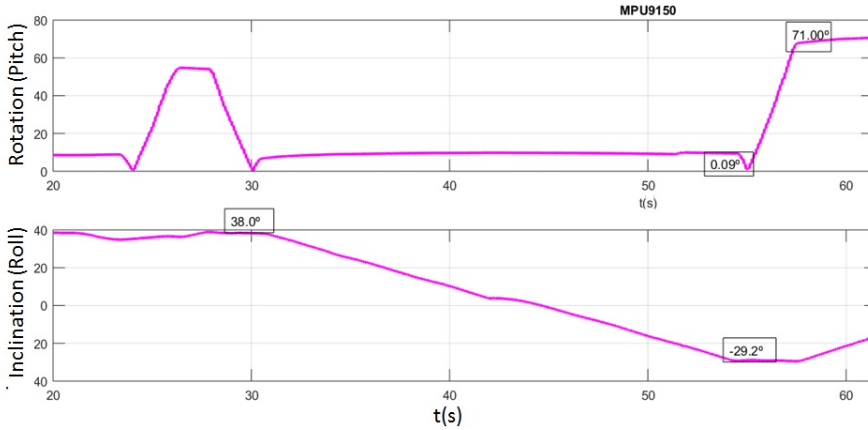


Figure 6.7. System specifications. (A) Rotation system from zero to the maximum value acquired with the MPU-9150. (B) Maximum inclination difference that was able to do, starting from the most negative inclination to the most positive inclination.

6.3.2 Slicing test

In order to test the viability of the device, it was attached to a real vibratome Leica VT 1200s (see Figure 6.7). During this test, the standard configuration was applied to the vibratome (speed = 0.05 mm/s). The automatic cutting device was configured to perform a tilt movement (inclination) in order to obtain a curved slice of tissue. Next, to debug the device, an agarose brain was created with a mold (based on the data of chapter 5) and used to perform the slices. As a result, a curved slice was obtained as shown in Figure 6.8. Even though the slice

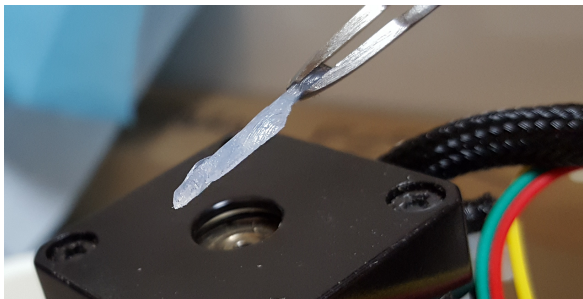


Figure 6.8. Slicing test with an agarose rat brain

is slightly thicker than it was desired, it is a good proof that the device works properly and with some improvements, it could achieve higher precision.

6.3.3 Graphical User Interface

In order to control the system a Graphical User Interface (GUI) was created in MATLAB (Figure 6.9) with the GUI toolbox. It permits to setup USB communications with Arduino and read the I²C protocol provided by the MPU. Arduino firmware interpreted the commands from MATLAB to control the movement accurately. Simultaneously MPU data are read by I²C bus and is shown in the GUI. In right side of the GUI the orientation of the Sample's platform can be viewed in real time. The 3D object on the lower left side of the GUI, mimics the movement of the platform, to make it easier to interpret.

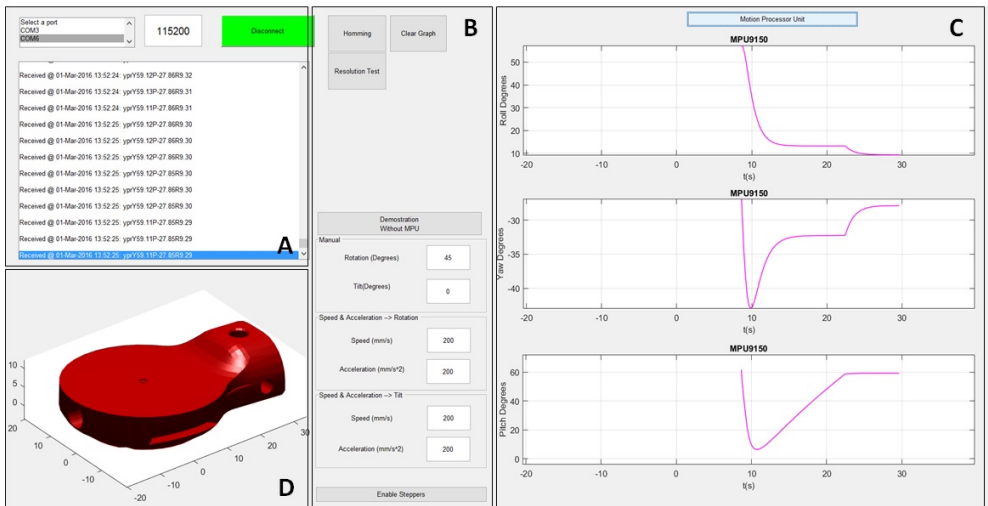


Figure 6.9. This Graphical User Interface (GUI) was made to control each movement of the system and to visualize all of orientation data. At zone A communications settings can be changed to communicate with the system properly. The device setting is provided in zone B. The sensor measurements can be shown in the C zone. Inside of D zone, a real time representation of the Sample's platform is shown while the system is working.

6.4 Conclusions

The concept of an automatic positioning device for cutting 3D tissue in living or fixed samples was proposed, developed and tested. It was designed to give researchers the ability to use it as an enhanced vibratome accessory. The device was designed and developed with professional 3D CAD software. The prototype was manufactured with selective laser sintering technologies. In addition, the device is easy to assemble and disassemble without any tools to make it easier to clean. The device means the user is able to change sample orientation when the slicing process has started. This makes the device a highly competitive product because it improves tissue research possibilities in almost all biological fields. This is especially true in neurological research where it is important to obtain the whole path or structures of the animal's brain. The presented automatic positioning device achieves very precise and smooth movements, as reflected in the tests performed with orientation sensors. The device makes it possible to slice samples along different paths or guidelines. The device is currently undergoing tests with a commercial vibratome in order to obtain slices of whole tracts.

Lung Tumor Movement Simulator for Radiotherapy

In Organization for Economic Co-operation and Development (OECD) countries, cancer is one of the main causes of death, lung cancer being one of the most aggressive. There are several techniques for the treatment of lung cancer, among which radiotherapy is one of the most effective and least invasive for the patient. However, it has associated difficulties due to the moving target tumor. It is possible to reduce the side effects of radiotherapy by effectively tracking a tumor and reducing target irradiation margins. This work presents a custom electromechanical system that follows the movement of a lung tumor. The developed device helps the verification of individualized radiation treatment plans and permits the improvement of radiotherapy quality assurance procedures.

The content presented in this chapter has been adapted from the following publication:

D. R. Quiñones, D. Soler-Egea, V. González-Pérez, J. Reibke, E. Simarro-Mondejar, R. Pérez-Feito, J. García-Manrique, V. Crispín, and D. Moratal, “Open Source 3D Printed Lung Tumor Movement Simulator for Radiotherapy Quality Assurance”, *Materials*, vol. 11, no. 8, p. 1317, 2018. DOI: 10.3390/ma11081317

7.1 Preface

As a result of all the knowledge, experience and skills acquired during the thesis development, it was decided to extrapolate this expertise to other fields outside of the neuroscience.

In collaboration with the Fundación Instituto Valenciano de Oncología (IVO), it was proposed to develop a Lung Tumor Movement Simulator that would help the researchers and clinicians of this center to plan the radiotherapy treatments for their patients.

7.2 Introduction

Lung cancer is the most common type of cancer in OECD countries. It is responsible for over 1.38 million deaths annually [236]. There are currently several treatments for lung cancer, including surgery, radiotherapy, chemotherapy and palliative care. One of the most effective is radiotherapy. It is because malignant cells are eliminated via ionizing radiation and it is less invasive for the patient [237]. Nowadays, more than half of all cancer patients receive radiotherapy, either alone or in combination with surgery or chemotherapy [238]. However, radiotherapy has detrimental side effects, as healthy tissue is also affected by these usually high-dose-rate radiation beams.

Radiotherapy involves the use of controlled doses of high-intensity radiation to kill cancer cells or to reduce the size of tumors. In the case of lung cancer, radiotherapy is used as a main treatment in patients for whom surgery is impossible. It can also be applied before or after the surgery, as palliative therapy

or to relieve blocked airways. Radiotherapy is generated outside the body, in a Linear Accelerator (LINAC), and is generally used to treat non-small cell tumor.

Regarding the side effects of radiotherapy, a distinction between acute and chronic effects is made. The formers are those that appear during treatment and usually disappear within a few weeks, such as fatigue and skin reactions, among others. Chronic side effects appear months or even years after treatment and may be permanent.

One of the essential parts of external radiotherapy treatment is planning [239]. Before starting treatment, it is important to calculate the dose needed, the emission angles and other parameters that will allow the patient to receive the right amount of radiation without affecting adjacent areas.

Compared to other parts of the body, the lungs are in constant motion [240], [241]. According to *Seppenwoolde et al.* the movement of the lung in this way is largely two-dimensional and it is possible to reproduce the movement of any part of the lung when the length and capacity of the breath is known.

Previous studies have shown that a human adult breathes between 16 and 20 times per minute, which means one breath (inhalation and exhalation) every 3–3.75 s [242]. Closer inspection of the lungs shows that not all points move at the same rate and, therefore, not at the same speed [243]. Nevertheless, the general movement can be equated to a hysteresis loop [244], [245], as shown in Figure 7.1. This is why lung tumor irradiation cannot be concentrated in a fixed tumor position at each phase of the breathing cycle, and it must be applied with small margins of the target volume to cover the tumor position during the entire respiratory cycle. To irradiate the tumor, it is necessary to follow the movement of the tumor [246] to plan the radiotherapy treatment.

Good planning will reduce the amount of radiation that healthy tissues receives, while reducing the side effects. To verify the treatment of sophisticated radiation techniques in lung cancer, a parametric simulator of the tumor movement is needed.

The imaging techniques currently available, such as the 4D Computer Tomography (4DCT), acquire images synchronized with respiratory movement [247], [248]. This permits to track the tumor position in each phase of the cycle

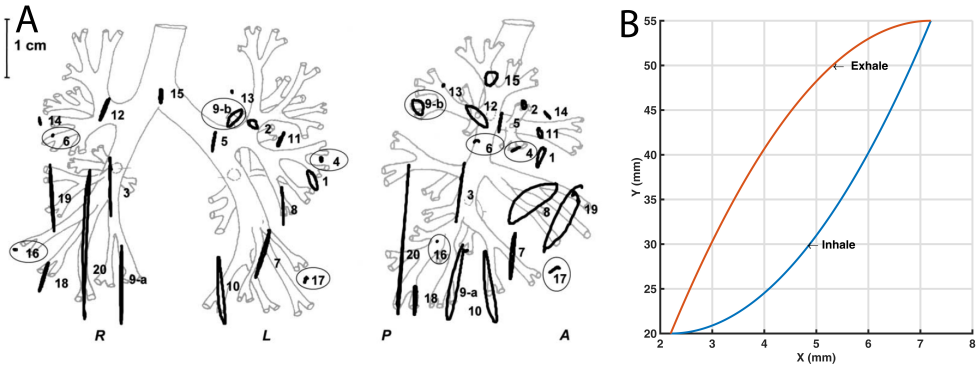


Figure 7.1. Hysteresis loop of lung tumors movement: (A) The orthogonal projections of the trajectories of the 21 tumors on (left) the coronal (LR-CC) and (right) the sagittal (AP-CC) plane is shown (reproduced with permission from [244]); and (B) One recreated hysteresis cycle that simulates the movement of the tumor is displayed.

and extract a custom path from patients [249]–[254]. These images are taken with the patient immobilized, in the same way in which the future treatment will be applied in each of the sessions.

In this work, we present a proof of concept of a lung tumor movement simulator prototype, which considers that not every human has the same breathing characteristic curve. In addition, it can be adapted to any possible specific height, width and speed of breathing movement. Although there are some commercial alternatives, they are not Open-Source. The Lung Tumor Movement Simulator was entirely created using 3D printed parts in order to achieve a customizable device that can be adapted for specific cases. Furthermore, it was printed with an Open-Source 3D printer that makes it affordable for every research center. With this device, individualized radiation treatment plans can be tested in advance.

7.3 Materials and Methods

7.3.1 *Linear Accelerator*

A LINAC is a device that is most commonly used to give external beam radiation therapy to patients with cancer. It supplies high-energy X-rays to the tumor region of the patient. These X-ray treatments can be designed to destroy cancer cells without affecting normal surrounding tissues.

The linear accelerator uses microwave technology to accelerate electrons and then allows these electrons to collide with a heavy metal target to produce high-energy X-rays [255]. These high energy X-rays are shaped as they exit the machine to target the tumor in the patient. The beam is shaped by a multi-leaf collimator that is incorporated into the head of the LINAC. The patient lies on a movable treatment couch and lasers are used to make sure that the patient is placed in the desired position. The ionizing beam is emitted from a part of the accelerator called a gantry, which can be rotated around the patient. Moreover, radiation can be delivered to the tumor from any angle, by rotating the gantry and by moving the treatment couch.

Because lungs are in constant motion, the tumor is constantly changing its position and this movement should be taken in account. This movement of the tumor is always studied before starting the treatment (Figure 7.1). To increase the LINACs accuracy and avoid irradiating healthy areas, there is a technique called tumor tracking [249] that is useful to analyze the movement of an internal lung tumor. Based on these tumor tracking studies, and to improve customized radiotherapy plan verification, the Lung Tumor Movement Simulator was created. It provides a good simulation of tumor movement and a good radiation measure because it holds a dosimeter in the Tip. In this case the Tip was designed to contain a Landauer OSL nanoDotTM(Landauer, Inc., Greenwood, IL, USA).

7.3.2 *Electromechanical Components*

To give motion to the mechanism, a pair of NEMA 17 stepper motors was used. The stepper motors have a minimum step angle of 1.8 degrees (200 steps/revolution). Each phase needs 280 mA to 7.4 V, allowing a torque of 650 g-cm (9 oz-in). To drive both stepper motors, a pair of stepper controllers DRV8825 (Texas Instruments, Dallas, TX, USA) was used, which features adjustable current limiting and six microstep resolutions (down to 1/32-step).

In cyclic or rotating movements, it is important to know the starting point of the rotation. For this reason, endstops are needed. Endstops sensors are electronic components that function as switches, sending signals when an element is placed in a certain position. There are various types such as mechanical, optical and magnetic. In the prototype two optical endstops are used because they can be activated by some element of the mechanism (Figure 7.2, element 3 and 9). At the same time, this type of sensor avoids the possible rebounds that may appear in mechanical sensors.

7.3.3 *Microcontroller*

The Arduino Mega 2560 (Smart Projects, Turin, Italy & SparkFun Electronics, Boulder, CO) development board is a printed circuit that allows the use of a microcontroller ATMEGA2560 (Microchip Technology Inc., AZ, USA) [173]. Arduino is commonly used in a high variety of research fields due to its versatility and low cost [170], [174]–[176].

This microcontroller controls 54 digital Input/Output pins, 15 pulse width modulation pins, and 16 analog pins, and is able to automate any system. Documentation and software are open source and available at the Arduino website. The programming software is based on the C/C++ language and the power supply of this development board can be powered through USB or main supply from 5 V to 12 V.

All of these features make Arduino perfect for this project, but, to connect the drivers to Arduino, which control the stepper motors, an Arduino-Shield was needed. The Reprap Arduino Mega Pololu Shield (RAMPS) is a board specially designed for the use of the selected drivers. This can control up to five stepper

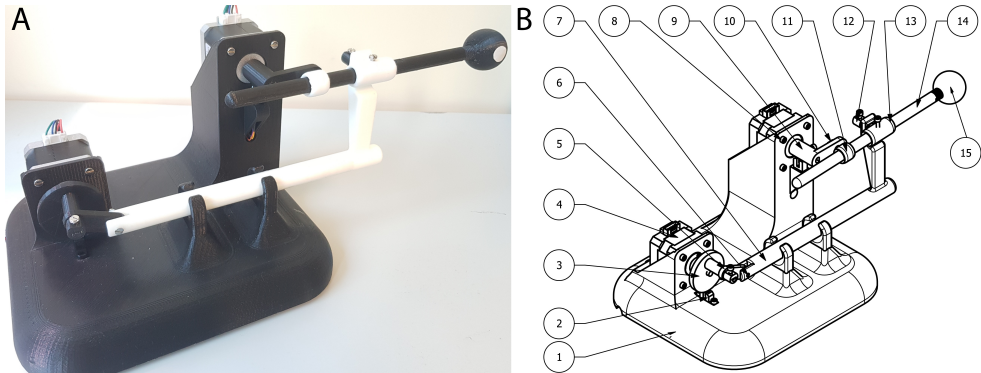


Figure 7.2. (A) Real Lung Tumor Movement Simulator prototype; and (B) Schematic parts of the prototype. See Table 7.1 for details.

motors and support the connection of various endstops. The RAMPS board can only be used together with an Arduino Mega 2560 board on which it is placed by inserting the male connectors of the RAMPS into female Arduino pins.

7.3.4 *Manufacture and Material*

The entire project was thought to be printable in any commercial or Open-Source 3D printer. A Prusa i3 MK2 with a precision of 50 microns per layer height, and a printing surface of 10.500 cm^3 ($25 \times 21 \times 20 \text{ cm}$ or $9.84 \times 8.3 \times 8 \text{ in}$) was used to print all of the parts. The entire prototype was manufactured with PLA material. This material was chosen because it achieves the specifications that are need for the prototype [256]. It is light and strong enough to enable the mechanism to function smoothly. Furthermore, it is biodegradable and environmentally friendly.

7.4 Results

7.4.1 *Prototype Design*

During the design of the Lung Tumor Movement Simulator (LTMS) (Figure 7.3), several mechanical designs were studied and proposed; in the end, a design composed of two sliders was chosen.

PART (Figure 7.2)	Description	Quantity	X(mm)	Y(mm)	Z(mm)	Weight (g)	Material
1	Base	1	209.50	180.00	145.00	550.00	poly(lactic acid) (PLA)
2	Endstop	2	-	-	-	-	-
3	Horizontal wheel	1	45.10	40.00	51.00	9.00	PLA
4	Stepper NEMA 17	2	42.00	42.00	38.00	285.00	PLA
5	Union bar	1	15.70	36.60	4.50	3.00	PLA
6	Cylinder pin	1	2.00	3.00	30.00	2.00	Stainless Steel
7	Horizontal bar	1	200.00	26.00	85.50	28.00	PLA
8	Screw M3 x 6	15	-	-	-	5.00	Stainless Steel
9	Vertical bar	1	22.00	44.90	30.00	6.00	PLA
10	Short retainer	1	4.00	10.90	9.10	1.00	PLA
11	Stem guide	1	33.00	13.40	16.20	3.00	PLA
12	Long retainer	2	9.00	10.90	9.10	2.00	PLA
13	Stem support	1	22.00	44.90	30.00	6.00	PLA
14	Stem	1	200.10	10.00	14.90	12.00	PLA
15	Tumor sphere (Tip)	1	29.20	30.00	30.00	8.00	PLA

Table 7.1. Prototype parts.

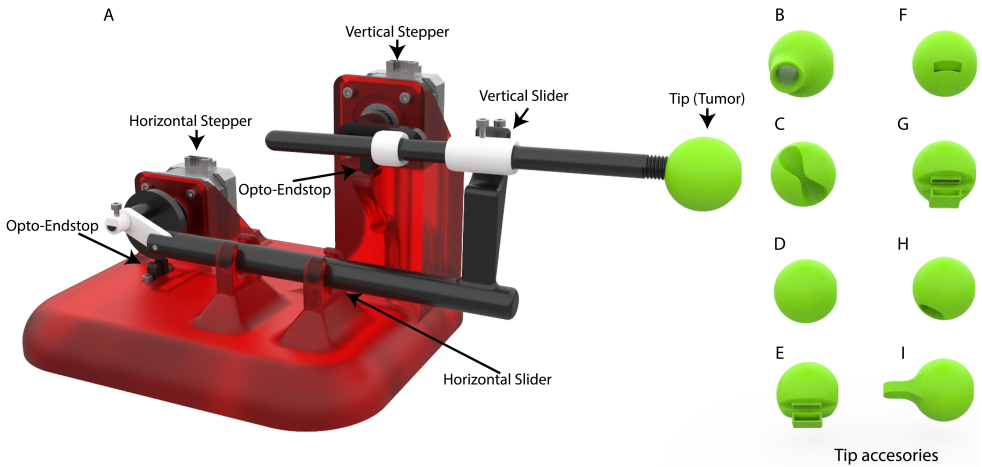


Figure 7.3. 3D model of the Lung Tumor Movement Simulator. Main design of the prototype A and eight tips model that were designed to give versatility to the model. Tips D–H were designed with the purpose of holding a nanoDot™ radiation dosimeter. Tips B, C and I were designed to hold a test tube with contrast fluids for other purposes.

This design is formed by two stepper motors, which move the mechanical elements (Figure 7.2) to achieve the desired movement. There is an upper motor, which controls the upwards and downwards motion of the Tip that simulates the tumor position. Then, there is a lower motor which controls the pushing forward and backward of the Tip, which represents the targeted tumor. The

entire prototype is composed of 15 different parts. Their dimensions and weights are shown in Table 7.1.

The biggest challenge during the design was how to achieve the synchronization of the two stepper motors in order to obtain an accurate path. This problem was overcome with the addition of two optical endstops. These endstops were placed underneath each stepper motor and a protuberance on each axis is what triggers the optic mechanism.

7.4.2 Movement and Path Simulation

To validate the prototype mechanism, it was necessary to evaluate the mobility of the whole system as shown in Figure 7.4. By using the feature of Movement Simulation from Unigraphics NX 11 (Siemens, Berlin, Germany), the Tip trajectory was simulated considering the gravity, friction and speed limits.

During the virtual simulation, it was observed that the Tumor Movement Area, which is shown in Figure 7.4, was the expected area for the tumor movement cycle. Furthermore, the simulation was done with the same speed for the two stepper motors and one specific mechanical configuration; however, if the speed or the length of the mechanical transmission were modified, the height and width of the desired area would be modified.

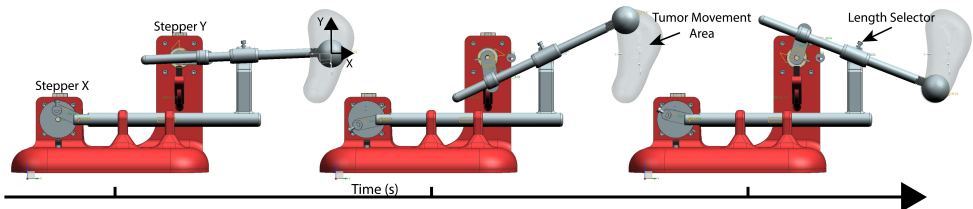


Figure 7.4. Virtual simulation of the desired area to cover with the LTMS in order to validate the viability of the system design.

7.4.3 Synchronizing the Movements

The rotation speed of the primary motor (Figure 7.5A), which is the operator of the horizontal movement, was fixed at a speed that depends on the respiratory frequency of the patient, so that a complete turn is made with the same duration as breathing is performed.

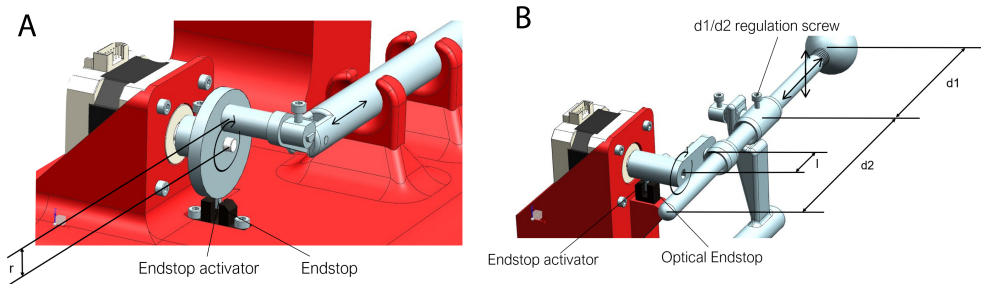


Figure 7.5. LMTS motors setup detail. A- Horizontal stepper motor; and B- vertical stepper motor. See main text for details.

To reconstruct the hysteresis cycle, the second stepper motor (Figure 7.5B), which controls vertical displacement, continuously modifies the rotation speed throughout the cycle. This cycle is divided into six parts, which corresponds to a 60-degree turn of the motor. The average speed in the set of the six sections is equal to the other engine to achieve a synchronized movement and a complete turn in the same time. Therefore, the different speeds on this engine are time dependent.

The parametric variables that affect the Tip (simulated tumor) trajectory are shown in Figure 7.5. The simulated tumor trajectory can be adjusted in several ways:

- In width: The width can be modified by changing the distance “ r ”.
- In height: To change the height of the movement (amplitude), it is necessary only to release a little screw that is at the joint of the vertical slider

(Figure 7.5B) and to move the rod forward or backward. This is represented by distances “ $d1$ ” and “ $d2$ ” (Equation 7.1).

- In timing: In the serial console, the breathing time can be set to move at the same frequency as the patient does.

$$h = 2 \cdot \left(\frac{d1 \cdot l}{d2} \right) \quad (7.1)$$

As a result of changing the distances, the output path is defined by Equation 7.2 and Equation 7.3. These equations describe the Tip trajectory during the inhalation and exhalation.

$$Y_{inhalation} = \left(\left(\sqrt{\frac{h}{(2 \cdot r)^2}} \right) \cdot x \right)^2 \quad (7.2)$$

$$Y_{exhalation} = \left(-(x - (2 \cdot r))^2 + (2 \cdot r)^2 \right) \cdot \sqrt{\frac{h}{(2 \cdot r)^2}} \quad (7.3)$$

7.4.4 Path Verification

To check the precision of the LTMS prototype, the movement was tracked (Figure 7.6 A,B) by creating a tracking workflow with Bonsai software [44]. Bonsai is a visual programming language that allows a modular, high-performance, open-source visual programming framework for the acquisition and online processing of data streams. It permits real time data acquisition and processing among several interfaces.

A real-time data analysis was performed to constantly track the position in X and Y of the Tip, while the prototype is running the breathing cycle. In this Bonsai workflow, the camera input with the overlapped tracking were recorded, as well as the X and Y positions of the Tip plus a time-stamp.

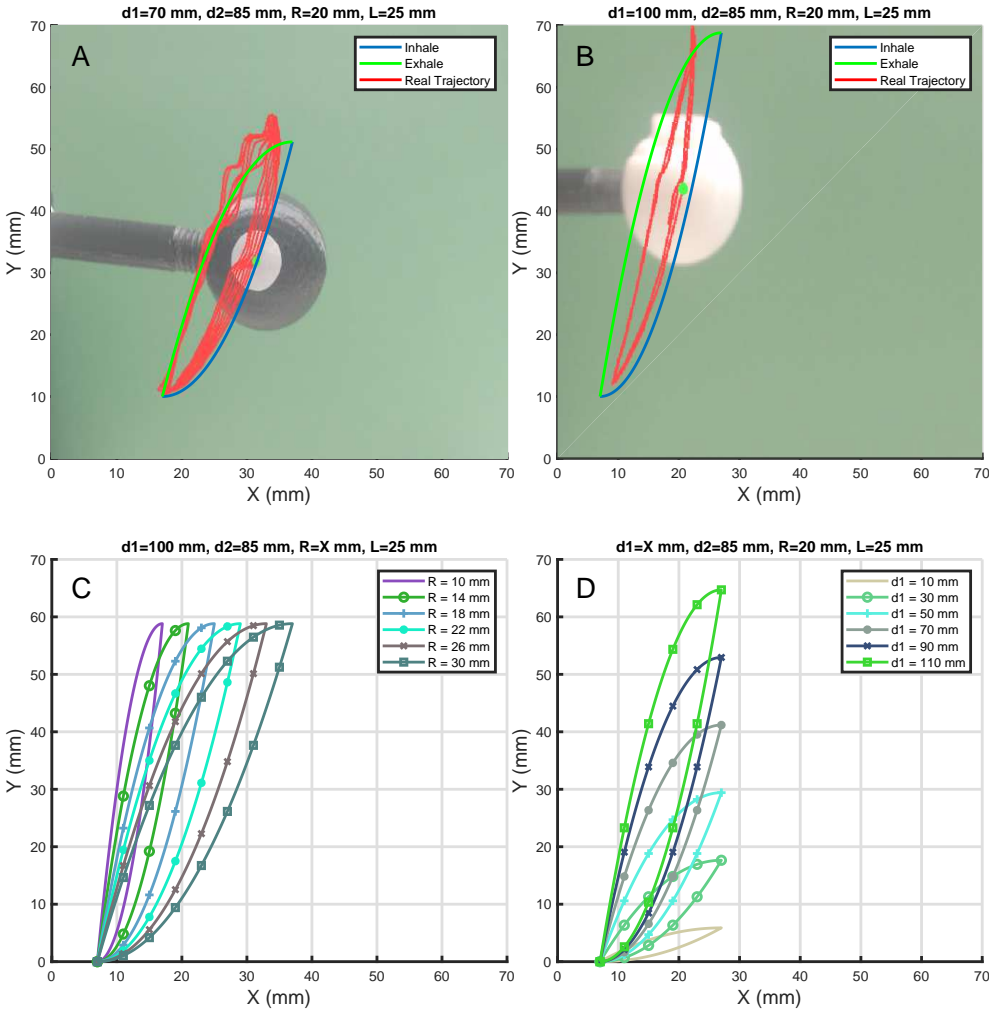


Figure 7.6. (A) Setup for a wider tumor trajectory is shown. (B) Setup for higher tumor trajectory is shown. (C) All possible trajectories by modifying the r parameter are displayed. (D) Possible trajectories by modifying $d1$ parameter are displayed.

This tracking is performed by transforming the acquired image from the camera to a Hue, Saturation, Value (HSV) image. A white sticker was attached to the Tip (sphere), which is shown in Figure 7.6A and Figure 7.6B, and by means of establishing an HSV threshold it was possible to discriminate the sticker contours against the Tip (simulated tumor). Then, the largest binary region was found,

which corresponded to the sticker, and the centroid of it was detected. These centroid coordinates correspond to the X and Y position of the simulated tumor.

The resulting curves of the prototype and program differ slightly from the desired hysteresis loop; even though the lower part matches well, the upper area deviates a maximum of 5 mm from the desired position, as shown in Figure 7.6A,B. Several tests were made with the system during 20 cycles. It deviates in the two first cycles until the synchronization process is done. After these two cycles the deviations were smaller than 1 mm in the higher setups and 4 mm in the wider setups. However, in future versions the above mentioned errors will be minimized by improving the mechanical design.

There are several combinations that could be set up with the prototype, and depending on which of the transmission components is used it is possible to achieve all of the combinations that are shown in Figure 7.6C and Figure 7.6D.

The 3D Printed Lung Tumor Movement Simulator for radiotherapy quality assurance has been presented (Figure 7.7) to a group of expert radiation oncologists and medical physicists from the Instituto Valenciano de Oncología, Valencia, Spain. These experts agree that small deviations from the theoretical loop are not worrying, as a real tumor does not move on a perfect line either; and so the radiation device should be flexible enough to reflect this kind of variation.

7.5 Discussion

In the radiotherapy field, movement of tumors due to the respiratory cycle makes treatment difficult and, for this reason, an area of research has focused on treatment planning [240], [241], [246]. There are devices that can be used to guarantee the quality and quantity of received radiation doses, which are commonly named phantoms. In this way, in the most complex cases, doctors and radiologists will perform a priori tests that ensure maximum precision before the treatment.

Although there are existing commercial devices such as QUASAR (Modus Medical Devices Inc., ON, Canada), Respiratory Gating Platform (Standard Imaging Inc., WI, USA) and Dynamic Thorax Phantom (CIRS Inc., VA, USA),

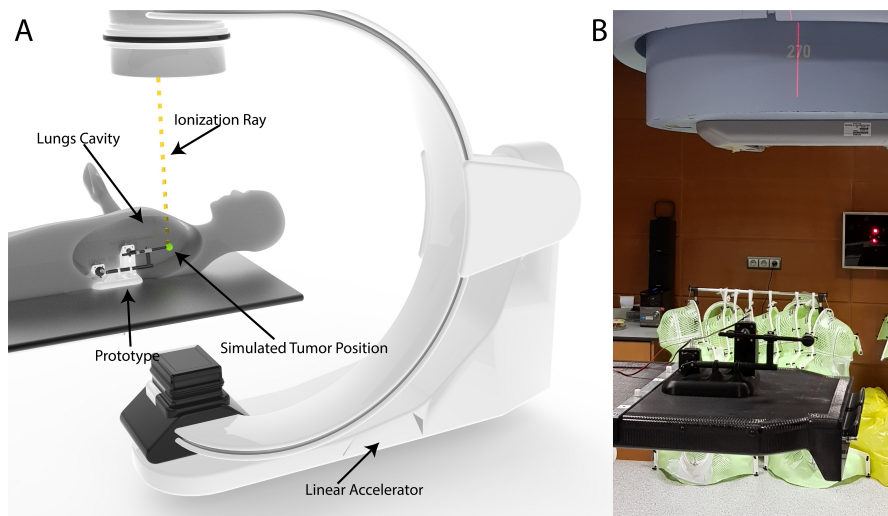


Figure 7.7. (A) Virtual reconstruction of the location where the prototype should be placed to simulate the tumor path is shown; and (B) the real Lung Tumor Movement Simulator placed inside a LINAC.

these alternatives are proprietary and difficult to customize. The creation of this prototype based on 3D printing and Open-Source is intended to serve as a basis for the expansion of these devices for research purposes.

The Respiratory Motion Phantom from QUASAR is a commercial device developed by Modus QA, which, in its latest version, reproduces in two dimensions the respiratory movement of patients for use in radiotherapy [257]. It is useful for testing treatments, the correction of these tests and the commissioning of the implementation of new systems. However, this device is a licensed product that cannot be customized, and it is not accessible for researchers. The aim of this project is to pave the way for researchers to improve the treatment simulations in a cost-effective way. In addition, it facilitates the creation of parametric components, which allow the simulated tumor path to be changed. One of the strongest features of this prototype is that all of the mechanisms are 3D printed and they can be modified as the researcher desires.

7.6 Conclusions

This project began with the idea of creating an Open-Source prototype that would follow the hysteresis loop of the movement of a human lung during a respiration cycle to track the movement of a tumor. We present an Open-Source Lung Tumor movement simulator, which is 3D printed for each patient and for each treatment. This prototype is completely customizable, and it paves the way for researchers, radiologists and nuclear medicine physicians to improve the radiation therapy for quality assurance procedures and outcomes.

This Lung Tumor Movement Simulator is programmable with the amplitude and frequency specific to each treatment and patient. These data are obtained thanks to the images obtained by techniques such as the 4D-CT and are translated through the serial interface that connects the computer and the hardware (drivers, motors, etc.). In the prototype, there is the possibility of introducing a dosimetric film or an ionization chamber to measure the dose of radiation absorbed. Furthermore, the Lung Tumor Movement simulator is cost-effective, because it is almost entirely 3D printed and the electronic components, as well as the motors, are not expensive.

The results of building and testing the new lung movement prototype are very promising. It has been shown that it is possible to create a simple and cost-effective machine to simulate the movement of a tumor in the lungs based on additive manufacturing. The prototype is ready to be tested and there are plans to undertake customized radiotherapy verification and research in a radiotherapy machine.

Chapter 8

Conclusions and Outlook

Research in neuroscience has always been a field that has covered many specialties. The objective of this thesis is to contribute to the field of neuroscience by addressing some technological deficiencies that are encountered in current animal experimentation . Hence, in this document, six projects, which aim to contribute to improving the “Principle of the three Rs”, are presented. The thesis further aims to demonstrate that there is still a lot of technology that can be applied to this field by presenting six new tools.

8.1 On the tracking devices

Humans and animals use their bodies as their primary interface with the outer world, and as powerful tools for expressing their inner worlds. Movement is, therefore, a phenomenon of interest to many researchers, including neuroscientists, surgeons, engineers, makers and artists.

Positional tracking systems are used to improve understanding of movement in a number of niches, such as performance art, athletics, neuroscience and medicine. Indeed, commercial solutions can track the movements of a human

inside a room with millimetric precision. However, these systems can track only a small number of subjects at a time; they suffer occlusions; are too expensive to be easily accessible; and their trackers are too large and inaccurate for research or clinical use.

For these reasons, two novel devices are presented. These devices are based on different technologies, which have the potential to accurately track multiple small animals, humans and other subjects. The first system is the RATT. This system has shown great potential in tracking multiple animals in a large enriched environment. Despite the system user interface, as well as the fact that the firmware needs to be slightly improved, this system is ready to undertake real experiments with rodents. The second tracking system that is presented is the Hive Tacker. This system is a novel tool that can be used in several fields, from neuroscience to virtual reality games. The system is at an early stage and it needs to be polished as a final product. However, behind this project, we are creating a big community, which supports the system and is very keen on helping to develop it. Moreover, both technologies are perfectly compatible with each other, and with currently available camera tracking systems. This provides the possibility of creating enriched environments featuring a high accuracy tracking system that does not suffer from current drawbacks.

Finally, we have long appreciated that movement on a macro scale is a phenomenon of interest to many, such as engineers, makers and artists, it has become increasingly clear that much could be gained from studying movement in greater detail and with higher precision specially in neuroscience.

8.2 On the control temperature devices

Anesthesia has an effect on an animal's physiology. Mammals, such as laboratory mice, are endothermic animals. However, they are unable to produce the heat necessary to regulate and maintain their body temperature while they are inside an MR scanner. For this reason, we have developed an Open-Source temperature control device for fMRI experimentation in mice, which is called ThermouseDuino. With the model and experimental results, we demonstrated the viability of the system for maintaining the temperature of the anesthetized animal within the physiological range and meeting user specifications that ensure its practical

use. TherMouseDuino, provides an automatic, safe and precise control of body temperature for anesthetized mice. This system is currently working in the Neuroscience Institute of San Juan de Alicante and it was tested with two strains of mice.

By using TherMouseDuino during the fMRI, we have observed that the mice under anesthesia are able to keep their temperature stable. This results in better BOLD signal acquisition and frees up the technician to do other tasks. In addition, this system can help in a large number of laboratories thanks to the fact that it is completely Open Source and its cost is low . Finally, this system can be modified to be interconnected with other devices and/or connected to a cooler in order to reduce the temperature if necessary.

8.3 On the 3D printed brain

Two-Dimensional (2D) representations limit our appreciation of complex structures, such as brain convolutions, and 2D displays of these models on computer screens prevent us from interacting with a model of the physical brain. With the participation of an experienced biologist, an eight-piece printed rat brain was created in this project. This 3D printed brain was designed to be easily assembled and disassembled. At the same time, this project presents a novel methodology to convert clinical and preclinical digital images into real 3D objects through free software.

8.4 On the histological cuts

In the last two decades, vibratomes have increasingly been used in neuroscientific laboratories. However, there is a drawback with existing commercial vibratomes: they only permit cuts in a single plane, which is defined by the user. In order to overcome this issue, an automatic positioning device for cutting 3D tissue in living or fixed samples was developed and tested. It was designed to give researchers the ability to use it as an enhanced vibratome accessory. Even though the development of the device is at an early stage and more testing needs to be done, it is a highly promising device that will contribute hugely to the fields of neuroscience and histology.

8.5 On the tumor movement simulator

Radiotherapy is one of the most effective cancer treatments and, by good planning, the amount of radiation that healthy tissue receives can be reduced, therefore also reducing the side effects. In order to verify the treatment of sophisticated radiation techniques in lung cancer, a parametric simulator of the tumor movement was created. The Lung Tumor Movement Simulator is programmable with the amplitude and frequency specific to each treatment and each patient in order to simulate the treatment before applying it to patients. This device has a high potential to improve radiotherapy quality assurance and paves the way for the radiophysics research required in this field.

8.6 On the future work

Work on the projects featured in this thesis began in with the idea of addressing some technological gaps in the neuroscientific field. Each of the projects started with the identification of a need or of a deficiency in current technology.

Now, it is time to look to the future and some work should be done, especially focused on the RATT project. These work should focus on improving the end-user software in order to make it more “*user-friendly*”. In addition, the Antennas should be redesigned in shape in order to optimize the communication with the bio-compatible glass tags. Moreover, the synchronization among all of the tiles should be optimized in order to minimize the speed of detection.

Regarding Hive Tracker, this project is currently being improved and it has a growing open source community at Hackaday.io. However, it needs some improvements to avoid light reflections and process the light flashes detection faster.

Regarding TherMouseDuino, the expansion of this system to other animals should enhance the usability of this device in other species. Moreover, it could be use to obtain heat transfer models of other rodents such as rats.

Regarding the Automatic Device for Cutting 3D Tissue, more test should be done in order to debug and optimize the movements. Test in real samples will be also good in order to have better feedback on the slicing process.

Chapter 9

Contributions

9.1 Research Internship

- Sainsbury Wellcome Centre for Neural Circuits and Behaviour - Kampff Lab, University College London, (April 4th, 2017 - July 6th, 2017), London, United Kingdom. Supervisor: Adam R. Kampff.

9.2 Publications in Journals

9.2.1 *International Journals*

- D. R. Quiñones, J. Ferragud-Agulló, R. Pérez-Feito, J. García-Manrique, S. Canals, and D. Moratal, “A Tangible Educative 3D Printed Atlas of the Rat Brain”, *Materials*, vol. 11, no. 9, p. 1531, 2018. DOI: 10.3390/ma11091531
- D. R. Quiñones, D. Soler-Egea, V. González-Pérez, J. Reibke, E. Simarro-Mondejar, R. Pérez-Feito, J. García-Manrique, V. Crispín, and D. Moratal, “Open Source 3D Printed Lung Tumor Movement Simulator for

Radiotherapy Quality Assurance”, *Materials*, vol. 11, no. 8, p. 1317, 2018. DOI: 10.3390/ma11081317

- D. R. Quiñones, L. M. Fernández-Mollá, J. Pacheco-Torres, J. M. Caramés, S. Canals, and D. Moratal, “TherMouseDuino: An affordable Open-Source temperature control system for functional magnetic resonance imaging experimentation with mice”, *Magnetic Resonance Imaging*, vol. 58, p. 9, 2019. DOI: 10.1016/j.mri.2019.01.009

9.2.2 National Journals

- V. Álvarez, D. R. Quiñones, D. Moratal, V. Crispín, R. Pérez-Feito, M. Á. Arroyo, N. Gómez, and V. González-Pérez, “Diseño de moldes personalizados con técnicas de impresión 3D para tratamientos de braquiterapia superficial y radioterapia externa”, *Revista de Física Médica, Sociedad Española de Física Médica (SEFM) [submitted]*, 2018

9.3 Patents

- D. Moratal Pérez, D. R. Quiñones Colomer, S. Canals Gamoneda, J. A. García Manrique, and R. Pérez Feito, *Dispositivo automático de posicionamiento para corte de tejido tridimensional en una muestra, vibratomo que lo comprende y su uso*, 2015
- D. Moratal Pérez, A. Cuevas López, J. Cambra Enguix, D. R. Quiñones Colomer, and S. Canals Gamoneda, *Baldosa y malla para la identificación y seguimiento de animales y sistema de identificación y seguimiento de animales*, 2017
- D. Moratal, R. Prat-Acín, M. Fernández-Rodríguez, and D. R. Quiñones, *Herramienta de registro de áreas cerebrales elocuentes mediante análisis de imagen, durante la cirugía de tumores cerebrales*, 2016

9.4 Publications in International Conference Proceedings

- D. R. Quiñoñes, R. Perez-Feito, J. A. Garcia-Manrique, S. Canals, and D. Moratal, “Automatic positioning device for cutting three-dimensional tissue in living or fixed samples. Proof of concept”, *2017 39th Annual International Conference of the IEEE Engineering in Medicine and Biology Society (EMBC)*, Jeju Island, South Korea, South Korea: IEEE, 2017, pp. 1372–1375. DOI: 10.1109/EMBC.2017.8037088
- D. R. Quiñoñes, A. Cuevas, J. Cambra, S. Canals, and D. Moratal, “RATT: RFID Assisted Tracking Tile. Preliminary results”, *2017 39th Annual International Conference of the IEEE Engineering in Medicine and Biology Society (EMBC)*, IEEE, 2017, pp. 4114–4117. DOI: 10.1109/EMBC.2017.8037761
- D. R. Quiñoñes, G. Lopes, D. Kim, C. Honnet, D. Moratal, and A. Kampff, “HIVE Tracker”, *Proceedings of the 9th Augmented Human International Conference on - AH '18*, vol. Part F1344, New York, New York, USA: ACM Press, 2018, pp. 1–8. DOI: 10.1145/3174910.3174935

9.5 Awards and Honours

- First award in Biotecnología y Biomedicina - Valencia Idea 2015. Sistema automático de posicionamiento para corte de tejido tridimensional en muestras vivas o fijadas - Concejalía de Juventud - Ayuntamiento de València - Gas Natural Cegas
- First award Concurso Emprendedor Universitario STARTUPV 2K18 - Modalidad TFG/TFM/TESIS [EMPRENDE], Cyclung - simulador del movimiento de un tumor en el pulmón durante el ciclo respiratorio para la mejora del tratamiento mediante técnicas de radioterapia student: David Soler-Egea, Supervisors: Quiñoñes-Colomer, Darío R. & Moratal Pérez D.

9.6 Others

- D. Kim, K Perkins, C Ramble, H Garnade, G. Lopes, D. R. Quiñones, R Campbell-Russo, F Lischenko, C O'Brien, R Nakajima, R. Hanlon, I Blaney, K McNaught, R Barrett, M Stopps, K Fergus, T.-G. A, D Osorio, T. E. Team, and A. Kampff, *Surprising Minds. Interactive installation and crowd human behaviour experiment*. Sea Life Brighton, Brighton, UK., 2017

9.7 Final Master Project Supervision

- M. Fernández Rodríguez, “Desarrollo de una herramienta de registro de áreas cerebrales elocuentes mediante análisis de imagen, como soporte al mapeo cerebral intraoperatorio con paciente despierto durante la cirugía de tumores cerebrales.” “Sup.: D. R. Quiñones, and D. Moratal”, Trabajo de Final de Grado del Grado de Ingeniería Biomédica, Universitat Politècnica de València, 2016
- L. M. Fernández Mollá, “Sistema regulador de temperatura basado en Arduino para experimentación con animales para la obtención de Imágenes por Resonancia Magnética Funcional.” “Supervisors: D. R. Quiñones, J. Pacheco-Torres, and D. Moratal.”, Trabajo Fin de Máster del Máster en Ingeniería Biomédica, Universitat Politècnica de València, 2016
- E. Simarro Mondejar, “Simulación mediante un sistema LEGO del movimiento de un tumor con el ciclo respiratorio en el tratamiento de cáncer de pulmón.” “ Supervisors: D. R. Quiñones, and D. Moratal.”, Trabajo Fin de Máster del Máster en Ingeniería Biomédica, Universitat Politècnica de València, 2015

9.8 Final Degree Project Supervision

- D. Soler-Egea, “Diseño y desarrollo de un simulador del movimiento de un tumor en el pulmón durante el ciclo respiratorio para la mejora del tratamiento mediante técnicas de radioterapia.” “Supervisors: D. R. Quiñones , and D. Moratal.”, Trabajo Final de Grado del Grado en Ingeniería Industrial, Universitat Politècnica de València, 2018
- A. Hernández Vega, “Desarrollo y fabricación de moldes personalizados para tratamiento de tumores mediante braquiterapia.” “Supervisors: D. R. Quiñones, and D. Moratal.”, Trabajo de Final de Grado del Grado de Ingeniería Biomédica, Universitat Politècnica de València, 2018
- J. Ferragud Agulló, “Desarrollo de un modelo anatómico cerebral de rata mediante técnicas de impresión 3D y análisis de imagen por resonancia magnética.” “Supervisors: D. R. Quiñones, and D. Moratal.”, Trabajo de Final de Grado del Grado de Ingeniería Biomédica, Universitat Politècnica de València, 2016
- C. Calatayud Guerrero, “Desarrollo de un puntero para el registro de áreas cerebrales elocuentes durante intervenciones quirúrgicas.” “Supervisors: D. R. Quiñones, and D. Moratal.”, Trabajo de Final de Grado del Grado de Ingeniería Biomédica, Universitat Politècnica de València, 2017
- I. Olivares Guerrero, “Desarrollo de un software para el registro de las áreas cerebrales elocuentes durante las intervenciones quirúrgicas.” “Supervisors: D. R. Quiñones, and D. Moratal.”, Trabajo de Final de Grado del Grado de Ingeniería Biomédica, Universitat Politècnica de València, 2017
- M. Sáez Sánchez, “Diseño y desarrollo de una herramienta para la detección del posicionamiento y orientación de una muestra biológica en un sistema de corte tridimensional mediante cámaras de video y análisis de imagen.” “Supervisors: D. R. Quiñones, and D. Moratal”, Trabajo de Final de Grado del Grado de Ingeniería Biomédica, Universitat Politècnica de València, 2016
- J. A. Cortés Granell, “Desarrollo de un reloj-contador electrónico modulable para un juego de tablero basado en fantasy football.” “Supervisors: D. R.

Quiñones, and D. Moratal.”, Trabajo Final de Grado del Grado en Ingeniería Industrial, Universitat Politècnica de València, 2015

List of Figures

1.1	Golgi Stain	3
1.2	The most famous used animal models for experimentation	6
2.1	Zebrafish camera tracking.	16
2.2	Particle filtering approach example	18
2.3	Behavior computer vision classifier	18
2.4	Inductive coupled RFID-System	21
2.5	Coin Tag	23
2.6	Mechanical layout of a glass transponder	24
2.7	An example of electrophysiology during behavior experiments	25
2.8	RATT simplified diagram block.	26
2.9	ARM Cortex M4F LPC4088	29
2.10	Biocompatible Crystal RFID Tags	30
2.11	RATT tiles interconnection	32
2.12	RATT environment concept.	34

2.13	RATT detailed diagram block.	35
2.14	Control Board	35
2.15	RF board	37
2.16	The Relationship between vertical distance and ampere-turns for a 5 cm radius antenna.	38
2.17	Magnetic field strength on the horizontal axis	38
2.18	Antenna PCB footprint	39
2.19	Antenna Simulation with MATLAB	40
2.20	Antenna Simulation with CST	41
2.21	Antenna Simulation with passive coils through CST	42
2.22	2D CAD of the structure.	43
2.23	Photo of the assembled structure	44
2.24	Co-tracking Setup.	46
2.25	Traking Aruco Markers.	47
2.26	Co-tracking multiple tags.	48
2.27	RSSI map	49
2.28	RATT versus Camera tracking mistakes	50
2.29	Camera tracking versus RATT	51
2.30	RATT environment	52
2.31	RATT environment with an L shape	53
3.1	Overall Hive Tracker system overview	59
3.2	Valve tracking system (from Valve Corp. , WA, USA).	59
3.3	Representation of the computed lines in the 3D space.	60
3.4	Light signal sequences	62

3.5 Accuracy comparison between a commercial controller and Hive Tracker proof-of-concept in an ideal room.	64
3.6 Accuracy comparison between commercial controller and Hive Tracker proof-of-concept in a non-ideal room.	65
3.7 Reflections off the walls	66
3.8 PCB design	68
3.9 Programmable peripheral interconnect (PPI)	69
3.10 Size/weight comparison.	70
3.11 Hive Tracker prototype, with a US 25 cent coin for size comparison.	71
4.1 Schematic diagram of the connected devices.	77
4.2 TherMouseDuino disassembly.	79
4.3 Data acquisition for experimental identification of the system. . . .	85
4.4 Selected data for the experimental identification of the system. . .	86
4.5 Measured and simulated model output.	87
4.6 Results obtained using the final regulator.	90
4.7 BOLD response for 20Hz electric stimulation in the perforant pathway.	91
5.1 Pipeline of the process from a CT or MRI set of images to a physical 3D printed model.	96
5.2 Statistical Parametrical Mapping toolbox.	97
5.3 Data labeling in Amira 3D software.	99
5.4 Smoothing process applied on the Basal Ganglia.	101
5.5 Interconnecting joins.	102
5.6 Final 3D model (disassembled) of the rat template.	103
5.7 Final 3D model of the rat template.	104

6.1	Microtome slicing process	109
6.2	Three-dimensional model of a slicing process of a mouse brain. . .	110
6.3	Automatic positioning device for cutting 3D tissue parts explosion.	111
6.4	Schematic illustration of the 3D positioning system.	113
6.5	Motion-capturing sensor MPU 9150	114
6.6	Real Automatic positioning device for cutting 3D tissue assembled with a commercial Leica VT 1200 S Vibratome.	115
6.7	System specifications	116
6.8	Slicing test with an agarose rat brain	116
6.9	Graphical user interface	117
7.1	Hysteresis loop of lung tumors movement	122
7.2	Real Lung Tumor Movement Simulator prototype	125
7.3	3D model of the Lung Tumor Movement Simulator	126
7.4	Virtual simulation of the desired area to cover with the LTMS in order to validate the viability of the system design.	127
7.5	LMTS motors setup detail	128
7.6	Simulator setups	130
7.7	Virtual reconstruction of the location where the prototype should be placed	132

List of Tables

2.1	RFID Bands, regulations and specifications	22
2.2	LPC4088 board features	29
2.3	Equation 2.2, 2.3 and 2.4 variables	45
3.1	Activation Timings	61
5.1	Regions clustering.	98
5.2	Measurements on X, Y, Z axes of each part, total assembly without container and total assembly with container.	103
7.1	Prototype parts.	126

Abbreviations and Acronyms

2D Two-Dimensional. 42, 43, 66, 94, 95, 100, 137

3D Three-Dimensional. vi, 8, 11, 27, 28, 34, 46, 58, 61, 66, 68, 69, 72, 93–97, 99–105, 107–112, 116, 122, 125, 126, 131–133

ABS Acrylonitrile butadiene styrene. 22, 23, 104

AFE Analog Front End. 31

ARM Advanced RISC Machine. 28, 29, 61, 67, 68

BLE Bluetooth Low-Energy. 67, 68

BOLD Blood Oxygen Level Dependent. vi, 73–75, 90

BOOTP Bootstrap Protocol. 32

CAD Computer-Aided Design. 28

CBF Cerebral Blood Flow. 74

CBV Cerebral Blood Volume. 74

CT Computed Tomography. 94, 96, 105

DHCP Dynamic Host Configuration Protocol. 32

- DMP** Digital Motion Processor. 113
- DNS** Domain Name System. 32
- fMRI** functional MRI. vi, 10, 73, 75, 76, 85, 89–91, 94
- FPGA** Field-Programmable Gate Array. 67–69
- FPS** Frames Per Second. 45
- GPIO** General Purpose Input/Output. 68
- GUI** Graphical User Interface. 27, 44, 46, 116, 117
- HF** High Frequency/RF (3-30 MHz). 22, 23, 26, 27
- HSV** Hue, Saturation, Value. 129
- I²C** Inter-Integrated Circuit. 28, 34, 36, 114, 116
- IC** Integrated Circuit. 60, 68
- IDE** Integrated Development Environment. 27
- IEC** International Electrotechnical Commission. 30, 31
- IMU** Integrated Motion Unit. 68
- IR** InfraRed. 60, 69
- ISO** International Organization for Standardization. 30, 31
- LF** Low Frequency (30-300 kHz). 22, 23
- LINAC** Linear Accelerator. 120, 122, 123, 131
- MCU** MicroController Unit. 31, 67–69
- MEMS** Micro-Electro-Mechanical Systems. 113
- MPU** Multiple Process Unit. 113, 114, 116
- MRI** Magnetic Resonance Imaging. vi, 7, 10, 75, 77, 94–99, 105

- OECD** Organization for Economic Co-operation and Development. 119, 120
- OSC** Open Sound Control. 61
- PCB** Printed circuit board. 23, 28, 31, 36, 39, 60, 65, 67, 68, 70, 76
- PID** Proportional-Integrative-Derivative. 76, 82
- PLA** poly(lactic acid). 104, 125
- PPI** Programmable Peripheral Interconnect. 67, 69
- RATT** RFID Assisted Tracking Tile. v, 10, 13, 19, 25–27, 33–36, 41, 42, 45–48, 50–53
- RF** Radio Frequency. 22, 26, 33–37, 41, 42, 148
- RFID** Radio Frequency IDentification. v, 10, 13, 19–22, 27, 28, 31, 34, 36, 39, 41, 45, 47, 49, 51
- RISC** Reduced Instruction Set Computing. 28, 147
- RSSI** Received Signal Strength Indicator. 25, 30, 42, 44–49
- SDK** Software Development Kit. 69
- SPI** Serial Peripheral Interface. 28, 31, 80
- UART** Universal Asynchronous Receiver-Transmitter. 28
- UDP** User Datagram Protocol. 32, 35, 46, 61
- UHF** Ultra High Frequency (300 MHz-3 GHz). 22, 23, 26
- USB** Universal Serial Bus. 28, 79, 80, 116
- VR** Virtual Reality. 10, 60, 61, 65, 72

Bibliography

- [1] G. K. York and D. A. Steinberg, “Chapter 3 Neurology in Ancient Egypt”, *Handbook of Clinical Neurology*, Elsevier B.V., 2009, pp. 29–36. DOI: 10.1016/S0072-9752(08)02103-9 (cit. on p. 2).
- [2] E. R. Kandel, J. H. Schwartz, T. M. Jessell, D. o. B. Jessell, M. B. Thomas, S. Siegelbaum, and A. J. Hudspeth, *Principles of neural science*. McGraw-hill New York, 2000, vol. 4 (cit. on p. 2).
- [3] S. Zaqout and A. M. Kaindl, “Golgi-Cox Staining Step by Step”, *Frontiers in Neuroanatomy*, vol. 10, 2016. DOI: 10.3389/fnana.2016.00038 (cit. on p. 3).
- [4] B. Hassard, “Bifurcation of periodic solutions of the Hodgkin-Huxley model for the squid giant axon”, *Journal of Theoretical Biology*, vol. 71, pp. 401–420, 1978. DOI: 10.1016/0022-5193(78)90168-6 (cit. on p. 2).
- [5] C. A. Nelson and M. Luciana, *Handbook of Developmental Cognitive Neuroscience*. 2008, vol. 0, p. 936. DOI: 10.1002/1521-3773(20010316)40:6<9823::AID-ANIE9823>3.3.CO;2-C (cit. on p. 2).

- [6] M. Aragona, G. D. Kotzalidis, and A. Puzella, “The many faces of empathy, between phenomenology and neuroscience”, *Archives of Psychiatry and Psychotherapy*, vol. 15, pp. 5–12, 2013. DOI: 10.12740/APP/19179 (cit. on p. 3).
- [7] T. Ofengenden, “Memory Formation and Belief”, *Dialogues in Philosophy, Mental and Neuro Sciences*, vol. 7, 2014 (cit. on p. 3).
- [8] J. L. Silverman, M. Yang, C. Lord, and J. N. Crawley, “Behavioural phenotyping assays for mouse models of autism”, *Nature Reviews Neuroscience*, vol. 11, pp. 490–502, 2010. DOI: 10.1038/nrn2851 (cit. on p. 3).
- [9] P. W. Glimcher, “Neuroeconomics: The Consilience of Brain and Decision”, *Science*, vol. 306, pp. 447–452, 2004. DOI: 10.1126/science.1102566 (cit. on p. 3).
- [10] D. Rakshit, K. M. Daily, and D. Blume, “Natural and unnatural parity states of small trapped equal-mass two-component Fermi gases at unitarity and fourth-order virial coefficient”, *Physical Review A*, vol. 85, p. 033634, 2012. DOI: 10.1103/PhysRevA.85.033634 (cit. on p. 3).
- [11] R. Adolphs, “Cognitive neuroscience of human social behaviour”, *Nature Reviews Neuroscience*, vol. 4, pp. 165–178, 2003. DOI: 10.1038/nrn1056 (cit. on p. 3).
- [12] C. Morin, “Neuromarketing: The New Science of Consumer Behavior”, *Society*, vol. 48, pp. 131–135, 2011. DOI: 10.1007/s12115-010-9408-1 (cit. on p. 3).
- [13] R. Gordon, J. Ciorciari, and T. van Laer, “Using EEG to examine the role of attention, working memory, emotion, and imagination in narrative transportation”, *European Journal of Marketing*, vol. 52, pp. 92–117, 2018. DOI: 10.1108/EJM-12-2016-0881 (cit. on p. 4).
- [14] M. A. Suckow, S. H. Weisbroth, and C. L. Franklin, *The laboratory rat*. Elsevier, 2006, p. 912 (cit. on pp. 4, 7).

- [15] J. L. Molina Martínez, G. Alonso Villavicencio, D. Heredia Ruiz, M. N. García Cruz, C. Sánchez Álvarez, M. Castro Gutiérrez, and L. Chaviano Álvarez, *Bioética en la experimentación animal*, 2015 (cit. on p. 4).
- [16] M. G. S. Consortium, “Initial sequencing and comparative analysis of the mouse genome”, *Nature*, vol. 420, pp. 520–562, 2002. DOI: 10.1038/nature01262 (cit. on p. 5).
- [17] A. L. Hodgkin and A. F. Huxley, “A quantitative description of membrane current and its application to conduction and excitation in nerve”, *The Journal of Physiology*, vol. 117, p. 500, 1952 (cit. on p. 5).
- [18] J del Castillo and B Katz, “Local activity at a depolarized nerve-muscle junction.”, *The Journal of physiology*, vol. 128, pp. 396–411, 1955 (cit. on p. 5).
- [19] D Lange, H. K. Hartline, and F Ratliff, “Inhibitory interaction in the retina: techniques of experimental and theoretical analysis.”, *Annals of the New York Academy of Sciences*, vol. 128, pp. 955–71, 1966 (cit. on p. 5).
- [20] E. R. Kandel, “The Molecular Biology of Memory Storage: A Dialogue Between Genes and Synapses”, *Science*, vol. 294, pp. 1030–1038, 2001. DOI: 10.1126/science.1067020 (cit. on p. 5).
- [21] H. J. Bellen, C. Tong, and H. Tsuda, “100 years of Drosophila research and its impact on vertebrate neuroscience: a history lesson for the future”, *Nature Reviews Neuroscience*, vol. 11, pp. 514–522, 2010. DOI: 10.1038/nrn2839 (cit. on p. 6).
- [22] J. O’Keefe and L. Nadel, “Précis of O’Keefe & Nadel’s The hippocampus as a cognitive map”, *Behavioral and Brain Sciences*, vol. 2, pp. 487–494, 1979. DOI: 10.1017/S0140525X00063949 (cit. on p. 6).
- [23] T. Hafting, M. Fyhn, S. Molden, M.-B. Moser, and E. I. Moser, “Microstructure of a spatial map in the entorhinal cortex”, *Nature*, vol. 436, pp. 801–806, 2005. DOI: 10.1038/nature03721 (cit. on p. 6).

- [24] M. A. Suckow, P. Danneman, and C. Brayton, *The Laboratory Mouse*. 2001, vol. 20007162, p. 600. DOI: 10.1201/9780849376276 (cit. on p. 7).
- [25] L. Giancardo, D. Sona, H. Huang, S. Sannino, F. Managò, D. Scheggia, F. Papaleo, and V. Murino, “Automatic Visual Tracking and Social Behaviour Analysis with Multiple Mice”, *PLoS ONE*, vol. 8, T. Burne, Ed., e74557, 2013. DOI: 10.1371/journal.pone.0074557 (cit. on pp. 14, 18).
- [26] U.-M. M. Jow, P. McMenamain, M. Kiani, J. R. Manns, and M. Ghovanloo, “EnerCage: A smart experimental arena with scalable architecture for behavioral experiments”, *IEEE Transactions on Biomedical Engineering*, vol. 61, pp. 139–148, 2014. DOI: 10.1109/TBME.2013.2278180 (cit. on pp. 14, 15, 24).
- [27] T. Wey, D. T. Blumstein, W. Shen, and F. Jordán, “Social network analysis of animal behaviour: a promising tool for the study of sociality”, *Animal Behaviour*, vol. 75, pp. 333–344, 2008. DOI: 10.1016/j.anbehav.2007.06.020 (cit. on p. 14).
- [28] J. W. Kalat, *Biological psychology*. Sinauer Associates Sunderland, 2013, p. 577. DOI: 10.1016/j.anbehav.2011.05.023 (cit. on p. 14).
- [29] L. Lewejohann, A. M. Hoppmann, P. Kegel, M. Kritzler, A. Krüger, and N. Sachser, “Behavioral phenotyping of a murine model of Alzheimer’s disease in a seminaturalistic environment using RFID tracking”, *Behavior Research Methods*, vol. 41, pp. 850–856, 2009. DOI: 10.3758/BRM.41.3.850 (cit. on pp. 14, 24).
- [30] R. C. Hinz and G. G. de Polavieja, “Ontogeny of collective behavior reveals a simple attraction rule”, *Proceedings of the National Academy of Sciences*, vol. 114, pp. 2295–2300, 2017. DOI: 10.1073/pnas.1616926114 (cit. on pp. 14, 24).
- [31] A. T. Schaefer and A. Claridge-Chang, “The surveillance state of behavioral automation”, *Current Opinion in Neurobiology*, vol. 22, pp. 170–176, 2012. DOI: 10.1016/j.conb.2011.11.004 (cit. on pp. 14, 15, 18, 24).

- [32] C. Desjardins, J. A. Maruniak, and F. H. Bronson, “Social Rank in House Mice: Differentiation Revealed by Ultraviolet Visualization of Urinary Marking Patterns”, *Science*, vol. 182, pp. 939–941, 1973. DOI: 10.1126/science.182.4115.939 (cit. on p. 14).
- [33] E. C. Grant and J. H. Mackintosh, “A Comparison of the Social Postures of Some Common Laboratory Rodents”, *Behaviour*, vol. 21, pp. 246–259, 1963. DOI: 10.2307/4533055 (cit. on p. 14).
- [34] G. Gheusi, R.-M. Bluthé, G. Goodall, and R. Dantzer, “Social and individual recognition in rodents: Methodological aspects and neurobiological bases”, *Behavioural Processes*, vol. 33, pp. 59–87, 1994. DOI: 10.1016/0376-6357(94)90060-4 (cit. on p. 14).
- [35] M. Baker, “Inside the minds of mice and men”, *Nature*, vol. 475, pp. 123–128, 2011. DOI: 10.1038/475123a (cit. on p. 14).
- [36] H. Dankert, L. Wang, E. D. Hoopfer, D. J. Anderson, and P. Perona, “Automated monitoring and analysis of social behavior in *Drosophila*”, *Nature Methods*, vol. 6, pp. 297–303, 2009. DOI: 10.1038/nmeth.1310 (cit. on p. 14).
- [37] K. Branson, A. A. Robie, J. Bender, P. Perona, and M. H. Dickinson, “High-throughput ethomics in large groups of *Drosophila*”, *Nature Methods*, vol. 6, pp. 451–457, 2009. DOI: 10.1038/nmeth.1328 (cit. on p. 14).
- [38] T. P. Patel, D. M. Gullotti, P. Hernandez, *et al.*, “An open-source toolbox for automated phenotyping of mice in behavioral tasks”, *Frontiers in Behavioral Neuroscience*, vol. 8, p. 349, 2014. DOI: 10.3389/fnbeh.2014.00349 (cit. on p. 15).
- [39] M. Reiser, “The ethomics era?”, *Nature Methods*, vol. 6, pp. 413–414, 2009. DOI: 10.1038/nmeth0609-413 (cit. on pp. 15, 16).
- [40] S. D. Pelkowski, M. Kapoor, H. A. Richendrfer, X. Wang, R. M. Colwill, and R. Creton, “A novel high-throughput imaging system for automated

- analyses of avoidance behavior in zebrafish larvae”, *Behavioural Brain Research*, vol. 223, pp. 135–144, 2011. DOI: 10.1016/j.bbr.2011.04.033 (cit. on p. 15).
- [41] S. Ohayon, O. Avni, A. L. Taylor, P. Perona, and S. Roian Egnor, “Automated multi-day tracking of marked mice for the analysis of social behaviour”, *Journal of Neuroscience Methods*, vol. 219, pp. 10–19, 2013. DOI: 10.1016/j.jneumeth.2013.05.013 (cit. on pp. 15, 18, 24).
- [42] A. Weissbrod, A. Shapiro, G. Vasserman, L. Edry, M. Dayan, A. Yitzhaky, L. Hertzberg, O. Feinerman, and T. Kimchi, “Automated long-term tracking and social behavioural phenotyping of animal colonies within a semi-natural environment.”, *Nature communications*, vol. 4, p. 2018, 2013. DOI: 10.1038/ncomms3018 (cit. on pp. 15, 24).
- [43] M. Shen, P. Szyszka, O. Deussen, C. G. Galizia, and D. Merhof, “Automated tracking and analysis of behavior in restrained insects”, *Journal of Neuroscience Methods*, vol. 239, pp. 194–205, 2015. DOI: 10.1016/j.jneumeth.2014.10.021 (cit. on p. 15).
- [44] G. Lopes, N. Bonacchi, J. Frazão, *et al.*, “Bonsai: an event-based framework for processing and controlling data streams.”, *Frontiers in Neuroinformatics*, vol. 9, p. 7, 2015. DOI: 10.3389/fninf.2015.00007 (cit. on pp. 15, 28, 62, 129).
- [45] A. Pérez-Escudero, J. Vicente-Page, R. C. Hinz, S. Arganda, and G. G. De Polavieja, “idTracker: tracking individuals in a group by automatic identification of unmarked animals.”, *Nature methods*, vol. 11, pp. 743–748, 2014. DOI: 10.1038/nmeth.2994 (cit. on pp. 15, 16, 24).
- [46] A. Isasi, S. Rodriguez, J. L. D. Armentia, and A. Villodas, *Location, tracking and identification with RFID and vision data fusion*. 2010, pp. 1–6 (cit. on pp. 15, 19, 24).

-
- [47] Y. Sztainberg and A. Chen, “An environmental enrichment model for mice.”, *Nature protocols*, vol. 5, pp. 1535–1539, 2010. DOI: 10.1038/nprot.2010.114 (cit. on p. 15).
- [48] W. S. Redfern, K. Tse, C. Grant, *et al.*, “Automated recording of home cage activity and temperature of individual rats housed in social groups: The Rodent Big Brother project”, *PLoS ONE*, vol. 12, J. Homberg, Ed., p. 26, 2017. DOI: 10.1371/journal.pone.0181068 (cit. on p. 15).
- [49] C. Restif, C. Ibáñez-Ventoso, M. M. Vora, S. Guo, D. Metaxas, and M. Driscoll, “CeleST: Computer Vision Software for Quantitative Analysis of *C. elegans* Swim Behavior Reveals Novel Features of Locomotion”, *PLoS Computational Biology*, vol. 10, A. Prlic, Ed., e1003702, 2014. DOI: 10.1371/journal.pcbi.1003702 (cit. on p. 15).
- [50] M. J. Silk, A. L. Jackson, D. P. Croft, K. Colhoun, and S. Bearhop, “The consequences of unidentifiable individuals for the analysis of an animal social network”, *Animal Behaviour*, vol. 104, pp. 1–11, 2015. DOI: 10.1016/j.anbehav.2015.03.005 (cit. on p. 15).
- [51] E. Dreosti, G. Lopes, A. R. Kampff, and S. W. Wilson, “Development of social behavior in young zebrafish”, *Frontiers in Neural Circuits*, vol. 9, p. 39, 2015. DOI: 10.3389/fncir.2015.00039 (cit. on pp. 16, 18, 24).
- [52] K. Branson and S. Belongie, “Tracking Multiple Mouse Contours (without Too Many Samples)”, *2005 IEEE Computer Society Conference on Computer Vision and Pattern Recognition (CVPR’05)*, vol. 1, IEEE, pp. 1039–1046. DOI: 10.1109/CVPR.2005.349 (cit. on p. 17).
- [53] Branson and Kristin, “Tracking multiple mice through severe occlusions”, PhD thesis, 2007 (cit. on p. 17).
- [54] H. Pistori, V. V. Viana Aguiar Odakura, J. B. Oliveira Monteiro, W. N. Gonçalves, A. R. Roel, J. de Andrade Silva, and B. B. Machado, “Mice and larvae tracking using a particle filter with an auto-adjustable observation

- model”, *Pattern Recognition Letters*, vol. 31, pp. 337–346, 2010. DOI: 10.1016/j.patrec.2009.05.015 (cit. on pp. 17, 18).
- [55] A. Klaeser, M. Marszalek, and C. Schmid, “A Spatio-Temporal Descriptor Based on 3D-Gradients”, *Proceedings of the British Machine Vision Conference 2008*, 2008, pp. 99.1–99.10. DOI: 10.5244/C.22.99 (cit. on p. 17).
- [56] G. Willems, T. Tuytelaars, and L. Van Gool, “An efficient dense and scale-invariant spatio-temporal interest point detector”, *Lecture Notes in Computer Science (including subseries Lecture Notes in Artificial Intelligence and Lecture Notes in Bioinformatics)*, vol. 5303 LNCS, 2008, pp. 650–663. DOI: 10.1007/978-3-540-88688-4-48 (cit. on p. 17).
- [57] H. Jhuang, T. Serre, L. Wolf, and T. Poggio, “A biologically inspired system for action recognition”, *IEEE 11th International Conference on Computer Vision*, pp. 1–8, 2007. DOI: 10.1109/ICCV.2007.4408988 (cit. on p. 17).
- [58] P. Dollár, V. Rabaud, G. Cottrell, and S. Belongie, “Behavior recognition via sparse spatio-temporal features”, *Proceedings - 2nd Joint IEEE International Workshop on Visual Surveillance and Performance Evaluation of Tracking and Surveillance, VS-PETS*, vol. 2005, 2005, pp. 65–72. DOI: 10.1109/VSPETS.2005.1570899 (cit. on p. 18).
- [59] C. T. Hsu, P. Dollár, D. Chang, and A. D. Steele, “Daily timed sexual interaction induces moderate anticipatory activity in mice”, *PLoS ONE*, vol. 5, 2010. DOI: 10.1371/journal.pone.0015429 (cit. on p. 18).
- [60] H. Jhuang, E. Garrote, X. Yu, V. Khilnani, T. Poggio, A. D. Steele, and T. Serre, “Automated home-cage behavioural phenotyping of mice”, *Nature Communications*, vol. 1, 2010. DOI: 10.1038/ncomms1064 (cit. on p. 18).
- [61] R. Tesoriero, J. Gallud, M. Lozano, and V. R. Penichet, “Tracking autonomous entities using rfid technology”, *IEEE Transactions on Consumer Electronics*, vol. 55, pp. 650–655, 2009. DOI: 10.1109/TCE.2009.5174435 (cit. on pp. 18, 19).

- [62] J. L. Brchan, L. Zhao, J. Wu, R. E. Williams, and L. C. Pérez, “A real-time RFID localization experiment using propagation models”, *2012 IEEE International Conference on RFID, RFID 2012*, 2012, pp. 141–148. DOI: 10.1109/RFID.2012.6193042 (cit. on p. 19).
- [63] T. Hori, T. Wada, Y. Ota, N. Uchitomi, K. Mutsuura, and H. Okada, “A multi-sensing-range method for position estimation of passive RFID tags”, *Proceedings - 4th IEEE International Conference on Wireless and Mobile Computing, Networking and Communication, WiMob 2008*, 2008, pp. 208–213. DOI: 10.1109/WiMob.2008.39 (cit. on p. 19).
- [64] L. M. Ni, Y. Liu, Y. C. Lau, and A. P. Patil, “LANDMARC: Indoor Location Sensing Using Active RFID”, *Wireless Networks*, vol. 10, pp. 701–710, 2004. DOI: 10.1023/B:WINE.0000044029.06344.dd (cit. on p. 19).
- [65] B. Danev, S. Capkun, R. Jayaram Masti, and T. S. Benjamin, “Towards Practical Identification of HF RFID Devices”, *ACM Transactions on Information and System Security*, vol. 15, pp. 1–24, 2012. DOI: 10.1145/2240276.2240278 (cit. on p. 19).
- [66] X. Liu, J. Peng, and T. Liu, “A novel indoor localization system based on passive RFID technology”, *Proceedings of 2011 International Conference on Electronic & Mechanical Engineering and Information Technology*, IEEE, 2011, pp. 4285–4288. DOI: 10.1109/EMEIT.2011.6023112 (cit. on p. 19).
- [67] D. Wei, W. Hung, and K. L. Wu, “A real time RFID locationing system using phased array antennas for warehouse management”, *2016 IEEE Antennas and Propagation Society International Symposium, APSURSI 2016 - Proceedings*, 2016, pp. 1153–1154. DOI: 10.1109/APS.2016.7696284 (cit. on p. 19).
- [68] K. S. Leong, M. L. Ng, and P. H. Cole, “Positioning analysis of multiple antennas in a dense RFID reader environment”, *Proceedings - 2006 Symposium on Applications and the Internet Workshops, SAINT 2006*

- Workshops*, vol. 2006, 2006, pp. 56–59. DOI: 10.1109/SAINT-W.2006.32 (cit. on p. 19).
- [69] M Galsworthy, I Amrein, P Kuptsov, I Poletaeva, P Zinn, A Rau, A Vyssotski, and H Lipp, “A comparison of wild-caught wood mice and bank voles in the Intellicage: assessing exploration, daily activity patterns and place learning paradigms”, *Behavioural Brain Research*, vol. 157, pp. 211–217, 2005. DOI: 10.1016/j.bbr.2004.06.021 (cit. on p. 19).
- [71] N. Krahnstoever, J. Rittscher, P. Tu, K. Chean, and T. Tomlinson, “Activity Recognition using Visual Tracking and RFID”, *2005 Seventh IEEE Workshops on Applications of Computer Vision (WACV/MOTION’05) - Volume 1*, 2005, pp. 494–500. DOI: 10.1109/ACVMOT.2005.17 (cit. on p. 19).
- [72] C.-S. Wang and L.-C. Cheng, “RFID & vision based indoor positioning and identification system”, *2011 IEEE 3rd International Conference on Communication Software and Networks*, pp. 506–510, 2011. DOI: 10.1109/ICCSN.2011.6014945 (cit. on p. 19).
- [73] K. Finkenzerler, *RFID Handbook*. Chichester, UK: John Wiley & Sons, Ltd, 2010. DOI: 10.1002/9780470665121 (cit. on pp. 20–22, 36).
- [74] R. J. Bodnar, “Biological Psychology: An Introduction to Behavioral, Cognitive, and Clinical Neuroscience”, *JAMA*, vol. 298, pp. 2680–2686, 2007 (cit. on p. 24).
- [75] A. M. Sodagar, G. E. Perlin, Y. Yao, K. Najafi, and K. D. Wise, “An implantable 64-channel wireless microsystem for single-unit neural recording”, *IEEE Journal of Solid-State Circuits*, vol. 44, pp. 2591–2604, 2009. DOI: 10.1109/JSSC.2009.2023159 (cit. on p. 24).
- [76] T. A. Szuts, V. Fadeyev, S. Kachiguine, *et al.*, “A wireless multi-channel neural amplifier for freely moving animals”, *Nature Neuroscience*, vol. 14, 2011, pp. 263–270. DOI: 10.1038/nn.2730 (cit. on p. 24).

- [77] E. Greenwald, M. Mollazadeh, C. Hu, W. Tang, E. Culurciello, and N. Thakor, “A VLSI neural monitoring system with ultra-wideband telemetry for awake behaving subjects”, *IEEE Transactions on Biomedical Circuits and Systems*, vol. 5, 2011, pp. 112–119. DOI: 10.1109/TBCAS.2011.2141670 (cit. on p. 24).
- [78] D. Fan, D. Rich, T. Holtzman, *et al.*, “A wireless multi-channel recording system for freely behaving mice and rats”, *PLoS ONE*, vol. 6, 2011. DOI: 10.1371/journal.pone.0022033 (cit. on p. 24).
- [79] S. B. Lee, M. Yin, J. R. Manns, and M. Ghovanloo, “A wideband dual-antenna receiver for wireless recording from animals behaving in large arenas”, *IEEE Transactions on Biomedical Engineering*, vol. 60, pp. 1993–2004, 2013. DOI: 10.1109/TBME.2013.2247603 (cit. on p. 24).
- [80] N. W. Simon and B. Moghaddam, “Neural processing of reward in adolescent rodents”, *Developmental Cognitive Neuroscience*, vol. 11, pp. 145–154, 2015. DOI: 10.1016/j.dcn.2014.11.001 (cit. on p. 25).
- [81] F. J. Romero-Ramirez, R. Muñoz-Salinas, and R. Medina-Carnicer, “Speeded up detection of squared fiducial markers”, *Image and Vision Computing*, vol. 76, pp. 38–47, 2018. DOI: 10.1016/j.imavis.2018.05.004 (cit. on pp. 28, 45).
- [82] R. Muñoz-Salinas, M. J. Marín-Jimenez, E. Yeguas-Bolivar, and R. Medina-Carnicer, “Mapping and localization from planar markers”, *Pattern Recognition*, vol. 73, pp. 158–171, 2018. DOI: 10.1016/j.patcog.2017.08.010 (cit. on pp. 28, 45).
- [83] Embedded Artists, *LPC4088 QuickStart Board* (cit. on p. 29).
- [84] P. H. Smith, “An Improved Transmission Line Calculator”, *Electronics*, vol. 17, pp. 130–325, 1944 (cit. on p. 30).
- [85] G. Gonzalez, *Microwave transistor amplifiers analysis and design*. 1996, p. 506. DOI: 10.1109/RFIC.2005.1489794 (cit. on p. 31).

- [86] T. Instrument, *Rev A HF Power Amplifier (Reference Design Guide)*, 2008 (cit. on p. 32).
- [87] D. Senić, D. Poljak, and A. Šarolić, “Electromagnetic field exposure of 13.56 MHz RFID loop antenna”, *Software, Telecommunications and Computer Networks (SoftCOM), 2010 International Conference on*, IEEE, 2010, pp. 121–125 (cit. on p. 36).
- [88] L Youbok, “Antenna circuit design for RFID applications”, *Microchip Technology Inc*, pp. 1–50, 2003 (cit. on pp. 36, 37).
- [89] A. Cuevas López, “Master thesis: Diseño de un sistema modular de identificación y localización mediante RFID de animales de experimentación en entornos de libertad controlada”, *Universitat Politècnica de València*, Tech. Rep., 2015, p. 61 (cit. on pp. 36, 38, 39).
- [90] Melexis, “13.56 MHz RFID systems and antennas design guide”, *Whitepaper - Melexis*, 2004 (cit. on p. 36).
- [91] R. L. Haupt, “Using MATLAB to control commercial computational electromagnetics software”, *Applied Computational Electromagnetics Society Journal*, 2008 (cit. on p. 36).
- [92] K. Lee, Y. Kim, and Y. C. Chung, “Design Automation of UHF RFID Tag Antenna Design Using a Genetic Algorithm Linked to MWS CST”, *4th IEEE International Symposium on Electronic Design, Test and Applications (delta 2008)*, IEEE, 2008, pp. 603–606. DOI: 10.1109/DELTA.2008.125 (cit. on p. 36).
- [93] M. Kisic, B. Dakic, M. Damnjanovic, A. Menicanin, N. Blaz, and L. Zivanov, “Design and simulation of 13.56 MHz RFID tag in ink-jet printing technology”, *Proceedings of the 36th International Spring Seminar on Electronics Technology*, IEEE, 2013, pp. 263–267. DOI: 10.1109/ISSE.2013.6648254 (cit. on p. 36).

- [94] K. Yang, D. Forte, and M. M. Tehranipoor, “UCR: An unclonable chipless RFID tag”, *2016 IEEE International Symposium on Hardware Oriented Security and Trust (HOST)*, IEEE, 2016, pp. 7–12. DOI: 10.1109/HST.2016.7495548 (cit. on p. 36).
- [95] F. Hirtenfelder, “Effective Antenna Simulations using CST MICROWAVE STUDIO®”, *2007 2nd International ITG Conference on Antennas*, IEEE, 2007, pp. 239–239. DOI: 10.1109/INICA.2007.4353972 (cit. on p. 36).
- [96] S. Basat, Kyutae Lim, J. Laskar, and M. Tentzeris, “Design and modeling of embedded 13.56 MHz RFID antennas”, *2005 IEEE Antennas and Propagation Society International Symposium*, vol. 4B, IEEE, 2005, pp. 64–67. DOI: 10.1109/APS.2005.1552740 (cit. on p. 36).
- [97] C. M. Studio, *Antenna Design and Simulation*, 2014 (cit. on p. 36).
- [98] A. O. Amos, H. Yskanda, A. Yasser, and D. Karim, “Effects of Coil Misalignments on the Magnetic Field and Magnetic Force Components between Circular Filaments”, *Journal of Machine to Machine Communications*, vol. 1, pp. 31–50, 2014. DOI: 10.13052/jmmc2246-137X.112 (cit. on p. 38).
- [99] R. Pieper and F. Dellsperger, “Personal computer assisted tutorial for Smith charts”, *Proceedings of the 33rd Southeastern Symposium on System Theory (Cat. No.01EX460)*, IEEE, 2001, pp. 139–143. DOI: 10.1109/SSST.2001.918506 (cit. on p. 39).
- [101] M. L. Anderson, “Embodied Cognition: A field guide”, *Artificial Intelligence*, vol. 149, pp. 91–130, 2003. DOI: 10.1016/S0004-3702(03)00054-7 (cit. on p. 56).
- [102] M. Wilson, “Six views of embodied cognition.”, *Psychonomic bulletin & review*, vol. 9, pp. 625–636, 2002 (cit. on p. 56).

- [103] M. Wilson and G. Knoblich, “The Case for Motor Involvement in Perceiving Conspecifics.”, *Psychological Bulletin*, vol. 131, pp. 460–473, 2005. DOI: 10.1037/0033-2909.131.3.460 (cit. on p. 56).
- [104] D. M. Wolpert, Z. Ghahramani, and J. R. Flanagan, “Perspectives and problems in motor learning”, *Trends in Cognitive Sciences*, vol. 5, pp. 487–494, 2001. DOI: 10.1016/S1364-6613(00)01773-3 (cit. on p. 56).
- [105] V. M. Preston-Dunlop and S. Lahusen, *Schritttanz: a view of German dance in the Weimar Republic*. Princeton Book Company Pub, 1990 (cit. on p. 56).
- [106] B. L. McNaughton, S. J. Y. Mizumori, C. A. Barnes, B. J. Leonard, M. Marquis, and E. J. Green, “Cortical Representation of Motion during Unrestrained Spatial Navigation in the Rat”, *Cerebral Cortex*, vol. 4, pp. 27–39, 1994. DOI: 10.1093/cercor/4.1.27 (cit. on p. 57).
- [107] E. I. Moser, E. Kropff, and M.-B. Moser, “Place Cells, Grid Cells, and the Brain’s Spatial Representation System”, *Annual Review of Neuroscience*, vol. 31, pp. 69–89, 2008. DOI: 10.1146/annurev.neuro.31.061307.090723 (cit. on p. 57).
- [108] H. Nishijo, T. Ono, S. Eifuku, and R. Tamura, “The relationship between monkey hippocampus place-related neural activity and action in space”, *Neuroscience Letters*, vol. 226, pp. 57–60, 1997. DOI: 10.1016/S0304-3940(97)00255-3 (cit. on p. 57).
- [109] J. O’Keefe and J. Dostrovsky, “The hippocampus as a spatial map. Preliminary evidence from unit activity in the freely-moving rat”, *Brain Research*, vol. 34, pp. 171–175, 1971. DOI: 10.1016/0006-8993(71)90358-1 (cit. on p. 57).
- [110] J O’Keefe, “A review of the hippocampal place cells.”, *Progress in Neurobiology*, vol. 13, pp. 419–439, 1979. DOI: 10.1016/0301-0082(79)90005-4 (cit. on p. 57).

-
- [111] J. F. Soechting and M Flanders, “Moving in Three-Dimensional Space: Frames of Reference, Vectors, and Coordinate Systems”, *Annual review of neuroscience*, vol. 15, pp. 167–191, 1992. DOI: 10.1146/annurev.ne.15.030192.001123 (cit. on p. 57).
- [112] L. P. Latash and M. L. Latash, *A New Book by N. A. Bernstein: On Dexterity and Its Development*. 1994, vol. 26, pp. 56–62. DOI: 10.1080/00222895.1994.9941662 (cit. on p. 57).
- [113] F. Röhricht, “Body oriented psychotherapy. The state of the art in empirical research and evidence-based practice: A clinical perspective”, *Body, Movement and Dance in Psychotherapy*, vol. 4, pp. 135–156, 2009. DOI: <http://dx.doi.org/10.1080/17432970902857263> (cit. on p. 57).
- [114] S. Vaynman and F. Gomez-Pinilla, “License to Run: Exercise Impacts Functional Plasticity in the Intact and Injured Central Nervous System by Using Neurotrophins”, *Neurorehabilitation and Neural Repair*, vol. 19, pp. 283–295, 2005. DOI: 10.1177/1545968305280753 (cit. on p. 57).
- [115] M. Windolf, N. Götzen, and M. Morlock, “Systematic accuracy and precision analysis of video motion capturing systems - exemplified on the Vicon-460 system”, *Journal of Biomechanics*, vol. 41, pp. 2776–2780, 2008. DOI: 10.1016/j.jbiomech.2008.06.024 (cit. on p. 57).
- [116] C.-Y. Chang, B. Lange, M. Zhang, S. Koenig, P. Requejo, N. Somboon, A. A. Sawchuk, and A. A. Rizzo, “Towards pervasive physical rehabilitation using Microsoft Kinect”, *Pervasive Computing Technologies for Healthcare (PervasiveHealth), 2012 6th International Conference on*, IEEE, 2012, pp. 159–162 (cit. on p. 57).
- [117] K. Winer, *9 DoF Motion Sensor Bakeoff*, *GitHub*, 2017 (cit. on p. 57).
- [118] K. Winer, *Affordable 9 DoF Sensor Fusion*, 2017 (cit. on p. 57).

- [119] S. Madgwick, “An efficient orientation filter for inertial and inertial/magnetic sensor arrays”, *Report x-io and University of Bristol (UK)*, vol. 25, 2010 (cit. on p. 57).
- [120] S. O. H. Madgwick, A. J. L. Harrison, and R. Vaidyanathan, “Estimation of IMU and MARG orientation using a gradient descent algorithm”, *2011 IEEE International Conference on Rehabilitation Robotics*, IEEE, 2011, pp. 1–7. DOI: 10.1109/ICORR.2011.5975346 (cit. on p. 57).
- [121] Y. Tian, X. Meng, D. Tao, D. Liu, and C. Feng, “Upper limb motion tracking with the integration of IMU and Kinect”, *Neurocomputing*, vol. 159, pp. 207–218, 2015. DOI: 10.1016/j.neucom.2015.01.071 (cit. on p. 58).
- [122] A. Pfister, A. M. West, S. Bronner, and J. A. Noah, “Comparative abilities of Microsoft Kinect and Vicon 3D motion capture for gait analysis”, *Journal of Medical Engineering & Technology*, vol. 38, pp. 274–280, 2014. DOI: 10.3109/03091902.2014.909540 (cit. on p. 58).
- [123] A. Schlegel and C. Honnet, “From Ordinary to Expressive Objects Using Tiny Wireless IMUs”, *Proceedings of the 4th International Conference on Movement Computing - MOCO '17*, pp. 1–8, 2017. DOI: 10.1145/3077981.3078040 (cit. on p. 58).
- [124] R. Freire, C. Honnet, and P. Strohmeier, “Second Skin: An Exploration of eTextile Stretch Circuits on the Body Video Figure”, *Tei*, vol. 17, pp. 653–658, 2017. DOI: 10.1145/3024969.3025054 (cit. on p. 58).
- [125] P. Strohmeier, C. Honnet, and S. von Cyborg, “Developing an Ecosystem for Interactive Electronic Implants”, *Biomimetic and Biohybrid Systems: 5th International Conference, Living Machines 2016, Edinburgh, UK, July 19-22, 2016. Proceedings*, N. F. Lepora, A. Mura, M. Mangan, P. F.M. J. Verschure, M. Desmulliez, and T. J. Prescott, Eds. Cham: Springer International Publishing, 2016, pp. 518–525. DOI: 10.1007/978-3-319-42417-0_56 (cit. on p. 58).

- [126] D. Wessel, M. Wright, and J. Schott, “Intimate Musical Control of Computers with a Variety of Controllers and Gesture Mapping Metaphors”, *Proceedings of the 2002 conference on New interfaces for musical expression*, pp. 1–3, 2002 (cit. on p. 62).
- [127] Ashtuchkin2017, *DIY Position Tracking using HTC Vive’s Lighthouse* (cit. on p. 63).
- [128] D. H. Eberly, *3D game engine design: a practical approach to real-time computer graphics*. New York and San Mateo, CA: CRC Press, 2006, p. 1040 (cit. on p. 63).
- [129] V. Lepetit, F. Moreno-Noguer, and P. Fua, “EPnP: An Accurate $O(n)$ Solution to the PnP Problem”, *International Journal of Computer Vision*, vol. 81, pp. 155–166, 2009. DOI: 10.1007/s11263-008-0152-6 (cit. on p. 66).
- [130] N. Semiconductors, *Programmable Peripheral Interface documentation* (cit. on p. 69).
- [131] G Paxinos and C Watson, “The rat brain in stereotaxic coordinates/George Paxinos”, *Charles Watson, Amsterdam*, 2007 (cit. on pp. 70, 71, 94, 97).
- [133] N. K. Logothetis, “The neural basis of the blood-oxygen-level-dependent functional magnetic resonance imaging signal”, *Philosophical Transactions of the Royal Society B: Biological Sciences*, vol. 357, pp. 1003–1037, 2002. DOI: 10.1098/rstb.2002.1114 (cit. on p. 74).
- [134] B. B. Biswal, J Van Kylen, and J. S. Hyde, “Simultaneous assessment of flow and BOLD signals in resting-state functional connectivity maps.”, *NMR in biomedicine*, vol. 10, pp. 165–70, 1997 (cit. on p. 74).
- [135] J. L. Boxerman, L. M. Hamberg, B. R. Rosen, and R. M. Weisskoff, “MR contrast due to intravascular magnetic susceptibility perturbations”, *Magnetic Resonance in Medicine*, vol. 34, pp. 555–566, 1995. DOI: 10.1002/mrm.1910340412 (cit. on pp. 74, 75).

- [136] H. Gudbjartsson and S. Patz, “Simultaneous calculation of flow and diffusion sensitivity in steady-state free precession imaging”, *Magnetic Resonance in Medicine*, vol. 34, pp. 567–579, 1995. DOI: 10.1002/mrm.1910340413 (cit. on p. 74).
- [137] I. Digernes, A. Bjørnerud, S. A. S. Vatnehol, G. Løvland, F. Courivaud, E. Vik-Mo, T. R. Meling, and K. E. Emblem, “A theoretical framework for determining cerebral vascular function and heterogeneity from dynamic susceptibility contrast MRI”, *Journal of Cerebral Blood Flow & Metabolism*, vol. 37, pp. 2237–2248, 2017. DOI: 10.1177/0271678X17694187 (cit. on p. 74).
- [138] K. Johar, A. Priya, and M. T. T. Wong-Riley, “Regulation of Na⁺/K⁺-ATPase by nuclear respiratory factor 1”, *Journal of Biological Chemistry*, vol. 287, pp. 40381–40390, 2012. DOI: 10.1074/jbc.M112.414573 (cit. on p. 74).
- [139] C. Reynell and J. J. Harris, “The BOLD signal and neurovascular coupling in autism”, *Developmental Cognitive Neuroscience*, vol. 6, pp. 72–79, 2013. DOI: 10.1016/j.dcn.2013.07.003 (cit. on p. 74).
- [140] J. C. Whitman, L. M. Ward, and T. S. Woodward, “Patterns of cortical oscillations organize neural activity into whole-brain functional networks Evident in the fMRI BOLD signal”, *Frontiers in Human Neuroscience*, vol. 7, p. 80, 2013. DOI: 10.3389/fnhum.2013.00080 (cit. on p. 74).
- [141] C. J. Keller, S. Bickel, C. J. Honey, *et al.*, “Neurophysiological investigation of spontaneous correlated and anticorrelated fluctuations of the BOLD Signal”, *Journal of Neuroscience*, vol. 33, pp. 6333–6342, 2013. DOI: 10.1523/JNEUROSCI.4837-12.2013 (cit. on p. 74).
- [142] K. R. Thulborn, D. Davis, P. Erb, M. Strojwas, and J. A. Sweeney, “Clinical fMRI: Implementation and Experience”, *NeuroImage*, vol. 4, S101–S107, 1996. DOI: 10.1006/nimg.1996.0060 (cit. on p. 74).

- [143] A. Moreno, P. Jego, F. de la Cruz, and S. Canals, “Neurophysiological, metabolic and cellular compartments that drive neurovascular coupling and neuroimaging signals”, *Frontiers in Neuroenergetics*, vol. 5, p. 3, 2013. DOI: 10.3389/fnene.2013.00003 (cit. on pp. 74, 75, 89).
- [144] S. Canals, M. Beyerlein, H. Merkle, and N. K. Logothetis, “Functional MRI Evidence for LTP-Induced Neural Network Reorganization”, *Current Biology*, vol. 19, pp. 398–403, 2009. DOI: 10.1016/j.cub.2009.01.037 (cit. on pp. 74, 75).
- [145] N. K. Logothetis, J. Pauls, M. Augath, T. Trinath, and A. Oeltermann, “Neurophysiological investigation of the basis of the fMRI signal”, *Nature*, vol. 412, pp. 150–157, 2001. DOI: 10.1038/35084005 (cit. on pp. 74, 75).
- [146] J. Paasonen, R. A. Salo, A. Shatillo, M. M. Forsberg, J. Närväinen, J. K. Huttunen, and O. Gröhn, “Comparison of seven different anesthesia protocols for nicotine pharmacologic magnetic resonance imaging in rat.”, *European neuropsychopharmacology : the journal of the European College of Neuropsychopharmacology*, vol. 26, pp. 518–31, 2016. DOI: 10.1016/j.euroneuro.2015.12.034 (cit. on pp. 74, 75).
- [147] K. A. Williams, M. Magnuson, W. Majeed, S. M. LaConte, S. J. Peltier, X. Hu, and S. D. Keilholz, “Comparison of α -chloralose, medetomidine and isoflurane anesthesia for functional connectivity mapping in the rat”, *Magnetic Resonance Imaging*, vol. 28, pp. 995–1003, 2010. DOI: 10.1016/j.mri.2010.03.007 (cit. on pp. 74, 75).
- [148] L. Pérez-Cervera, J. M. Caramés, L. M. Fernández-Mollá, A. Moreno, B. Fernández, E. Pérez-Montoyo, D. Moratal, S. Canals, and J. Pacheco-Torres, “Mapping Functional Connectivity in the Rodent Brain Using Electric-Stimulation fMRI.”, *Methods in molecular biology (Clifton, N.J.)*, vol. 1718, pp. 117–134, 2018. DOI: 10.1007/978-1-4939-7531-0_8 (cit. on pp. 74, 83, 89).

- [149] H. Senoo, “Physiology of Stress and Starvation-like Conditions”, *The Laboratory Rat*, Elsevier, 2000, pp. 447–460. DOI: 10.1016/B978-012426400-7.50062-5 (cit. on p. 75).
- [150] S. Wegener and E. C. Wong, “Longitudinal MRI studies in the isoflurane-anesthetized rat: long-term effects of a short hypoxic episode on regulation of cerebral blood flow as assessed by pulsed arterial spin labelling”, *NMR in Biomedicine*, vol. 21, pp. 696–703, 2008. DOI: 10.1002/nbm.1243 (cit. on p. 75).
- [151] N. C. Owens, Y Ootsuka, K Kanosue, and R. M. McAllen, “Thermoregulatory Control of Sympathetic Fibres Supplying the Rat’s Tail”, *The Journal of Physiology*, vol. 543, pp. 849–858, 2002. DOI: 10.1113/jphysiol.2002.023770 (cit. on p. 75).
- [152] P. E. Sharp and M. C. LaRegina, *The laboratory rat*. Academic Press, 1998 (cit. on p. 75).
- [153] C. Huang, O. T.-W. Ng, Y.-S. Ho, M. G. Irwin, R. C.-C. Chang, and G. T.-C. Wong, “Effect of Continuous Propofol Infusion in Rat on Tau Phosphorylation with or without Temperature Control”, *Journal of Alzheimer’s Disease*, vol. 51, pp. 213–226, 2016. DOI: 10.3233/JAD-150645 (cit. on p. 75).
- [154] M. K. Huss, H. H. Chum, A. G. Chang, K. Jampachairsi, and C. Pacharinsak, “The Physiologic Effects of Isoflurane, Sevoflurane, and Hypothermia Used for Anesthesia in Neonatal Rats (*Rattus norvegicus*).”, *Journal of the American Association for Laboratory Animal Science : JAALAS*, vol. 55, pp. 83–8, 2016 (cit. on p. 75).
- [155] A. Schroeter, F. Schlegel, A. Seuwen, J. Grandjean, and M. Rudin, “Specificity of stimulus-evoked fMRI responses in the mouse: The influence of systemic physiological changes associated with innocuous stimulation under four different anesthetics”, *NeuroImage*, vol. 94, pp. 372–384, 2014. DOI: 10.1016/j.neuroimage.2014.01.046 (cit. on p. 75).

- [156] E. Jonckers, R. Delgado y Palacios, D. Shah, C. Guglielmetti, M. Verhoye, and A. Van der Linden, “Different anesthesia regimes modulate the functional connectivity outcome in mice”, *Magnetic Resonance in Medicine*, vol. 72, pp. 1103–1112, 2014. DOI: 10.1002/mrm.24990 (cit. on p. 75).
- [157] T. Wu, J. Grandjean, S. C. Bosshard, M. Rudin, D. Reutens, and T. Jiang, “Altered regional connectivity reflecting effects of different anesthesia protocols in the mouse brain”, *NeuroImage*, vol. 149, pp. 190–199, 2017. DOI: 10.1016/j.neuroimage.2017.01.074 (cit. on p. 75).
- [158] F. Schlegel, A. Schroeter, and M. Rudin, “The hemodynamic response to somatosensory stimulation in mice depends on the anesthetic used: Implications on analysis of mouse fMRI data”, *NeuroImage*, vol. 116, pp. 40–49, 2015. DOI: 10.1016/j.neuroimage.2015.05.013 (cit. on p. 75).
- [159] J. Grandjean, A. Schroeter, I. Batata, and M. Rudin, “Optimization of anesthesia protocol for resting-state fMRI in mice based on differential effects of anesthetics on functional connectivity patterns”, *NeuroImage*, vol. 102, pp. 838–847, 2014. DOI: 10.1016/j.neuroimage.2014.08.043 (cit. on p. 75).
- [160] P. Flecknell, *Laboratory animal anesthesia: A practical introduction for research workers and technicians*. San Diego: Academic Press Inc., 1996, p. 1987 (cit. on p. 75).
- [161] G. Dispersyn, L. Pain, and Y. Touitou, “Circadian disruption of body core temperature and rest-activity rhythms after general (Propofol) Anesthesia in Rats”, *Anesthesiology*, vol. 110, pp. 1305–1315, 2009. DOI: 10.1097/ALN.0b013e3181a10225 (cit. on p. 75).
- [162] E. A. Kiyatkin, “The hidden side of drug action: brain temperature changes induced by neuroactive drugs”, *Psychopharmacology*, vol. 225, pp. 765–780, 2013. DOI: 10.1007/s00213-012-2957-9 (cit. on p. 75).

- [163] M. S. Smirnov and E. A. Kiyatkin, “Behavioral and temperature effects of delta 9-tetrahydrocannabinol in human-relevant doses in rats”, *Brain Research*, vol. 1228, pp. 145–160, 2008. DOI: 10.1016/j.brainres.2008.06.069 (cit. on p. 75).
- [164] E Kiyatkin and P Brown, “Brain and body temperature homeostasis during sodium pentobarbital anesthesia with and without body warming in rats”, *Physiology & Behavior*, vol. 84, pp. 563–570, 2005. DOI: 10.1016/j.physbeh.2005.02.002 (cit. on p. 75).
- [165] T. Tsurugizawa, Y. Takahashi, and F. Kato, “Distinct effects of isoflurane on basal BOLD signals in tissue/vascular microstructures in rats”, *Scientific Reports*, vol. 6, p. 38977, 2016. DOI: 10.1038/srep38977 (cit. on p. 75).
- [166] N. P. Blockley, V. E. M. Griffeth, A. B. Simon, and R. B. Buxton, “A review of calibrated blood oxygenation level-dependent (BOLD) methods for the measurement of task-induced changes in brain oxygen metabolism”, *NMR in Biomedicine*, vol. 26, pp. 987–1003, 2013. DOI: 10.1002/nbm.2847 (cit. on p. 75).
- [167] J Pacheco-Torres, A Moreno, B Fernández, L Pérez-Cervera, J. Caramés, L. Fernández-Mollá, E Pérez-Montoyo, D Moratal, and S Canals, “Functional MRI of synaptic plasticity, in "Handbook of in vivo neural plasticity techniques: A systems neuroscience approach to the neural basis of memory and cognition"”, Denise Manahan-Vaughan, Ed., Amsterdam, The Netherlands: Elsevier, 2018 (cit. on pp. 75, 89).
- [168] J. Guerreiro, A. Lourenço, H. Silva, and A. Fred, “Performance Comparison of Low-cost Hardware Platforms Targeting Physiological Computing Applications”, *Procedia Technology*, vol. 17, pp. 399–406, 2014. DOI: 10.1016/j.protcy.2014.10.204 (cit. on p. 76).
- [169] G. Lockridge, B. Dzwonkowski, R. Nelson, and S. Powers, “Development of a Low-Cost Arduino-Based Sonde for Coastal Applications”, *Sensors*, vol. 16, p. 528, 2016. DOI: 10.3390/s16040528 (cit. on p. 76).

- [170] P. Teikari, R. P. Najjar, H. Malkki, K. Knoblauch, D. Dumortier, C. Gronfier, and H. M. Cooper, “An inexpensive Arduino-based LED stimulator system for vision research.”, *Journal of neuroscience methods*, vol. 211, pp. 227–36, 2012. DOI: 10.1016/j.jneumeth.2012.09.012 (cit. on pp. 76, 79, 124).
- [171] P. Artoni, S. Landi, S. S. Sato, S. Luin, and G. M. Ratto, “Arduino Due based tool to facilitate in vivo two-photon excitation microscopy”, *Biomedical Optics Express*, vol. 7, p. 1604, 2016. DOI: 10.1364/BOE.7.001604 (cit. on p. 76).
- [172] V. A. Korolyov and V. T. Potapov, “Biomedical fiber-optic temperature and pressure sensors”, *Biomedical Engineering*, vol. 46, pp. 79–82, 2012. DOI: 10.1007/s10527-012-9272-y (cit. on p. 78).
- [173] A. D’Ausilio, “Arduino: a low-cost multipurpose lab equipment.”, *Behavior research methods*, vol. 44, pp. 305–13, 2012. DOI: 10.3758/s13428-011-0163-z (cit. on pp. 79, 124).
- [174] T. Besson, D. Debayle, S. Diochot, M. Salinas, and E. Lingueglia, “Low cost venom extractor based on Arduino board for electrical venom extraction from arthropods and other small animals”, *Toxicon*, vol. 118, pp. 156–161, 2016. DOI: 10.1016/j.toxicon.2016.05.001 (cit. on pp. 79, 124).
- [175] A. Sheinin, A. Lavi, and I. Michaelovski, “StimDuino: An Arduino-based electrophysiological stimulus isolator”, *Journal of Neuroscience Methods*, vol. 243, pp. 8–17, 2015. DOI: 10.1016/j.jneumeth.2015.01.016 (cit. on pp. 79, 124).
- [176] A. S. Ali, Z. Zanzinger, D. Debose, and B. Stephens, “Open Source Building Science Sensors (OSBSS): A low-cost Arduino-based platform for long-term indoor environmental data collection”, *Building and Environment*, vol. 100, pp. 114–126, 2016. DOI: 10.1016/j.buildenv.2016.02.010 (cit. on pp. 79, 124).

- [177] K. Ogata and Y Yang, *Modern control engineering*, 5th ed. Upper Saddle River, New Jersey: Pearson Education, 1990 (cit. on pp. 81, 88).
- [178] A. Shitzer, E. Arens, and H. Zhang, “Compilation of basal metabolic and blood perfusion rates in various multi-compartment, whole-body thermoregulation models”, *International Journal of Biometeorology*, vol. 60, pp. 1051–1064, 2016. DOI: 10.1007/s00484-015-1096-5 (cit. on p. 81).
- [179] J. M. Barker, C. E. Cooper, P. C. Withers, and A. P. Cruz-Neto, “Thermoregulation by an Australian murine rodent, the ash-grey mouse (*Pseudomys albocinereus*)”, *Comparative Biochemistry and Physiology Part A: Molecular & Integrative Physiology*, vol. 163, pp. 336–342, 2012. DOI: 10.1016/j.cbpa.2012.07.011 (cit. on p. 81).
- [180] R. C. Dorf and N. K. Sinha, “Modern Control Systems”, *IEEE Transactions on Systems, Man, and Cybernetics*, vol. 11, pp. 580–580, 1981. DOI: 10.1109/TSMC.1981.4308749 (cit. on pp. 81, 82).
- [181] I. J. Koenka, J. Sáiz, and P. C. Hauser, “Instrumentino: an open-source software for scientific instruments”, *CHIMIA International Journal for Chemistry*, vol. 69, pp. 172–175, 2015 (cit. on p. 83).
- [182] R. Anderson and D. Cervo, “Pro Arduino”, *Pro Arduino*, vol. 28, Berkeley, CA: Apress, 2013, ch. 7, p. 316. DOI: 10.1007/978-1-4302-3940-6 (cit. on p. 83).
- [183] A. Moreno, R. G. Morris, and S. Canals, “Frequency-Dependent Gating of Hippocampal–Neocortical Interactions”, *Cerebral Cortex*, vol. 26, pp. 2105–2114, 2016. DOI: 10.1093/cercor/bhv033 (cit. on pp. 83, 89).
- [184] E. Alvarez-Salvado, V. Pallares, A. Moreno, and S. Canals, “Functional MRI of long-term potentiation: imaging network plasticity”, *Philosophical Transactions of the Royal Society B: Biological Sciences*, vol. 369, pp. 20130152–20130152, 2013. DOI: 10.1098/rstb.2013.0152 (cit. on p. 89).

- [186] R. J. Perrin, A. M. Fagan, and D. M. Holtzman, “Multimodal techniques for diagnosis and prognosis of Alzheimer’s disease”, *Nature*, vol. 461, pp. 916–922, 2009. DOI: 10.1038/nature08538 (cit. on p. 94).
- [187] D. E. Linden, “The Challenges and Promise of Neuroimaging in Psychiatry”, *Neuron*, vol. 73, pp. 8–22, 2012. DOI: 10.1016/j.neuron.2011.12.014 (cit. on p. 94).
- [188] S. Teipel, A. Drzezga, M. J. Grothe, *et al.*, “Multimodal imaging in Alzheimer’s disease: validity and usefulness for early detection”, *The Lancet Neurology*, vol. 14, pp. 1037–1053, 2015. DOI: 10.1016/S1474-4422(15)00093-9 (cit. on p. 94).
- [189] C. W. Woo, L. J. Chang, M. A. Lindquist, and T. D. Wager, “Building better biomarkers: Brain models in translational neuroimaging”, *Nature Neuroscience*, vol. 20, pp. 365–377, 2017. DOI: 10.1038/nn.4478 (cit. on p. 94).
- [190] I. Ivanov, “The Neuroimaging Gap - Where do we go from Here?”, *Acta Psychopathologica*, vol. 03, 2017. DOI: 10.4172/2469-6676.100090 (cit. on p. 94).
- [191] O. Kastrup, I. Wanke, and M. Maschke, “Neuroimaging of infections”, *NeuroRX*, vol. 2, pp. 324–332, 2005. DOI: 10.1602/neurorx.2.2.324 (cit. on p. 94).
- [192] D. Preece, S. B. Williams, R. Lam, and R. Weller, “Let’s Get Physical: Advantages of a physical model over 3D computer models and textbooks in learning imaging anatomy”, *Anatomical Sciences Education*, vol. 6, pp. 216–224, 2013. DOI: 10.1002/ase.1345 (cit. on p. 94, 105).
- [193] Y.-x. Zheng, D.-f. Yu, J.-g. Zhao, Y.-l. Wu, and B. Zheng, “3D Printout Models vs. 3D-Rendered Images: Which Is Better for Preoperative Planning?”, *Journal of Surgical Education*, vol. 73, pp. 518–523, 2016. DOI: 10.1016/j.jsurg.2016.01.003 (cit. on p. 94).

- [194] Z. Li, Z. Li, R. Xu, M. Li, J. Li, Y. Liu, D. Sui, W. Zhang, and Z. Chen, “Three-dimensional printing models improve understanding of spinal fracture—A randomized controlled study in China”, *Scientific Reports*, vol. 5, p. 11 570, 2015. DOI: 10.1038/srep11570 (cit. on p. 94).
- [195] J Kettenbach, T Wong, D Kacher, N Hata, R. B. Schwartz, P. M. L. Black, R Kikinis, and F. A. Jolesz, “Computer-based imaging and interventional MRI: Applications for neurosurgery”, *Computerized Medical Imaging and Graphics*, vol. 23, Pergamon, 2008, pp. 76–80. DOI: 10 . 1016 / S0895 - 6111(99)00022-1 (cit. on p. 94).
- [196] A. J. Schwarz, A. Danckaert, T. Reese, A. Gozzi, G. Paxinos, C. Watson, E. V. Merlo-Pich, and A. Bifone, “A stereotaxic MRI template set for the rat brain with tissue class distribution maps and co-registered anatomical atlas: Application to pharmacological MRI”, *NeuroImage*, vol. 32, pp. 538–550, 2006. DOI: 10.1016/j.neuroimage.2006.04.214 (cit. on pp. 94, 97, 98).
- [197] A. Marro, T. Bandukwala, and W. Mak, “Three-Dimensional Printing and Medical Imaging: A Review of the Methods and Applications”, *Current Problems in Diagnostic Radiology*, vol. 45, pp. 2–9, 2016. DOI: 10.1067/j.cpradiol.2015.07.009 (cit. on p. 95).
- [198] M. H. Michalski and J. S. Ross, “The Shape of Things to Come”, *JAMA*, vol. 312, p. 2213, 2014. DOI: 10.1001/jama.2014.9542 (cit. on p. 95).
- [199] M. Ratto and R. Ree, “Materializing information: 3D printing and social change”, *First Monday*, vol. 17, 2012. DOI: 10.5210/fm.v17i7.3968 (cit. on p. 95).
- [200] F. Rengier, A. Mehndiratta, H. von Tengg-Kobligk, C. M. Zechmann, R. Unterhinninghofen, H.-U. Kauczor, and F. L. Giesel, “3D printing based on imaging data: review of medical applications”, *International Journal of Computer Assisted Radiology and Surgery*, vol. 5, pp. 335–341, 2010. DOI: 10.1007/s11548-010-0476-x (cit. on p. 95).

- [201] M. S. Mannoor, Z. Jiang, T. James, Y. L. Kong, K. A. Malatesta, W. O. Soboyejo, N. Verma, D. H. Gracias, and M. C. McAlpine, “3D printed bionic ears”, *Nano Letters*, vol. 13, pp. 2634–2639, 2013. DOI: 10.1021/nl4007744 (cit. on p. 95).
- [202] J. R. Guy, P. Sati, E. Leibovitch, S. Jacobson, A. C. Silva, and D. S. Reich, “Custom fit 3D-printed brain holders for comparison of histology with MRI in marmosets”, *Journal of Neuroscience Methods*, vol. 257, pp. 55–63, 2016. DOI: 10.1016/j.jneumeth.2015.09.002 (cit. on p. 95).
- [203] K. J.K. J. Friston, J. Ashburner, S. Kiebel, T. Nichols, and W. D. Penny, *Statistical parametric mapping : the analysis of funtional brain images*. Elsevier/Academic Press, 2007, p. 647 (cit. on p. 98).
- [204] K. J. Friston, A. P. Holmes, K. J. Worsley, J. P. Poline, C. D. Frith, and R. S. Frackowiak, “Statistical parametric maps in functional imaging: A general linear approach”, *Human Brain Mapping*, vol. 2, pp. 189–210, 1994. DOI: 10.1002/hbm.460020402 (cit. on p. 98).
- [205] G. Flandin and M. J. U. Novak, “fMRI data analysis using SPM”, *fMRI*, Berlin, Heidelberg: Springer Berlin Heidelberg, 2013, pp. 51–76. DOI: 10.1007/978-3-642-34342-1_6 (cit. on p. 98).
- [206] J. W. Eaton, D. Bateman, and S. Hauberg, *GNU Octave version 3.0. 1 manual: a high-level interactive language for numerical computations*. New York, NY, USA: SoHo Books, 2007 (cit. on p. 98).
- [207] B. Mueller, “Additive Manufacturing Technologies - Rapid Prototyping to Direct Digital Manufacturing”, *Assembly Automation*, vol. 32, 2012. DOI: 10.1108/aa.2012.03332baa.010 (cit. on p. 102).
- [208] J. Gulánová, I. Kister, N. Káer, and L. Gulán, “A Comparative Study of various AM Technologies Based on Their Accuracy”, *Procedia CIRP*, vol. 67, pp. 238–243, 2018. DOI: 10.1016/j.procir.2017.12.206 (cit. on p. 102).

- [209] P. S. D'Urso, T. M. Barker, W. J. Earwaker, L. J. Bruce, R. L. Atkinson, M. W. Lanigan, J. F. Arvier, and D. J. Effeney, "Stereolithographic biomodelling in cranio-maxillofacial surgery: a prospective trial", *Journal of Cranio-Maxillofacial Surgery*, vol. 27, pp. 30–37, 1999. DOI: 10.1016/S1010-5182(99)80007-9 (cit. on p. 105).
- [210] A. Müller, K. G. Krishnan, E. Uhl, and G. Mast, "The Application of Rapid Prototyping Techniques in Cranial Reconstruction and Preoperative Planning in Neurosurgery", *Journal of Craniofacial Surgery*, vol. 14, pp. 899–914, 2003. DOI: 10.1097/00001665-200311000-00014 (cit. on p. 105).
- [211] J. Guarino, S. Tennyson, G. McCain, L. Bond, K. Shea, and H. King, "Rapid Prototyping Technology for Surgeries of the Pediatric Spine and Pelvis", *Journal of Pediatric Orthopaedics*, vol. 27, pp. 955–960, 2007. DOI: 10.1097/bpo.0b013e3181594ced (cit. on p. 105).
- [212] C. Canstein, P. Cachot, A. Faust, A. Stalder, J. Bock, A. Frydrychowicz, J. Küffer, J. Hennig, and M. Markl, "3D MR flow analysis in realistic rapid-prototyping model systems of the thoracic aorta: Comparison with in vivo data and computational fluid dynamics in identical vessel geometries", *Magnetic Resonance in Medicine*, vol. 59, pp. 535–546, 2008. DOI: 10.1002/mrm.21331 (cit. on p. 105).
- [213] F. L. Giesel, A. Mehndiratta, H. von Tengg-Kobligk, A. Schaeffer, K. Teh, E. Hoffman, H.-U. Kauczor, E. van Beek, and J. M. Wild, "Rapid Prototyping Raw Models on the Basis of High Resolution Computed Tomography Lung Data for Respiratory Flow Dynamics", *Academic Radiology*, vol. 16, pp. 495–498, 2009. DOI: 10.1016/j.acra.2008.10.008 (cit. on p. 105).
- [214] S. K. Malyala, Y. Ravi Kumar, and C. Rao, "Organ Printing With Life Cells: A Review", *Materials Today: Proceedings*, vol. 4, pp. 1074–1083, 2017. DOI: 10.1016/j.matpr.2017.01.122 (cit. on p. 105).

- [215] K. R. Foster, “3-Dimensional Printing in Medicine: Hype, Hope, and the Challenge of Personalized Medicine”, *Philosophy of Engineering and Technology*, Springer, Cham, 2017, pp. 211–228. DOI: 10.1007/978-3-319-45193-0_16 (cit. on p. 105).
- [217] G. W. Griffiths and W. E. Schiesser, *Histology and Cell Biology - Abraham Kierszenbaum.pdf*, 2002 (cit. on p. 108).
- [218] R. Paniagua, Nistal, P M and Sesma, U. Álvarez, B Fraile, R Anadón, F. Sáez, and M. De Miguel, *Citología e histología vegetal y animal*. McGraw-Hill Interamericana, 1998 (cit. on p. 108).
- [219] P Lipton, P. G. Aitken, F. E. Dudek, *et al.*, “Making the best of brain slices: comparing preparative methods.”, *Journal of neuroscience methods*, vol. 59, pp. 151–6, 1995 (cit. on p. 108).
- [220] E. Clérin, Y. Yang, V. Forster, V. Fontaine, J.-A. Sahel, and T. Lévillard, “Vibratome Sectioning Mouse Retina to Prepare Photoreceptor Cultures”, *Journal of Visualized Experiments*, pp. 1–9, 2014. DOI: 10.3791/51954 (cit. on p. 108).
- [221] H. M. Abdelaal, H. O. Kim, R. Wagstaff, R. Sawahata, P. J. Southern, and P. J. Skinner, “Comparison of Vibratome and Compresstome sectioning of fresh primate lymphoid and genital tissues for in situ MHC-tetramer and immunofluorescence staining”, *Biological Procedures Online*, vol. 17, p. 2, 2015. DOI: 10.1186/s12575-014-0012-4 (cit. on p. 108).
- [222] A. Marciniak, C. M. Cohrs, V. Tsata, *et al.*, “Using pancreas tissue slices for in situ studies of islet of Langerhans and acinar cell biology”, *Nature Protocols*, vol. 9, pp. 2809–2822, 2014. DOI: 10.1038/nprot.2014.195 (cit. on p. 108).
- [223] J. Brechbahl, M. Klaey, F. Moine, E. Bovay, N. Hurni, M. Nenniger-Tosato, and M.-C. Broillet, “Morphological and physiological species-dependent characteristics of the rodent Grueneberg ganglion”, *Frontiers in Neu-*

- roanatomy*, vol. 8, pp. 1–14, 2014. DOI: 10.3389/fnana.2014.00087 (cit. on p. 108).
- [224] Z. He, M. Fernandez-Fuente, M. Strom, L. Cheung, I. C. Robinson, and P. Le Tissier, “Continuous On-Line Monitoring of Secretion from Rodent Pituitary Endocrine Cells Using Fluorescent Protein Surrogate Markers”, *Journal of Neuroendocrinology*, vol. 23, pp. 197–207, 2011. DOI: 10.1111/j.1365-2826.2010.02104.x (cit. on p. 108).
- [225] S. A. Joseph, D. T. Piekut, and K. M. Knigge, “Immunocytochemical localization of luteinizing hormone-releasing hormone (LHRH) in Vibratome-sectioned brain.”, *Journal of Histochemistry & Cytochemistry*, vol. 29, pp. 247–254, 1981. DOI: 10.1177/29.2.6166655 (cit. on p. 108).
- [226] H. Kubota, S. Katsurabayashi, a. J Moorhouse, N. Murakami, H. Koga, and N. Akaike, “GABAB receptor transduction mechanisms, and cross-talk between protein kinases A and C, in GABAergic terminals synapsing onto neurons of the rat nucleus basalis of Meynert”, *The Journal of Physiology*, vol. 551, pp. 263–276, 2003. DOI: 10.1113/jphysiol.2003.046524 (cit. on p. 108).
- [227] I. J. Llewellyn-Smith and J. B. Minson, “Complete penetration of antibodies into vibratome sections after glutaraldehyde fixation and ethanol treatment: light and electron microscopy for neuropeptides.”, *Journal of Histochemistry & Cytochemistry*, vol. 40, pp. 1741–1749, 1992. DOI: 10.1177/40.11.1431060 (cit. on p. 108).
- [228] T. Hökfelt and A Ljungdahl, “Modification of the Falck-Hillarp formaldehyde fluorescence method using the Vibratome: simple, rapid and sensitive localization of catecholamines in sections of unfixed or formalin fixed brain tissue.”, *Histochemie. Histochemistry. Histochimie*, vol. 29, pp. 325–39, 1972 (cit. on p. 108).
- [229] R. Gibb and B. Kolb, “A method for vibratome sectioning of Golgi-Cox stained whole rat brain.”, *Journal of neuroscience methods*, vol. 79, pp. 1–4, 1998 (cit. on p. 108).

-
- [230] J Geiger, J Bischofberger, I Vida, U Fröbe, S Pfitzinger, H Weber, K Haverkamp, and P Jonas, “Patch-clamp recording in brain slices with improved slicer technology”, *Pflügers Archiv - European Journal of Physiology*, vol. 443, pp. 491–501, 2002. DOI: 10.1007/s00424-001-0735-3 (cit. on p. 108).
- [231] D Gruber, K. Gilling, and a Albrecht, “5-HT receptor-mediated modulation of granule cell inhibition after juvenile stress recovers after a second exposure to adult stress”, *Neuroscience*, vol. 293, pp. 67–79, 2015. DOI: 10.1016/j.neuroscience.2015.02.050 (cit. on p. 108).
- [232] T. Siegfried and F. Red, *Vibrating microtome with automated measurement of vertical runout*, 2007 (cit. on p. 109).
- [233] L. Ankri, Y. Yarom, and M. Y. Uusisaari, “Slice It Hot: Acute Adult Brain Slicing in Physiological Temperature”, *Journal of Visualized Experiments*, e52068, 2014. DOI: 10.3791/52068 (cit. on p. 109).
- [234] M. Wirth and F. Thiesse, “Shapeways and the 3d printing revolution”, 2014 (cit. on p. 113).
- [236] C. Fitzmaurice, D. Dicker, and A. Pain, “The Global Burden of Cancer 2013”, *JAMA Oncology*, vol. 1, p. 505, 2015. DOI: 10.1001/jamaoncol.2015.0735 (cit. on p. 120).
- [237] C. F. Mountain, “Revisions in the international system for staging lung cancer”, *Chest*, vol. 111, pp. 1710–1717, 1997 (cit. on p. 120).
- [238] K. D. Miller, R. L. Siegel, C. C. Lin, A. B. Mariotto, J. L. Kramer, J. H. Rowland, K. D. Stein, R. Alteri, and A. Jemal, “Cancer treatment and survivorship statistics, 2016”, *CA: A Cancer Journal for Clinicians*, vol. 66, pp. 271–289, 2016. DOI: 10.3322/caac.21349 (cit. on p. 120).
- [239] P Mayles and A Nahum, *Handbook of Radiotherapy Physics*, P Mayles, A Nahum, and J Rosenwald, Eds. Taylor & Francis, 2007. DOI: 10.1201/9781420012026 (cit. on p. 121).

- [240] G. S. Mageras, A. Pevsner, E. D. Yorke, *et al.*, “Measurement of lung tumor motion using respiration-correlated CT”, *International Journal of Radiation Oncology Biology Physics*, vol. 60, pp. 933–941, 2004. DOI: 10.1016/j.ijrobp.2004.06.021 (cit. on pp. 121, 131).
- [241] K. J. Borm, M. Oechsner, J. J. Wilkens, J. Berndt, M. Molls, H. Geinitz, and M. N. Duma, “The impact of CT window settings on the contouring of a moving target: A phantom study”, *Clinical Radiology*, vol. 69, e331–e336, 2014. DOI: 10.1016/j.crad.2014.03.006 (cit. on pp. 121, 131).
- [242] A. C. Guyton, J. E. Hall, E. John, I. Fernández Bernaldo de Quirós, J. L. Agud Aparicio, and I. Alvarez Baleriola, *Guyton & hall: tratado de fisiología medica (12ª ed.)* 12th. Elsevier España S.A., 2011, p. 1112 (cit. on p. 121).
- [243] G. Guidi, N. Maffei, A. Ciarmatori, M. G. Mistretta, G. Gottardi, T. Costi, C. Vecchi, and G. Baldazzi, “Real-time lung tumour motion modeling for adaptive radiation therapy using lego mindstorms”, *Journal of Mechanics in Medicine and Biology*, vol. 15, p. 1540019, 2015 (cit. on p. 121).
- [244] Y. Seppenwoolde, H. Shirato, K. Kitamura, S. Shimizu, M. van Herk, J. V. Lebesque, and K. Miyasaka, “Precise and real-time measurement of 3D tumor motion in lung due to breathing and heartbeat, measured during radiotherapy”, *International Journal of Radiation Oncology Biology Physics*, vol. 53, pp. 822–834, 2002. DOI: 10.1016/S0360-3016(02)02803-1 (cit. on pp. 121, 122).
- [245] R. S. Harris, “Pressure-volume curves of the respiratory system”, *Respiratory care*, vol. 50, pp. 78–99, 2005 (cit. on p. 121).
- [246] M. C. Aznar, G. F. Persson, I. M. Kofoed, D. E. Nygaard, and S. S. Korreman, “Irregular breathing during 4DCT scanning of lung cancer patients: Is the midventilation approach robust?”, *Physica Medica*, vol. 30, pp. 69–75, 2014. DOI: 10.1016/j.ejmp.2013.03.003 (cit. on pp. 121, 131).

-
- [247] S. Sarudis, A. Karlsson Hauer, J. Nyman, and A. Bäck, “Systematic evaluation of lung tumor motion using four-dimensional computed tomography”, *Acta Oncologica*, vol. 56, pp. 525–530, 2017. DOI: 10.1080/0284186X.2016.1274049 (cit. on p. 121).
- [248] Y. Wang, Y. Bao, L. Zhang, *et al.*, “Assessment of respiration-induced motion and its impact on treatment outcome for lung cancer.”, *BioMed research international*, vol. 2013, p. 872739, 2013. DOI: 10.1155/2013/872739 (cit. on p. 121).
- [249] S. Shimizu, H. Shirato, S. Ogura, H. Akita-Dosaka, K. Kitamura, T. Nishioka, K. Kagei, M. Nishimura, and K. Miyasaka, “Detection of lung tumor movement in real-time tumor-tracking radiotherapy”, *International Journal of Radiation Oncology Biology Physics*, vol. 51, pp. 304–310, 2001. DOI: 10.1016/S0360-3016(01)01641-8 (cit. on pp. 122, 123).
- [250] K. J. Redmond, D. Y. Song, J. L. Fox, J. Zhou, C. N. Rosenzweig, and E. Ford, “Respiratory Motion Changes of Lung Tumors Over the Course of Radiation Therapy Based on Respiration-Related Four-Dimensional Computed Tomography Scans”, *International Journal of Radiation Oncology*Biolog*Physics*, vol. 75, pp. 1605–1612, 2009. DOI: 10.1016/j.ijrobp.2009.05.024 (cit. on p. 122).
- [251] K. Harada, N. Katoh, R. Suzuki, Y. M. Ito, S. Shimizu, R. Onimaru, T. Inoue, N. Miyamoto, and H. Shirato, “Evaluation of the motion of lung tumors during stereotactic body radiation therapy (SBRT) with four-dimensional computed tomography (4DCT) using real-time tumor-tracking radiotherapy system (RTRT)”, *Physica Medica*, vol. 32, pp. 305–311, 2016. DOI: 10.1016/j.ejmp.2015.10.093 (cit. on p. 122).
- [252] L. Knybel, J. Cvek, L. Molenda, N. Stieberova, and D. Feltl, “Analysis of Lung Tumor Motion in a Large Sample: Patterns and Factors Influencing Precise Delineation of Internal Target Volume”, *International Journal of Radiation Oncology Biology Physics*, vol. 96, pp. 751–758, 2016. DOI: 10.1016/j.ijrobp.2016.08.008 (cit. on p. 122).

- [253] A. Fassi, J. Schaerer, M. Fernandes, M. Riboldi, D. Sarrut, and G. Baroni, “Tumor Tracking Method Based on a Deformable 4D CT Breathing Motion Model Driven by an External Surface Surrogate”, *International Journal of Radiation Oncology Biology Physics*, vol. 88, pp. 182–188, 2014. DOI: 10.1016/j.ijrobp.2013.09.026 (cit. on p. 122).
- [254] J. Ruben, A. Seeley, V. Panettieri, and T. Ackerly, “Variation in Lung Tumour Breathing Motion between Planning Four-dimensional Computed Tomography and Stereotactic Ablative Radiotherapy Delivery and its Dosimetric Implications: Any Role for Four-dimensional Set-up Verification?”, *Clinical Oncology*, vol. 28, pp. 21–27, 2016. DOI: 10.1016/j.clon.2015.08.010 (cit. on p. 122).
- [255] T. P. Wangler, *RF Linear Accelerators*. Weinheim, Germany: Wiley-VCH Verlag GmbH & Co. KGaA, 2008, p. 450. DOI: 10.1002/9783527623426 (cit. on p. 123).
- [256] A. P. Mathew, K. Oksman, and M. Sain, “Mechanical properties of biodegradable composites from poly lactic acid (PLA) and microcrystalline cellulose (MCC)”, *Journal of Applied Polymer Science*, vol. 97, pp. 2014–2025, 2005. DOI: 10.1002/app.21779 (cit. on p. 125).
- [257] L. Dunn, T. Kron, P. N. Johnston, L. N. McDermott, M. L. Taylor, J. Callahan, and R. D. Franich, “A programmable motion phantom for quality assurance of motion management in radiotherapy”, *Australasian Physical & Engineering Sciences in Medicine*, vol. 35, pp. 93–100, 2012. DOI: 10.1007/s13246-011-0114-0 (cit. on p. 132).